



**Politecnico
di Torino**

Politecnico di Torino

Master of Science in Biomedical Engineering

2020/2021

July 19th, 2021

"The alveolus-on-a-chip: a biomimetic, microfluidic in vitro model of the alveolar-capillary barrier"

Supervisor:

Prof. Gianluca Ciardelli

Prof. Matteo Cocuzza

Prof.ssa Chiara Tonda Turo

Dr. Simone Luigi Marasso

Candidate:

Eleonora Palumbo

Tables of contents

Abstract	7
1. INTRODUCTION	8
1.1 Lung: anatomy and physiology	8
1.1.1 The conductive tract.....	8
1.1.2 The gas exchange tract	8
1.1.3 The mechanical stretching in the alveoli.....	9
1.1.4 Lung diseases.....	10
1.2 In vitro organ models	11
1.2.1 Animal models.....	11
1.2.1.1 Limitations	12
1.2.2 In vitro 2D models	12
1.2.2.1 Limitations	14
1.2.3 In vitro 3D models	14
1.2.3.1 Spheroids	15
1.2.3.2 Organoids	15
1.2.3.3 Scaffolds.....	16
Decellularized scaffolds	16
Precision-cut lung slices.....	17
Polymeric scaffolds.....	17
1.2.3.4 Hydrogels.....	17
Bioprinting.....	18
1.3 Organ-on-chip	19
1.3.1 Introduction.....	19
1.3.1.1 Advantages and applications.....	19
1.3.2 Microfluidic device fabrication techniques	20
1.3.2.1 Materials.....	20
1.3.2.2 Fabrication techniques	21
A) Soft lithography	21
B) Laser ablation.....	22
C) Replica molding.....	23
1.3.3 Lung-on-chip.....	24
1.3.3.1 ALI barrier	24

<i>Medium throughput breathing human primary cell alveolus-on-chip model by Stucki et al.</i>	24
1.3.3.2 Drug screening	26
<i>A primary human lung alveolus-on-a-chip model of intravascular thrombosis for assessment of therapeutics by Jain et al.</i>	26
1.3.3.3 Toxicological studies	27
<i>Reconstituting Organ-Level Lung Functions on a Chip by Huh et al.</i>	27
1.3.3.4 Disease modelling	28
<i>Lung cancer</i>	28
<i>Polmonary edema</i>	29
<i>Asthma and COPD</i>	29
<i>Cystic fibrosis</i>	29
<i>Liquid plug</i>	29
<i>Epithelium damage and protection during reopening of occluded airways in a physiologic microfluidic pulmonary airway model by Tavana et al.</i>	30
<i>Personalized medicine</i>	30
1.4 <i>The alveolar-capillary basement membrane for ALI culture</i>	31
1.4.1.1 Membrane properties	31
1.4.1.2 Electrospinning	31
1.4.1.3 Membrane material selection	32
1.4.2 <i>Scientific literature</i>	34
2. AIM OF THE WORK	40
3. MATERIALS AND METHODS	41
3.1. <i>Materials</i>	41
3.1.1 <i>Polydimethylsiloxane (PDMS)</i>	41
3.1.2 <i>Polycaprolactone (PCL)</i>	41
3.1.3 <i>Gelatin</i>	42
3.1.3.1 γ -glycidossipropiltrimetossilano (GPTMS)	43
3.1.4 <i>Solution solvents</i>	43
3.1.4.1 Acetic acid	43
3.1.4.2 Formic acid	43
3.1.4.3 Chloroform	44
3.1.5 <i>Cells</i>	44
3.1.5.1 A549	44
3.1.5.2 HULEC-5a	45

3.1.6 Immunostaining	45
3.1.6.1 DAPI	45
3.1.6.2 Phalloidin	45
3.2 Methods	46
3.2.1 Alveolus-on-a-chip design	46
3.2.1.1 Top layer	46
3.2.1.2 Bottom layer	47
3.2.2 Alveolus-on-a-chip fabrication	48
3.2.2.1 Mold fabrication	48
3.2.2.2 Top and bottom layers fabrication	49
3.2.3 Nanofibrous mats fabrication	50
3.2.3.1 Preparation of PCL electrospun mats	50
3.2.3.2 Preparation of PCL/gelatin mats	51
3.2.4 Microfluidic device assembling	51
3.2.5 Field Emission Scanning Electron Microscopy (FE-SEM)	53
3.2.6 Images analysis	54
3.2.7 Mechanical characterization of electrospun nanofibers	54
3.2.7.1 Uniaxial mechanical tests	55
3.2.7.2 Biaxial mechanical tests	56
3.2.8 Cell culture	56
3.2.9 Immunostaining	58
3.2.10 Confocal laser scanning microscopy	58
3.2.11 Cell viability assay	59
4. RESULTS AND DISCUSSION	60
4.1 Fabrication of the lung on chip	60
4.1.1 Laser ablation and production of the PMMA mold	60
4.1.1.1 Top layer mold	60
4.1.1.2 Bottom layer mold	61
4.1.2 Replica molding and fabrication of the layers in PDMS	62
4.1.2.1 Top layer	62
4.1.2.2 Bottom layer	62
4.1.3 Electrospinning and membranes production	65
4.1.3.1 Parameters optimization	65
4.1.3.2 Morphological characterization	67

4.1.3.3 Mechanical characterization	70
4.1.4 Assembly of the device	72
4.2 Leakage tests	73
4.3 Cellular tests.....	74
4.3.1 Evaluation of the material biocompatibility.....	75
4.3.2 Optimization of the cell concentration.....	78
4.3.3 Cells adhesion and vitality in the microfluidic device.....	81
5.CONCLUSIONS	84
Bibliography	87

Abstract

The lung disease burden has increased due to some factors such as pollution, smoking, pathogenic bacteria and virus. Among them, lung cancer has become the leading cause of cancer death worldwide due to its high recurrence, metastasis formation and drug resistance. For these reasons, *in vitro* models that reproduce the lung environment and individualized treatment are required to improve therapies efficacy. Organs-on-chips can be a powerful technology to accomplish this goal. In this thesis work, an alveolus-on-chip, which mimics the alveolar-capillary barrier, is described. The developed microfluidic device consists of two layers separated by an electrospun polycaprolactone/gelatin (PCL/Gel) membrane, where the co-culture of lung epithelial cells (A549) and lung endothelial cells (HULEC-5a) was performed by seeding the two cell lines in the upper and bottom layer of the PCL/Gel membrane, respectively. In addition, the chip allows for carrying out the breathing motion by the mechanical stimulation of the membrane and to generate the air-liquid interface (ALI) on the co-culture for reproducing an *in vivo*-like ambient. The device was designed through Rhinoceros and fabricated using the replica molding technique by casting polydimethylsiloxane (PDMS) inside the mold (obtained by laser ablation of polymethylmethacrylate (PMMA)). The achieved devices were analysed by optical microscopy showing that the geometry was reproduced correctly maintaining the desired dimensions. Instead, the electrospinning technology was exploited to fabricate PCL and PCL/Gel membranes, whose morphology was analysed through scanning electron microscopy while uniaxial and biaxial cyclic tests were used to measure their mechanical properties. All the membranes revealed a random configuration and good fatigue resistance, in particular PCL/Gel nanofibers showed to be bead-free and with small diameters. Finally, the cellular adhesion on the two sides of the polymeric substrates was analysed through the staining of the nuclei and the actin filaments of A549 and HULEC-5a with DAPI and phalloidin, respectively. Results suggest that cells adhere better on PCL/Gel membrane, as demonstrated in cell viability assay (resazurin) which was conducted to monitor cells metabolic activity inside the device. This thesis work was carried out under the DEFLECT (“Advanced platform for the early detection of not small cells lung cancer”) project, financed by Piedmont Region in the framework of “Health & WellBeing” Platform.

1. INTRODUCTION

1.1 Lung: anatomy and physiology

Lungs are the main organ of the respiratory system; whose primary function is gas exchanging across the alveolar-capillary barrier. Carbon dioxide is taken by red cells from human body cells and it is carried to lung where diffusive exchanging phenomena with oxygen occur. In this way carbon dioxide is eliminated from the body during the exhalation and oxygen can be released through blood to all kind of cells for nourishment [1]. Other pulmonary functions are the maintenance of pH blood, the blood reservoir for lung vasculature and the removal of particles [2].

The respiratory way is divided in two regions. The first one is composed by the extrathoracic part which contains the nasal cavity, mouth, pharynx and larynx, and by the tracheobronchial part, which is formed by trachea, main bronchi, bronchi and bronchioles including terminal bronchioles. The second one is called the alveolar-interstitial region, which contains the alveolar sacs and the alveoli [1].

1.1.1 The conductive tract

This region has a tree-like shape with its branches: it is formed by the trachea which divides into two main bronchi that, at this time, separate into five lobar bronchi, three of them enter in the right lung and two in the left one. The lobar bronchi divide gradually into smaller diameter structures until they reach the bronchioles conformation [1]. Conduct air is the most important function of this part, together with humidity and temperature control. In addition, here is where particles from external air are inhaled and deposited [1]. The pseudostratified layer epithelium is formed by two types of cells ciliated and non-ciliated (Clara cells) from a columnar, in the higher airways, to cuboidal conformation at a lower level [1].

1.1.2 The gas exchange tract

Terminal bronchioles, alveolar ducts and sacs are this section's actors. The alveolar sacs have a grape-like structure (Figure 1.1) with an air volume of $4.5 \times 10^{-3} \text{ m}^3$ and contain in total around 300 million of alveoli, that are the lung's fundamental units, where the principal gas exchange phenomena happen. The total surface area of the alveoli is 150 m^2 and the diameter is about 200-300 μm for each one; this small size guarantees the diffusive gas exchanges because it maximizes the surface area [1]. Exchanges occur at alveolar-capillary barrier's level, which is an air-liquid interface (about 1.1 μm of thickness), composed by alveolar epithelial cells (in contact with air) and capillary endothelial cells (in contact with blood) divided by a basement membrane. The latter consists of fibrils of collagen and elastin with a thickness of about 50 nm [1] [3].

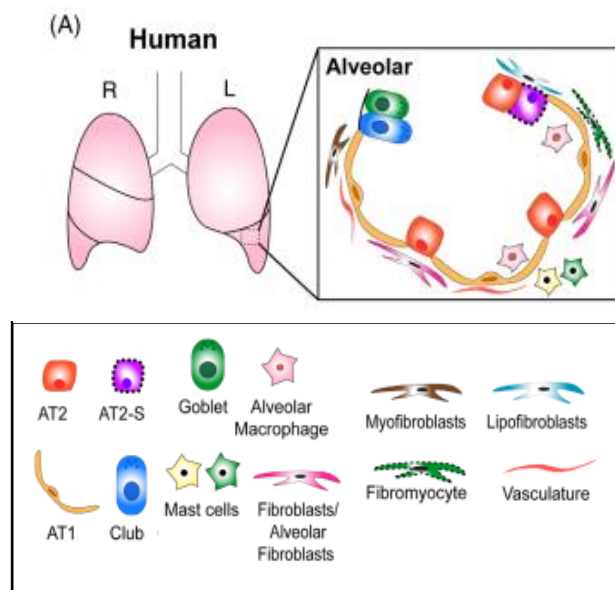


Figure 1.1 Cellular composition of the alveolar-capillary barrier [4].

The main function of this barrier is the transportation of solutes and proteins [5]. Tight junction proteins are present to ensure the integrity of the barrier, like the zonula occludens (ZO-1) which binds the epithelial cells to form the epithelial continuum and the VE cadherin which does the same for the endothelial cells [5].

There are two types of epithelial cells:

- the Type I, that are the more numerous because they cover about the 93% of surface, are flat and squamous, involved in gas exchange and immune response [1].
- the Type II are cuboidal and secrete the surfactant (a mixture of proteins and lipids), which is responsible for reducing surface tension; they compose the 7% of the surface and they have also the role of precursor of type I cells during lung repair [1].

There are other cells in the alveolar barrier such as endothelial cells, fibroblasts, nerve cells, lymphoid cells, macrophages and dendritic cells. In particular, the last two, together with the capillary epithelium and the connective tissue have the role to preventing harmful particles passage into the blood by clearing the surfactant and by removing the pathogens [1].

1.1.3 The mechanical stretching in the alveoli

During inspiration the air-liquid interface is compressed and then released throughout expiration provoking a cyclic mechanical stress to the cells. In a normal lung at rest 10-12 breaths take place every minute (with a frequency of 0.2 Hz) where the tidal volume is about 500 mL [3]. In this condition the linear strain feels by the basement membrane is about 4% and it can be higher during a physical effort, about 12 % and reaches 20% in an unhealthy lung [3]. The Young's elastic modulus in a healthy lung

tissue is about 1-2 kPa and it can reach 16.5 kPa in a pathological condition as in the case of idiopathic pulmonary fibrosis (IPF). On cells surface there are mechanical receptors that feel the stretch and turn it to biochemical signal. Indeed, mechanical stress influences proliferation, differentiation and migration of the epithelial cells [3].

1.1.4 Lung diseases

Lung diseases affect airways, lung tissue and pulmonary circulation and they are classified as obstructive which feature mucus and liquid plug formation, restrictive where the pulmonary volume is reduced and infectious with the presence of pathogens [2]. Respiratory diseases are one of the major causes of death in the world [2]. In fact, lung cancer is considered the leading cause of cancer death [2] because of the metastasis formation and its drug resistance [6]. There are different types of lung cancer such as small-cell lung cancer and nonsmall-cell lung cancer which need to be well treated and controlled, monitoring the metastasis and studying individualized therapies [6]. Chronic Obstructive Pulmonary Disease (COPD) is an obstructive pathology which damages the alveoli walls and the lung parenchyma by oxidative stress. Instead, the idiopathic pulmonary fibrosis (IPF) is an interstitial disease characterized by fibroblast foci and honeycomb regions and which presents an inevitable progression. Another debilitating disease is the acute respiratory distress syndrome (ARDS) which is an inflammatory disorder in which neutrophils, after invading the airways area, release proinflammatory cytokines provoking the breakdown of the alveolar-capillary barrier [4].

So, it is necessary to improve methods and systems for studying how lungs work and what are the principle mechanisms that lie behind pulmonary diseases for discovering and deploying new therapies.

1.2 In vitro organ models

To better understand and investigate the human organ physiology as well as the development and treatment of tissue, different approaches have been tried: *in vivo* models, like animal experiments, and *in vitro* models, such as 2D and 3D systems and, in recent years, microfluidic devices.

The cell type chosen for the *in vitro* studies are taken from isolated tissue, primary culture, or from a continuous cell line, secondary culture. The first one is a heterogeneous ensemble of different cell type but from each isolation only a few numbers of cells can be extracted, and they are, also, difficult to reproduce. Instead, the second one is easy to reproduce, homogeneous and stable but lack of phenotypic differentiation [1].

In lung tissue studies *in vitro* alternative cell cultures are used to model the epithelial barrier, based on the tissue's section to be analysed. The cell lines chosen for the airway epithelial barrier are Calu-3 and the 16HBE14o-, both of them are human origin cells which permit the formation of tight junctions. The BEAS-2B cells are another type of line used for the reproduction of the airway epithelial structure but differently from the others they do not form tight junctions. The alveolar epithelial barrier is replicate by using A549 cells, that originates from human lung carcinoma and differentiate in alveolar epithelial type II cells [1].

In the following paragraphs, the different approaches to organ models are summarized, with a particular focus on lung tissue's studies. At the beginning the most inconvenient model, animal one, is presented, secondary the 2D and 3D systems are evaluated, underlining all the pros and cons of each type. At the end microfluidic devices are discussed with an overview of the lung-on-chip present in the relevant literature.

1.2.1 Animal models

The human body is complex and the reaction to a stimulus involves varying related mechanisms which cannot be fully replicated with *in vitro* systems. For this reason, animal models were introduced and, nowadays, they are used for drug screening and efficacy studies, to assess new therapies [7].

For example, *Carrington et al.* developed a murine model for the analysis of the role of platelets in the pulmonary fibrosis evaluating the lung function reduction and the histological changes. To induce fibrosis in mice, Intranasal administration of low doses of bleomycin was performed over a period of 7 days and it was found that platelet depletion leads to a fibrosis reduction and a decrease of function changes [8].

Instead, *You et al.* developed a mouse model for lung squamous cells carcinoma (SSC). They treated a 6-8-week-old mouse with N-nitroso-trischloroethylurea (NTCU), topically (by skin painting) for 7 to 9

months to induce neoplastic lesions. They succeeded to reproduce all the neoplastic stages of squamous cell carcinoma from bronchiolar hyperplasia to invasive SCC, demonstrating the importance of this model in lung cancer chemoprevention. Indeed, an antitumor B (ATB) was tested in this mouse lung model proving that ATB operates as a chemoprotective agent from the cancer progression. Whereas, the green tea can prevent the passage from the hyperplastic stage to the malignant stage [9].

1.2.1.1 Limitations

The animal trials bring with them some scientific [10], ethic and economic complaints [11]. In fact, drug tests which give good results on animals most of the time fail on human beings [11]. In addition, animal models are not capable to replicate human diseases or to correctly predict the effects of toxic pathogens on humans [10]. This is due to the genetic differences between the two species and to the different responses at the external stimuli [10]. Moreover, the use of living beings for scientific tests is criticized by society which is more and more on the path of ethical and sustainable choices, not to mention that conduct these trials is expensive because animals require facilities to house and care [12].

1.2.2 In vitro 2D models

Submerge conditions are typically used to model the lung epithelium. The protocol requires that cells are cultured on plastic wells or flasks and covered with medium which releases nutrients and growth factors [3]. However, through the years, an air-liquid interface (ALI) method was performed, by which epithelial cells are cultivated on a porous membrane (usually polyethylene terephthalate, PET) with cells exposed to the air on the apical side and to the medium on the basal surface (Figure 1.2) [3]. The ALI conditions are more physiologic than the submerged ones because they allow to polarize the epithelial cells, mimicking the epithelial barrier's function and to cultivate other cell lines in a co-culture system, like the endothelial cells on the basal side [3].

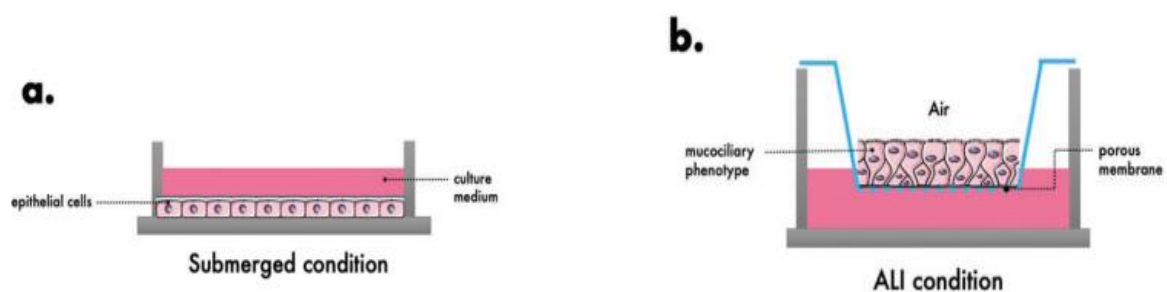


Figure 1.2. In vitro lung cell culture systems: a) under submerged conditions b) under ALI condition

There are different studies which propose a comparison between these two methods. For example, *Grainger et al* cultured Calu-3 cells on liquid covered system (LLI) and on air-liquid interface system (ALI) analysing differences on morphology and permeability. Analysis by transmission electron microscopy (TEM) shows that cells under LLI culture are assembled in a monolayer, differently, ALI culture exhibits a pseudostratified layer with more columnar cells. For both systems, tight junctions and apical microvilli were observed. The transepithelial flux of fluorescein-sodium and the variation of molecular weight dextrans labelled with fluorescein isothiocyanate were employed to assess the barrier's permeability showing a lower transportation in LLI culture [13]. Likewise, *Kreft et al* investigated a Calu-3 cells culture on a LLI and an ALI bringing back similar results. In fact, ALI model results to be more resemblant with the human lung epithelium displaying a pseudostratified columnar epithelium instead of just cuboidal like seen in LLI models (Figure 1.3). Moreover, microvilli are more numerous and elongated in ALI system, while tight junctions are present in all models, as seen by electron microscopy. As well as cells covered with medium exhibit a lower permeability then the ones with air contact, as shown in dextran permeability studies [14].

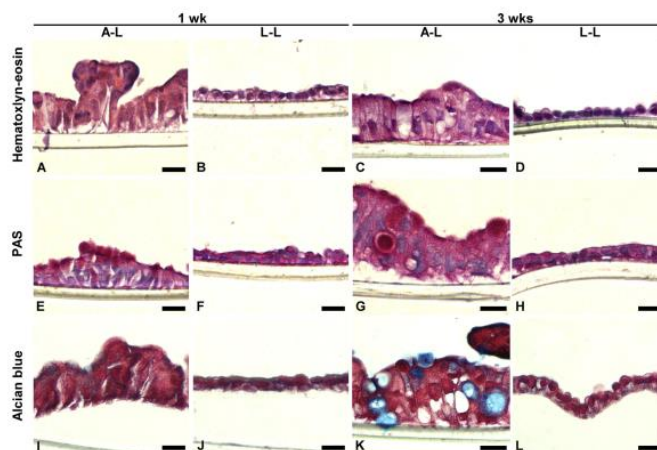


Figure 1.3. Cellular tests conduct by *Kreft et al* which demonstrate a monolayer formation after submerged conditions and a pseudostratified under ALI conditions after 1 week and 3 weeks of culture

In other studies, cells are cultivated only on Transwell Inserts, which allow to create an ALI system thanks to the porous membrane, for analysing epithelial resistance and barrier function [16]. *Wu et al* characterized the alveolar epithelium using A549 lung adenocarcinoma cells seeded on transwell insert coated with collagen (Figure 1.4). The TEM revealed that in ALI culture, compared with the submerged one, cells were more compacted with the presence of junctions and mucus. Throughout immunofluorescent staining assay, the higher expression of specific markers, AQP-5 and TTF-1, of the alveolar epithelial type I cells in ALI culture was demonstrated as compared with the submerged

culture. Moreover, the epithelial tight junction protein ZO-1 and the alveolar epithelial type two cells marker, SP-C, were detected. All these genes displayed their maximum expression after two weeks of ALI; this evinces that 1-2 weeks is the best range of time to cultivate the A549 cell line for maintaining the alveolar properties. In addition, Scanning electron microscopy (SEM) showed that submerged culture had smooth surfaces on the contrary cells under ALI conditions exhibited rough surfaces [16].

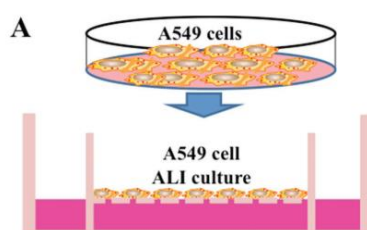


Figure 1.4. Scheme of the cell culture in the analysis of Wu et al.

Transwell systems gives, also, the possibility to co-culture different cell types for better simulate the physiological function, like *Dekali et al* did in their study that aims to analyse non-functionalized (51 and 110 nm) and aminated (52 nm) fluorescent polystyrene (PS) nanobeads translocation through the membrane. The cell lines chosen by this paper are: pulmonary epithelial cells (Calu-3 cell line) and macrophages (THP-1 differentiate cells) cultivated on the apical side and pulmonary endothelial cells (HPMEC-ST1.6R cell line) on the basal side of a microporous polyester membrane. They found that macrophages internalize nanoparticles like they do in vivo by affecting barrier integrity. In conclusion, this system has good barrier properties suitable for studying NP transportation, but only small non-functionalized nanoparticles can reach the basal side underlining that the membrane do not perform a neutral role in the NP passage and need to be improved [17].

1.2.2.1 Limitations

Nevertheless, 2D systems are low cost and easy to replicate technique, with well establish protocols, they exhibit different disadvantages. Indeed, they cannot reproduce a 3D environment, such as the cell-cell or cell-extracellular matrix (ECM) interactions, with a dynamic setting. Moreover, concentration gradients do not exist in this kind of analysis and nutrient and drugs can be release with a uniform concentration. So, 2D models do not allow to best describe the physiological environment and its response to the stimuli [18].

1.2.3 In vitro 3D models

Considered all the 2D system drawbacks a 3D models are needed because they allow to better mimic the cellular environment complexity [19], such as the cell-cell and cell-ECM interactions [18],

reproducing the tissue physiological and pathological function, such as behaviour and characteristics of cancer [7]. In addition, they describe drug response more accurately than 2D models, in fact they could be a possible alternative to animal models [18] [19] [7].

They are divided into different categories: spheroids and organoids, tissue-engineered models or scaffolds and hydrogels. In the following all these groups are described reporting the relevant literature for lung.

1.2.3.1 Spheroids

Spheroids are cellular spheres between 20 μm to 1 mm of size, that spontaneously aggregate. There are several methods for shaping them, such as hanging drop method, stirring or incorporating cells into hydrogel matrices, instead, scaffolds are not needed for their formation [7].

Spheroids can be used for rapid and high-throughput analysis and in research for modelling tumor [7], like *Xu et al.* did for lung cancer [20]. They examined the doxorubicin radiosensitivity in non-small cell lung cancer spheroids, A549 cell line, embedding doxorubicin into Poly(ethylene glycol)-poly(ϵ -caprolactone)-Pluronic P105 (PEG-PCL-Pluronic P105) micelles where spheroids are incubated with drug loaded micelles and irradiated. By confocal laser scanning microscopy and quantitative flow cytometry, it is found that micelles improve cellular doxorubicin accumulation and decrease its release. By colony forming assay it is seen that cells treated with radiation plus doxorubicin-loaded micelles died more than the ones treated with only radiation, showing the radiosensitivity property of doxorubicin-loaded micelles. In conclusion researchers demonstrate that incorporating doxorubicin into micelles enhances its anticancer effect [20].

Spheroids have some limitations; in fact, it is very challenging to control their size during their formation and they cannot reproduce angiogenesis and host immune reaction [7].

1.2.3.2 Organoids

An organoid is defined “as multicellular, stem-cell-derived systems in which cells spontaneously self-organize into properly differentiated, functional cell types that resemble in vivo counterparts and recapitulate part of the key features of the organ” by *Lancaster et al.*[21]. This structure can be cultured under submerged condition or embedded in a hydrogel matrix [21] and mechanical cues could be integrated, such as fluid shear stress, compression, and tension [10].

There are three types of cell lines chosen for the organoid development: embryo stem cells (ESC), pluripotent stem cells (iPSC) or primary stem cells from adult lung [10] [21].

For instance, *Miller et al.* employed pluripotent stem cells to create a lung organoid. First, they created some foregut spheroids from human pluripotent stem cells (hPSCs) which are left to differentiate in

two kind of lung organoids, a human lung organoid and a but tip progenitor organoid. The first one has an airways-like epithelium surrounded by mesenchymal and epithelial cells which express alveolar markers (AECI and AECII), that is perfect for studying the fetal lung development. The second one contains a population of cells like human fetal lung bud tip progenitors which can accomplish the task of precursor of epithelial cells [22].

Organoids are often used for disease model like *Wilkinson et al.* have done, who developed a lung organoid for idiopathic pulmonary fibrosis with the aim of finding a personalized drug therapy. To form the organoids, they inserted, in a rotative bioreactor, collagen functionalized alginate beads together with fetal lung fibroblasts and after that, to induce the hallmarks of IPF, shaped organoids are treated with an exogenous transforming growth factor- β 1 (TGF- β 1). This implies an increased level of collagen1 and α -SMA in treated organoids like happens in patients affected by IPF. Other cell lines could be added after the fibroblast adhesion to the beads but only with the presence of fibroblasts organoids are created [23].

Like spheroids, also organoids are difficult to control in size and it is challenging to maintain cells in position for analysis [19].

1.2.3.3 Scaffolds

Scaffold are a support for seeding the cells which structure aims to mimic the ECM's design for generating an organ or tissue [7]. Two kind of scaffolds are outlined in the literature: decellularized and polymeric scaffolds.

Decellularized scaffolds

They are created by removing all the cellular and nuclear materials but preserving the ECM structure from animals or human organs. After that scaffolds are re-cellularised with primary mesenchymal stem cells or human lung donor stem cells [15] [24].

For example, *Gahedi et al.* used iPSCs derived from the alveolar epithelium for re-cellularising rat or human adult lung. They described a protocol that allows to obtain definitive endoderm (DE), anterior foregut endoderm (AFE) and finally AETI and AETII cells from iPSCs. The cells seeded in repopulated scaffolds are cultured in a bioreactor where vascular perfusion and liquid ventilation occur. Type I markers are not detected in scaffolds even if they are able to proliferate in there. For this reason, cyclic mechanical stimuli are needed [25].

The vascular network differentiation and survival of cells is difficult to obtain with re-cellularized systems. Furthermore, ECM matrix could be damage by the aggressive decellularization reagents like detergents [15] [24].

Precision-cut lung slices

PCLS is a method for creating microslices of tissue using a vibratome [10]. The lung tissue is infused in heated liquid agarose and then solidified. This sequential process allows to maintain the alveolar structure when tissues are cut [4]. The tissue used is taken from a healthy donor, diseased lungs or by explanting lungs from mouse embryos and it could be important for studying tissue microarchitecture and features, also in diseased ones [3][10]. For example, human- idiopathic pulmonary fibrosis (IPF)-derived PCLS were employed to study AT2 cells behaviour and activation in fibrosis patients [4].

There are some limitations for this technique. The first one regards donor variation due to differences in genetic backgrounds [4], that can create an experimental variation, highlight the importance of founding personalised therapies [4] [10]. Moreover, this type of organ is difficult to obtain and they are subjected to contamination [10].

Polymeric scaffolds

Synthetic and natural materials are employed to fabricate polymeric scaffolds. There are different techniques used for fabricating the scaffolds. One of the most used is the electrospinning that permits the production of nano-porous fibrous mats which mimic the architecture of physiological ECM. Nowadays, rapid prototyping manufacturing technique emerged due to the need to reproduce complex system [7][24][26].

Shigemura et al. fabricated a polyglycolic acid sheet for pulmonary emphysema using adipose stromal cells. These cells secrete a lot of regenerative factors like hepatocyte grow factor which seems to be beneficial for remaining emphysematous tissue. Seeded sheet were used to cover the cut after lung volume reduction surgery in rat. It was observed that after one week from the implantation vascular and alveolar regeneration occurred faster than in lung subjected to only surgery [27].

1.2.3.4 Hydrogels

Hydrogels are three-dimensional systems used to develop an *in vitro* artificial ECM reproducing the three-dimensional (3D) microenvironment of native tissue. [25] They are used to encapsulate cells and ECM signals with the function to promote cell proliferation, angiogenesis and wound tissue expansion [7]. Collagen, alginate and Matrigel are the most used gel materials in constructing 3D models. This gel could be associate with microfluidic devices, to create a multicellular system without transport limitation and scaffolds [7].

De Hilster et al. describe an ECM hydrogel from normal and disease lung (COPD and IPF) which replicate the organ mechanical properties. To do this the lung was decellularized, reduced in powder and then transformed in a hydrogel and following the stiffness and viscoelastic properties are evaluated demonstrating that this hydrogel could simulate the lung environment [28].

Bioprinting

Bioprinting is a bio-additive manufacturing layer-by-layer technique which consists in deliver directly cells and bioactive matrix components building a 3D construct [20]. Advantages of bioprinting are the possibility to control temporally and spatially the material deposition and to replicate standard and reproducible healthy and pathological and cellularize models [29].

Horvat et al. used bioprinting to model the alveolar air-liquid interface delivering epithelial (A549) and endothelial (EA.hy926) cells divided by Matrigel acting as the basal membrane (Figure 1.5). First of all they analysed the differences between mono and co-culture manually seeded cells and printed cells pointing out that both mono and co-culture printed cells form a confluent thin monolayer instead of growing in clustered multilayers like it has been seen in manually seeded cells. Moreover, co-culture printed cells shows cell-cell interactions that lack in manual approaches. In conclusion, printed cells show a high viability and a tighter layer than cells seed with classic methods [29].

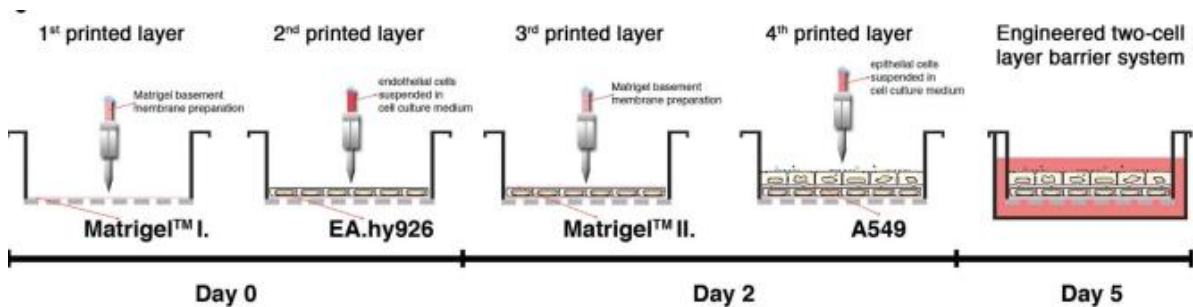


Figure 1.5. Schematic illustration of the bioprinting process

1.2.3.5 Limitations

Some drawbacks of 3D models are to be recorded, among them the lack of dynamicity and perfusion, the absence of mechanical stimuli, such as the flow shear stress, compression or traction, and the difficulty to carry out real-time analysis [18] [19]. In addition, a lot of systems miss of a multiscale architecture and a tissue-tissue interaction like interaction between the vascular endothelium and the surrounding tissue [19]. All these disadvantages underline that 3D models cannot describe a complex environment, like human organs are, with an ensemble of cells that communicate among them receiving biochemical and mechanical stimuli. For these reasons, microfluidic devices are necessary because they allow to mimic a physiological or pathological tissue bringing back the mechanical and chemical features.

1.3 Organ-on-chip

1.3.1 Introduction

An organ-on-chip is a microfluidic device whose purpose is to mimic the fundamental unit of an organ throughout a low cost and reproducible process in a controlled environment [12]. Three principal points should be considered: the 3D architecture of the tissue of interest, the tissue-tissue interface and the mechanical/ biochemical stimuli [30].

The simplest system of this chip is composed by a single chamber, containing a single cells culture, which is perfused by a combination of micrometric channels [19]. The cells, inside the microfluidic device, can be solicited mechanically, by applying a cyclic stress, a compression and the fluid flow shear stress, and biochemically with soluble factors and nutrients [18].

1.3.1.1 Advantages and applications

The microfluidic devices have countless advantages that allow them to become a future alternative to the animal models and the classical *in vitro* systems [31].

Indeed, the physiological micro-environment with a 3D architecture can be simulated inside the chip by seeding different cells lines and by promoting the cell-cell interactions [19]. Furthermore, rapid and high-resolution real-time analysis may be carried out due to the usage of optical transparent materials. The samples require for the tests are less than in the classical methods, so these devices have the benefit of being more economic [32] [30] [18]. The fluid passage is dynamic through the use of syringe pumps that ensures a controlled flux with the diffusive gradient of the solutes [18].

Via OOCs drug tests can be implemented by investigating drug efficacy and resistance and the its transportation. In addition, these devices allow to model a disease (like lung cancer) and make a diagnosis of the same with the future intention of evaluating a personalized therapy by using human-induced pluripotent stem cells (hiPSCs) [31].

In addition, to achieve more biomimetic device, it is possible to select tissue engineering techniques for employing materials that better mimic the ECM-like structure than polydimethylsiloxane (PDMS) [26].

1.3.2 Microfluidic device fabrication techniques

1.3.2.1 Materials

To select the more suitable material for the application of interest, there are different characteristics to evaluate: the biocompatibility, the sterilization method, the physicochemical properties and the cost [33]. In particular for biomedical applications a material should be optically transparent for microscopic analysis which allows to observe the cell culture, gas permeable to ensure enough oxygen to the cells, chemically and thermally resistant for avoiding material damage and have low absorption to avoid the alteration the tissue response to drugs [33].

Over the years, several materials have been employed in microfluidic chips, the most commonly used are glass, silicon and polymers.

Inorganic materials (glass and silicon)

These materials have a variety of good features for which they have been chosen for microfluidic applications. In fact, glass is optically transparent, chemically inert, electrically insulating and has a low fluorescent emission, whereas silicon has a high resistance to organic solvents, a high thermo-conductivity and it is an easily available source [34] [35]. Despite that, their hardness and the high cost of fabrication required put some limits on their application; in particular, for biomedical scopes, the lack of permeability does not allow a long-term cell culture. In addition, silicon is opaque, so this can hinder analysis with the microscope [34].

For all these reasons the need to use other materials arise.

Polymers

They can be divided into three groups according to their physical properties.

1) Thermosets are liquid or solid at room temperature and if they are heated or irradiated, they will start to cross-link. The curing process is irreversible even if they are heated again. Two main examples of this kind of polymers are the SU-8, a photoresist usually employed as a master, and the polyamide [36].

2) Thermoplastics are processable around glass transition temperature (T_g) because they soften at that temperature. Differently from the thermosets they can be reshaped more times after the curing process which then it is not irreversible. The most famous are poly(methyl methacrylate) (PMMA), polycarbonate (PC), polystyrene (PS), polyethylene terephthalate (PET), and polyvinylchloride (PVC) [34] [36].

PMMA

It is a thermoplastic transparent with a T_g of about 105°C. Its production has a lower cost compared to the one of glass and silicon, and it is easy to form, in fact all the classical technologies of fabrication can be employed, like laser ablation, hot embossing and injection moulding. The polymer has good mechanical, optical and chemical properties but it is hydrophobic, because of the lack of ionizable groups, so surface modification strategies have been explored, such as covalent modifications [35].

3) Elastomers have longer chains compared to the other polymers and physically entangled, in fact if they are elastically deformed, they can return to the original shape. In addition, they have a low cost, an easy handling and a high permeability to carbon dioxide and oxygen that make them a perfect material for cells applications [36].

PDMS

PDMS is composed by a polymeric chain with repeating Si-O groups and CH₃ groups on the side. It is the most used elastomer for the microfluidic device fabrication that can be made by a process of crosslinking and polymerization [35]. This last one is enhanced by heat treatment; in fact, it can be treated with temperatures from 60°C to 90°C for 1h-4h to complete the curing and achieve the final product [35]. PDMS has a variety of good properties that make it an optimal material for the fabrication microfluidic devices. It is chemically inert, thermally stable, gas permeable, easy to handle and to product [37]. In addition, its fabrication is cheaper than the silicon one and it can be bonded to a wide range of materials [35]. Moreover, it is optically transparent, non-fluorescent, biocompatible and safe; so, it is suitable, in particular, for biomedical applications [37].

1.3.2.2 Fabrication techniques

There are two types of fabrications techniques photolithography based and replication based. In the first one light is used to reproduce the pattern of interest on photosensitive material, in which the resolution depends on the wavelength applied [35]. In addition, it demands high cost because it needs the utilisation of cleanrooms [38]. The second one, instead, require a mold fabrication on which a polymer is poured [35]. In this section the technique employed in this thesis project are examined.

A) Soft lithography

This technique allows to reproduce the desired pattern on polymeric photomasks, masters, and molds with a high resolution and complex design.

The most used material in this technology is SU-8 that is an epoxy-based negative photoresist which is employed for the fabrication of the master. In brief, soft lithography includes the deposition of the

polymeric material (SU-8) on glass or silicon substrates through a spin coater, which permits the homogeneous and controlled spreading of the material on the surface. After that, the polymer is exposed to UV light through a mask; this last step is preceded and followed by a thermal treatment (called prebake and post bake, respectively), and finally the geometry is developed on the master. Because SU-8 is a negative resist during the exposure the parts that encounter the UVs become rigid and insoluble, instead the areas not touched by the light are then removed. The final master is subjected to silanization in order to avoid its adhesion to the PDMS stamp that, subsequently, is poured over the SU-8 mold and cured (Figure 1.6) [38]. In conclusion, soft lithography is a low-cost process with the capacity to design complex pattern and, also, with a high accuracy of replication and the possibility to reuse several times the master [38].

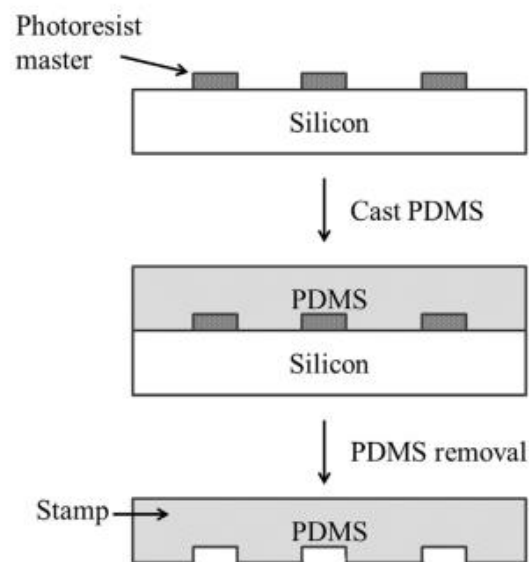


Figure 1.6. The figure describes graphically the soft-lithography technique

B) Laser ablation

It is a rapid and easy reproducible technique in which a high intensity laser beam is employed for writing the wanted design on the master surface by evaporating the substrate material at the focal point. To reproduce the geometry, the master can be exposed to the energy beam thanks to a mask or the laser beam can move directly along x and y directions. Typically, the type of laser chosen for this application is a pulsed one but the interaction of the laser with the master implies a change of surface chemistry. So, to get over this critical point, it is selected a CO₂ laser beam as an alternative, which has continuous beam that cuts the material. Laser ablation is a good way to design on thermoset and thermoplastic polymer like PMMA on which pouring elastomers [36].

C) Replica molding

A polymer, generally PDMS, is poured on a mold, made of silicon or photoresist like the SU-8 (produced, usually, by photolithography), where it let be cured. When the elastomer is crosslinked, the replica is peeled off the mold and it is bonded to another PDMS replica or a glass slide to form a closed design. This technique produces high resolution replicas and 3D geometries. Furthermore, the devices have all the good properties of PDMS, such as optical transparency and biocompatibility, that make it suitable for biomedical applications. In addition, it is a simple technology, versatile in design, cheap and rapid. However, some defects may be encounter in replicas due to the removal of the polymer from the mold [39].

1.3.3 Lung-on-chip

The complex features and functions that can be replicate in the lung-on-chip allow them to succeed as preclinical tools for research and medicine in respiratory field [40]. In fact, these devices make it possible to mimic the lung anatomy of the section of interest at true scale, in particular the air-liquid interface (ALI barrier) by developing a membrane-on-chip. The second hallmarks that should be reproduce in the lung-on-chip is the respiratory stress which affects cells cyclically [41]. The alveolar sac expands when external air enters the lung and retracts when the air is pulled out. This implies a 3D cyclic stress, usually imposed with a 10% of deformation and frequency of 0.2Hz (because 10/12 cyclic breath per minute are counted) [42]. Furthermore, the shear stress caused by the blood perfusion upon the endothelium is mimicked by the cell culture medium flowing along the microchannels, which guarantees the supply of nutrient and grow factors [41]. Moreover, these microfluidic devices can recreate several pathological conditions by controlling the different values of airflow stress and flow shear stress. Therefore, they can be exploited to evaluate the disease behaviour [41].

In the following, some examples of literature work which developed lung-on-chip devices are reported, divided by application.

1.3.3.1 ALI barrier

These devices reproduce the alveolar-capillary interface with the objective of evaluating the barrier structure features and permeability [43]. To do that researchers designed OOCs formed by two chambers split by a PDMS porous membrane for, simulating the basal membrane of lung. The epithelial cells are seeded on the top of this membrane whereas the endothelial cells are cultured on the basal side and they are left to grow under air-liquid conditions, in which the culture medium, that perfuses through the channel placed on the basal chamber, nourishes both endothelial and epithelial cells. In addition, it is possible to replicate the mechanical stress by applying vacuum which has the task of stretching the PDMS membrane equipped with cells. This cyclic stress is important to investigate the cell response and the barrier permeability [43].

Medium throughput breathing human primary cell alveolus-on-chip model by Stucki et al. [42].

Goal

Mimicking an in vivo-like environment seeding human primary alveolar type I (ATI) and type II-like (ATII) epithelial cells and lung endothelial cells on a circular PDMS membrane by submitting cells to a three-dimensional cyclic stress.

Microfluidic device design and fabrication

The lung-on-chip consist of two parts: fluidic and pneumatic. The first one is formed by two layers with a membrane (3.5 μm of thickness) sandwiched between them; the top layer features a circular well

that leaves the epithelial cells completely open to the atmosphere whereas the bottom layer contains a channel dedicated for the medium passage. The second one presents two valves and another PDMS membrane called microdiaphragm (40 μm of thickness) which is needed for the mechanical actuation. In fact, the device has two operation modes (Figure 1.7): the medium exchange mode on which the two valves are opened and the fresh medium can run; the breathing mode on which the two valves are closed and the microdiaphragm is cyclically deflected by an electropneumatic setup, this deflection is transferred to the thin membrane due to the incompressibility of the fluid. Both the fluidic and the pneumatic part are produced by soft lithography.

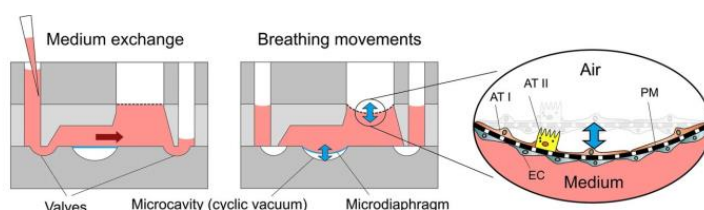


Figure 1.7. Scheme of the two operation modes

Results

The Primary human alveolar epithelial cells (hAEpCs cells) are seeded on the membrane under static and submerged conditions for two days when they reach the confluence and the ALI is performed. After three days of ALI, cells display high expression of AT I cell marker caveolin-1 and tight junction protein Zo-1, that is a prerequisite for cell differentiation on the chip. The co-culture (VeraVec cells seeded on the basal chamber and hAEpCs cells on the apical) has been performed for 22 days keeping intact the integrity of the barrier, assessed by the transepithelial electrical resistance (TEER). This is measured revealing that it increases for 7 days, after which it reaches a plateau. Rather, the shear stress of the medium exchange was calculated via mathematical model determined to be 5×10^{-1} dyne cm^{-2} an order of magnitude smaller than the one founding in the human vessels (3^{-10} dyne cm^{-2}). Therefore, a viability test is assessed using presto blue assay that asses the viability of cells until the day 6 (when the experiment was stopped). Moreover, the viability in dynamic conditions has been higher than in static conditions. Instead, permeability tests showed that the permeability of a small hydrophilic tracer, FITC-sodium, and of a macromolecule mimetic, RITC-dextran, increase when cells are stressed for 72h cyclically.

Conclusion

This microfluidic device can be an important tool for drug analysis and personalized medicine applications; in fact, it is capable of mimicking and valuing the alveolar barrier.

1.3.3.2 Drug screening

Thanks to their properties, lung-on-chip devices can be an excellent way to discover new therapies for disabling diseases, to produce a simple, high-throughput, sensitive and time-efficient devices which need of low samples for carrying on the investigation [43].

A primary human lung alveolus-on-a-chip model of intravascular thrombosis for assessment of therapeutics by Jain et al. [44].

Goal

To study the lung responses during an inflammation-induced thrombosis showing the fundamental role of the epithelium in the inflammation and evaluating the effects of an anti-thrombotic therapeutic.

Microfluidic device design and fabrication

It is composed by two layer both containing a channel, the upper for the air passage and the lower for the culture medium perfusion, separated by a PDMS membrane on which cells (human umbilical vascular endothelial cells (HUVECs) and primary human alveolar (mixture of type I and II) epithelial) are seeded (Figure 1.8). The PDMS replicas are produced by soft lithography.

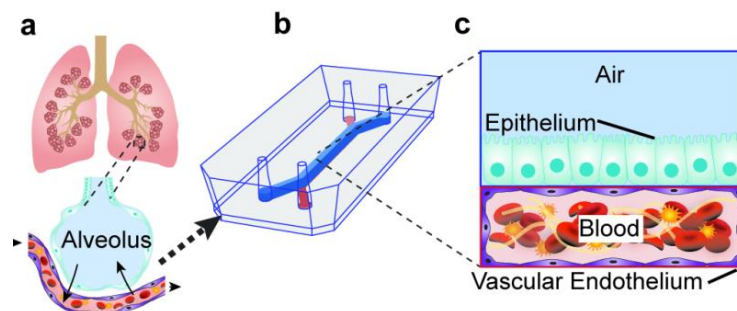


Figure 1.8. The figure shows how the alveolar-capillary barrier is mimicked in this microfluidic device

Results

This chip allows to maintain cells alive for 12 days under laminar flow showing cell-cell interactions, like ZO-1 in the epithelium and VE-cadherin in the endothelium. In addition, the device outlines the platelet dynamics and shape discovered in thrombus conditions in vivo. In fact, stimulating the endothelial cells with the inflammatory cytokine and the tumour necrosis factor-TNF- α before the blood perfusion, a platelet recruitment is seen followed by a thrombus formation with a tear drop-like morphology. Throughout a tracer dye it is shown that the barrier has a low permeability. In fact, adding the TNF- α to the epithelial chamber in doses more and more high resulted in a dose-dependent increase in vascular permeability. So, TNF- α has a pro-inflammatory effect resulting in the activation of endothelium and in thrombus formation. Moreover, lipopolysaccharide (LPS) endotoxin is added to

the alveolar section provoking a vascular leakage and increasing the barrier permeability. The effect of parmodulin-2 (PM2) that is a protease activated receptor-1 (PAR-1) inhibitor, which mediate tissue inflammation, is analysed, finding that this antithrombotic therapeutic exhibits a cytoprotective and antithrombotic activity by decreasing the thrombi formation and the permeability.

Conclusion

For all the evidence seen before, this chip stands as an ideal candidate for testing new anti-thrombotic drug and therapy with the future perspective of seeding cells directly obtained from biopsies in order to use lung cells differentiated from induced pluripotent stem cells.

1.3.3.3 Toxicological studies

Nanoparticles are involved in this kind of studies where their transportation from the apical (alveolar) side to the vascular chamber is evaluated. Since the toxic effect of the nanoparticles increase when the breathing motion is implemented, the importance of the mechanical stimulation in lung research is demonstrated. So, lung-on-chip could be used for toxicity test replacing the animal models in the near future [43].

Reconstituting Organ-Level Lung Functions on a Chip by Huh et al. [45].

Goal.

reconstructing a microfluidic device that encloses the principle features of the alveolar-capillary barrier, the air-liquid interface and the respiratory cyclic stress, and examining the responses to bacteria, inflammatory cytokines and nanoparticles.

Microfluidic device design and fabrication.

the device is composed of two layers; both present a central channel (for the air in the upper layer and for the medium in the lower layer) and two side channels for the vacuum application. A PDMS porous membrane separates the two chambers forming a layered chip. The side channels are connected by silicon tubes to a vacuum pump controlled by a software that allow the mechanical stretching of the membrane (Figure 1.9). Soft lithography was used to produce the replicas.

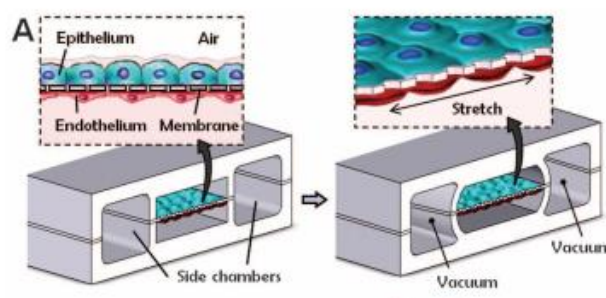


Figure 1.9. Representation of the lung-on-chip function

Results.

the epithelial cells (NCI-H441) can remain alive for a prolonged time (more than 2 weeks) after the air-liquid interface is assessed (on day 5), increasing the surfactant production and the electrical resistance (that demonstrates the tight junction formation and the barrier integrity). The mechanical application instead produces an alignment in the endothelial cells (EGM-2MV human lung microvascular endothelial cells).

By incorporating immune cells in the medium there is a release of cytokines by the epithelial cells and by adding the TNF- α in the alveolar microchannel the endothelium is activated increasing the expression of intercellular adhesion molecule-1 (ICAM-1) and promoting the human neutrophils adhesion. Moreover, it is evaluated the bacterial response by integrating in the apical side the Living Escherichia coli bacteria constitutively expressing green fluorescent protein (GFP) and showing the endothelium activation. For toxicology analysis, 12 nm silica nanoparticles have been used and introduced in the epithelial side demonstrating the negative effect on the endothelium that increases the expression of ICAM-1, observed when breathing motion is implemented. In fact, silica nanoparticles and carboxylated quantum dots, in combination with mechanical stimulus produce an acute inflammatory condition in the lung shown by the ROS levels rise. Whereas this event it is not seen with nanoparticles made of other materials.

Conclusion.

This microfluidic device is a good tool for studying various aspects and behaviours of the lung providing a low-cost alternative to animal models and in vitro studies for drug and toxicologic analysis.

1.3.3.4 Disease modelling

Here, the lung disease investigated with the lung-on-chip are described.

Lung cancer

The tumor-on-chip can be used to explore new therapies and drugs for examining the efficiency and sensitivity; for example, nanotherapeutics have been considered in recent studies. In addition, individual parameters can be tested to choose the better treatment for each patient [43].

Hassel et al. developed an organ on chip where they seeded human non-small cell lung cancer (NSCLC) and they studied the response of the tumour to Tyrosine Kinase Inhibitors (TKIs), an anti-cancer drug. They showed how the breathing motion suppresses the growth and invasion of the tumor cells into the endothelial side and how without mechanical stress tumor cells become resistant to drugs [46].

Polmonary edema

Edema is a condition which occurs due to vascular leakage where the vascular fluid accumulates in the alveolar space [2].

Huh et al. investigated this condition that comes out in cancer patient treating the vascular channel with the interleukin-2 (IL-2). Results displayed how the combination of IL-2 and the cyclic stress increased the vascular leakage. In addition, perfusing fibrinogen and prothrombin with IL-2 causes the formation of in vivo-like fibrin clots [47].

Asthma and COPD

Benam et al. developed a device composed of mucociliary and bronchiolar epithelium and vascular endothelium with immune cells circulating in the fluid flow to investigate the inflammatory process and the therapeutic response in asthma and COPD. By perfusing interleukin 13, a mediator of allergic asthma, an increase of goblet cells and inflammatory cytokines and a decrease of the cilia beating frequency are shown. To mimic the inflammatory response cells are exposed to polyinosinic-polycytidylic acid (Poly I:C), a viral mimic that implies the secretion of pro-inflammatory cytokines. This chip allows to evaluate the synergic effect of epithelium and endothelium in the inflammatory disorders [48].

Cystic fibrosis

Bacteria colonize lung provoking inflammation and failure of the respiratory capacity [43].

Skolimowski et al. developed a two-chambers chip with a membrane in the middle, on the top of this membrane an alginate hydrogel, which mimic the mucus, is formed whereas on the bottom there is the Calu3 cells culture. *P. aeruginosa* bacteria are added on the top side to produce the biofilm in the hydrogel. An antibiotic is inserted in the medium flow in the bottom channel to analyse the efficacy of the treatment [2].

Liquid plug

Mucus plugs are associated with the pulmonary disease like COPD, asthma and edema but also in patients that need artificial ventilation during a surgery and prevent gas exchanges and air flow. During inspiration the liquid plugs are pushed along the airways leads to airway rupture and reopening that cause epithelial injury [2].

Epithelium damage and protection during reopening of occluded airways in a physiologic microfluidic pulmonary airway model by Tavana et al. [49].

Goal

Analysis of a monolayer epithelium response at liquid plugs propagation.

Microfluidic device design and fabrication

The device is composed of two PDMS layers with a porous membrane between the two. Furthermore, in the top layer are present a series of channels for air and liquid passage for the formation of the plug (Figure 1.10). The layers are produced by soft lithography.

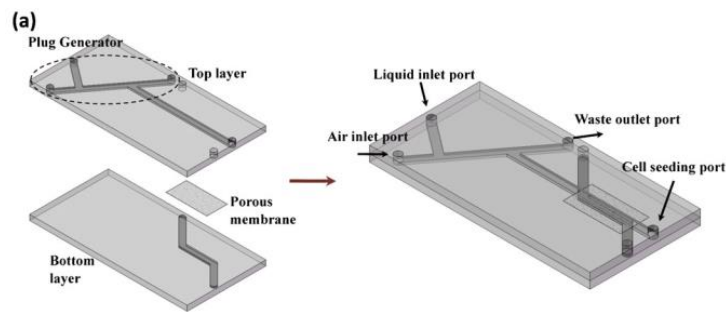


Figure 1.10. Schematic diagram of the microfluidic device

Results

A549 are seeded on the top of the membrane leaved in submerged culture until they reach the confluence (after 3 days), when ALI is created. During the first 4 days of ALI, TEER has increased, demonstrating the tight junctions formation; on day 4, phosphate buffer saline plug propagation started generated plug every 30 second with a speed of 3mm/s. Cell viability tests showed a good vitality after the first four days when liquid plug where not yet propagated, instead vitality after 3 days of liquid plug propagation decreased significantly. The same results can be detected for immunostaining of tight junction which is clearly decreased after 3 days of plugs. Moreover, they discovered that surfactant protects from plug injury producing a protective layer.

Conclusion

This is a good model to investigate the surface tension cause by lung disease. It can be used to studies therapy of surfactant replacement for treating ARDS.

Personalized medicine

Lung-on-chip can be employed in the future for developing new therapies based on the individual patient cells. Using specific parameters picked up from the patients or group, researches can find the perfect treatment or chemotherapy for each individual enhancing therapy results [43].

1.4 The alveolar-capillary basement membrane for ALI culture

1.4.1.1 Membrane properties

The membrane used to mimic the lung barrier should have the same characteristics of the native one (Table 1.1). Elasticity is the most important characteristic of the membrane because it must endure to the cyclic mechanical stress between 10% of deformation, in case of normal lung tissue model, to 20%, in case of pathological conditions [3]. Additionally, wettability is a relevant surface property which should be high (contact angle under 70°) because hydrophilicity is required by cells for their growth and proliferation [3]. Moreover, also geometrical features must be considered, like porosity and thickness since they are significant for creation of cell-cell interactions and transportation of biomolecules. The physiological basement membrane has 0.62 μm of thickness and pore diameter lower than 2.5 nm. Instead, in the literature the values chosen for the pore diameter are about 3-10 μm , that allow to forming the epithelial-endothelial interactions, and for the thickness 10 μm , because lower values are difficult to manage but higher thickness carries an increased resistance to the mechanical stress and lacks to mimic well the diffusive exchanges [3].

Parameter	Value
Stiffness of human alveolar tissue	1-3 kPa
Pore diameter of alveolar-capillary barrier	0.5-2.5 nm
Thickness of basement membrane	50 nm
Thickness of air-blood tissue barrier	0.62 μm
Total alveolar-capillary barrier thickness	1.1 μm

Table 1.1. Key parameters of the alveolar-capillary barrier [3]

1.4.1.2 Electrospinning

Electrospinning is a manufacture technique which allows to produce nano-porous mats sheets for biomedical applications, such as tissue engineering. The fibers are assembled to form a 3D substrate that has an ECM-like structure.

To manufacture nano-porous mats the high voltage usage is required. The technique involves filling a syringe with the polymeric solution to be spun and the Taylor's cone formation on the syringe nozzle

tip that occurs after the high voltage application between the nozzle and a collector. After the Taylor's cone creation, the solution is extruded by the syringe in wires that are attracted, thanks to a potential difference, by a collector where fibers are deposited under a nano-porous sheet's shape (Figure 1.11) [50].

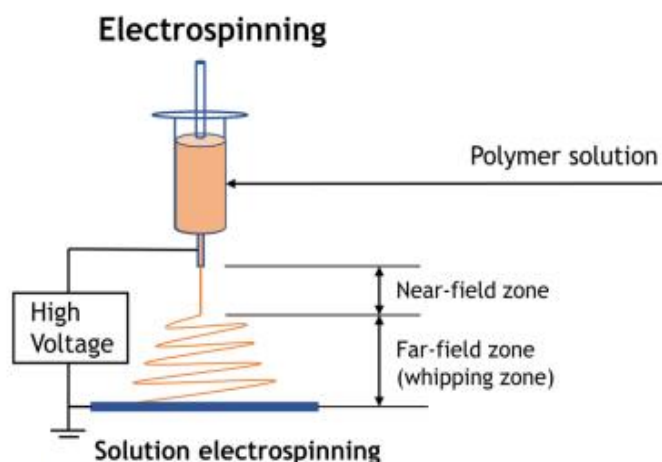


Figure 1.11. Schematic illustration of the electrospinning technique [51]

The process can be controlled by three kind of parameters: the solution parameters, like viscosity, surface tension, concentration, polymer molecular weight and structure, conductivity and the solvent evaporation; the processing parameters that include voltage, flow rate, distance between the tip and the collector, nozzle tip diameter and collector geometry; the ambient parameters, such as temperature and humidity [50].

Electrospun fibers have a high surface to volume ratio, high porosity, a variable pore-size range and a nano to micro scale ECM-like structure. In addition, it is a very versatile technique indeed a wide selection of materials can be chosen to be electrospun and if necessary fibers can be functionalized. In conclusion electrospinning is a simple, efficient, low cost and reproducible method suitable for mimic the *in vivo* environment complexity [50].

1.4.1.3 Membrane material selection

Electrospinning is a perfect technique for modelling the air-blood barrier. In the literature, PDMS is the material more widely selected for manufacture this kind of membrane due to its low Young's modulus of 1-3 MPa ideal for cyclic elastic movements but, because of its properties, it is not so simple to electrospun [3]. For this reason, other materials, with good mechanical properties, should be investigated, such as synthetic/natural polymers. For example, polycaprolactone (PCL), which is

biodegradable and biocompatible, could be a valid alternative, together with polyethylene terephthalate (PET) and polycarbonate Urethane (PCU) which have been used for epithelial culture [3]. This kind of synthetic materials, despite their good mechanical properties, are hydrophobic and so they are not suitable for cell growing without a pre-functionalization. Another alternative are natural polymers which derived and/or mimic the ECM composition, such as laminin, collagen and fibronectin; so, they are more accepted by cells, but they lack of good mechanical properties [3]. A good compromise between these two kinds of polymers are the composite that are formed by both synthetic and natural ones; this mean that both mechanical and bioactive properties are expressed. For example, PCL/gelatin blend is used for lung application, to model the alveolar-capillary barrier [3].

For all the reason above electrospinning is perfect for fabricating nano-porous sheets used to model the air-liquid interface in lung.

1.4.2 Scientific literature

In the following, some case studies from scientific literature, that employ electrospinning to reproduce the air-blood barrier, are described. In these, different cell cultures and different polymeric materials are exploited. In addition, a microfluidic device is described that involves the use of an electrospun membrane as a substrate for the cell culture, instead of one made of PDMS.

1) *Basement Membrane Mimics of Biofunctionalized Nanofibers for a Bipolar-Cultured Human Primary Alveolar-Capillary Barrier Model by Nishiguchi et al.* [52].

Goal

Modelling the alveolar-capillary barrier by seeding human primary endothelial and epithelial cells on poly(ϵ -caprolactone) (PCL) and bioinert six-armed, star-shaped poly(ethylene oxide-stat-propyleneoxide) with isocyanate end groups (NCO-sPEG) electrospun membranes (Figure 1.12). In addition, comparing the bipolar cell layer with the conventional membranes in terms of structure and permeability.

Materials and methods

To prepare the solution for the electrospinning, 6 wt % PCL and NCO-sPEG at the ratio of 20 wt % to PCL were dissolved in hexafluoroisopropanol (HFIP). After that 10 μ l of 0.2% trifluoroacetic acid was added to the solution to increase conductivity. The electrospinning parameters are varied for optimize the process: voltage (10-20 kV), distance (10-18 cm), and flow rate (0.1-1.0 mL h⁻¹).

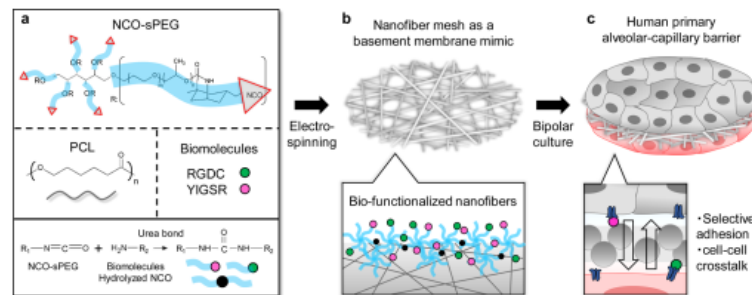


Figure 1.12. Schematic illustration of the bilayer cell culture on the PCL/NCO-sPEG meshes

Results

SEM analysis shows that fibers have an average pore size of 1.5 μ m with a porosity of 71%, instead classic transwell membranes have 3 μ m of pore diameter and a porosity of 14%. Also, mechanical tests are conducted for valuing the membrane properties following the physiological parameters, 0.25 Hz, 15 % of deformation and 30 cycles. An elastic modulus of 5.2 MPa on 10 μ m thick meshes is found. To interact with the ECM, peptides with free amine groups (lysine or N terminus) are added to the solution in HFIP and incubated for 1h before the solutions are electrospun. By measuring the fluorescence with a confocal scanning laser micrograph (CLSM) of the fibers labelled with fluoresceinamine, used as

model reaction of the peptide modification, it is seen the successful modification (Figure 1.13). To optimize the best culture conditions, a human lung carcinoma cell line (NCI H441) and human umbilical vein endothelial cell (HUVEC) have been seeded before the trials with the primary human cells. It is seen that cells culture on meshes without peptide do not adhere underlining the importance of functionalization. In particular, RGD and LM peptides were used for co-culture permitting the formation of interface between the two type of cells confirmed by TEM and confocal microscopy. Moreover, lamellar bodies are detected demonstrating the surfactant formation. In further experiments also human pulmonary alveolar epithelial cells (HPAEC) and primary human pulmonary microvascular endothelial cells (HPMEC) have been seeded showing the formation adherent junctions.

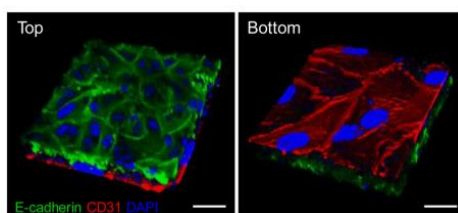


Figure 1.13. 3D reconstructed CLSM images of bipolar cultured HPAEC and HPMEC

Conclusion

This membrane is an optimum tool for understanding lung diseases and it could be used for the development for a lung oxygenator for chronic lung diseases therapies.

2) *Human co- and triple-culture model of the alveolar-capillary barrier on a basement membrane mimic by Dohle et al. [53].*

Goal

The study proposes a cellular triple-culture, composed by microvascular endothelial cells (ISO-HAS-1), lung adenocarcinoma epithelial cells (NCI H441) and human leukaemia monocyte cell line (THP1), cultured on PCL electrospun membranes which mimic the alveolar-capillary barrier (Figure 1.14).

Materials and methods

The solution was prepared by dissolving PCL at 6 wt% in HFIP then 10 μ L of 0.2 % trifluoroacetic acid solution have been added to increase the conductivity of the solution. Subsequently electrospun meshes have been fabricated with the following parameters: 20 kV; 15 cm distance from the collector; 0.5 mL/h. Lastly, the manufactured sheets were incubated in 0.01 wt% of bovine collagen I solution for coating and washed with PBS before seeding cells.

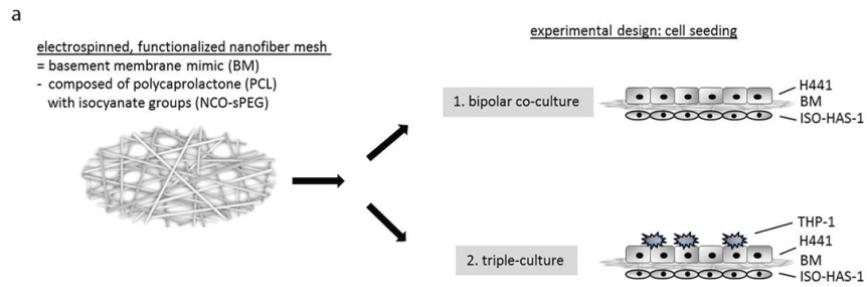


Figure 1.14. Schematic illustration of the co-culture and triple-culture on the electrospun membranes

Result

A viability assay (MTS assay) is performed to exclude cytotoxic effect of the PCL-collagen coated membranes giving back no negative effects. After that the TEER of the bipolar co-culture is evaluated both on PCL-collagen coated meshes and Transwell inserts used as control to assess the barrier quality. TEER values increase over the cultivation's period in both substrates, post-treating with dexamethasone which enhances the formation of tight junctions, reaching a value of $300 \Omega \cdot \text{cm}^2$ after 10 days. Also, a permeability assay was done examining the leakage of a fluorescent dye across the membrane, finding less transportation from the apical to the basal chamber in cultured fibers than in non-cultured. Via immunofluorescence staining the endothelial cells show the CD31 marker, instead, epithelial cells are stained positive for E-cadherin, an adherens junction protein, and β -catenin, present during the formation of adherent junctions, which demonstrates the cell-cell interaction (Figure 1.15). For the triple-culture, THP-1 cells are seeded on top of the epithelial cells at day 7, after the differentiation into M1, pro-inflammatory phenotype. The NCL H441 cells shows a more stratified layer after the macrophages supplement respect to the mono or bilayer present in the co-cultures.

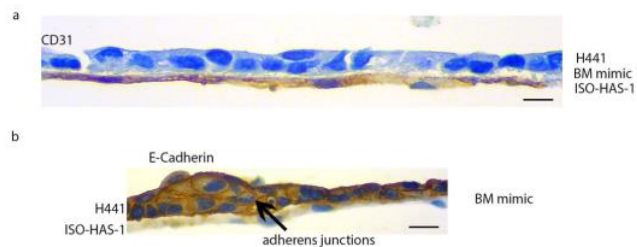


Figure 1.15. Immunostaining for a) the endothelial cell specific marker CD31 and b) adherent junction protein E-cadherin

Conclusion

This alveolar-capillary model simulates well the physiological barrier. In fact, it exhibits an increased TEER value during the cultivation and the presence of the adherent junctions. The immune response can also be studied by adding macrophages to the culture, analysing the effect of pathogens or toxic factors.

3) *A novel electrospun biphasic scaffold provides optimal three-dimensional topography for in vitro co-culture of airway epithelial and fibroblast cells by Morris et al. [54].*

Goal

The paper aims to fabricate a biphasic electrospun PET scaffold with nano- and micro- structure for culturing epithelial lung cells (CALU-3), which need to grow on nanoporous fibers, and lung fibroblast (MRC5), which prefer microporous fibers.

Materials and Methods

PET is dissolved in trifluoroacetic acid (TFA) and dichloromethane (DCM) (with a ratio 1:1) at 10% (w/v) or 30% (w/v) PET to produce nanofibers or microfibers scaffolds respectively.

Electrospinning parameters used are 15 kV; 15 cm of distance from the collector; 0.5 mL/h for the nanofiber and 2 mL/h for the microfiber. To create the biphasic property the solutions are electrospun sequentially with the parameters described, microfibers are electrospun before the nanofibers.

Results

Thanks to SEM the fibres diameters and porosity are evaluated experiencing non-beaded scaffolds with $0.25 \pm 0.002 \mu\text{m}$ for the nanofibers and $2.5 \pm 0.02 \mu\text{m}$ for the micro ones and more than 80% of porosity (Figure 1.16).

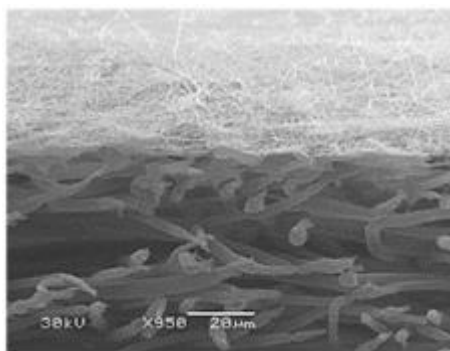


Figure 1.16. SEM of the biphasic scaffold

The CALU-3 cells are seeded both on nanofibers and microfibers forming a confluent monolayer at day 14 only on the first one. Moreover, also TEER measurements and E-cadherin immunostaining demonstrate the CALU cells prefer growing on nanofibers; indeed, the former, that is an index of barrier formation, increases during the culture only on nanofibers and the second, that is an indicator of junction formation, is stained positive only in nanofibers. On the contrary fibroblast on microfibers

are more elongated and show a greater viability than fibroblasts growing on nanofibers. The co-culture on biphasic scaffold shows good barrier properties, in fact, by immunostaining E-cadherin and occluding are stained positive (Figure 1.17). In addition, the barrier functions increase due to fibroblast presence raising the electrical resistance and reducing dextran's permeability.

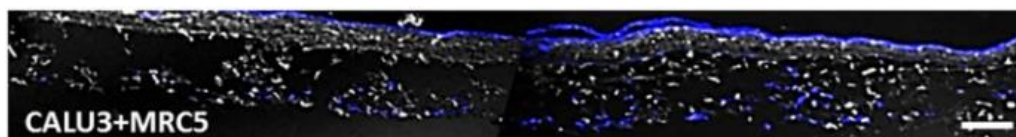


Figure 1.17. Section of the biphasic scaffold cultured with the CALU-3 cells and the MRC-5 cells

Conclusion

This study demonstrates that the electrospinning technique is able to develop a 3D topography that fits cells preferences about substrates where they like living on. In particular, this scaffold could be used to mimic the airway diseases such as asthma.

4) Using a Novel Microfabricated Model of the Alveolar-Capillary Barrier to Investigate the Effect of Matrix Structure on Atelectrauma by Higueta-Castro. [26].

Goal

The scientists developed a microfluidic device which mimics the alveolar barrier, the cells are seeded on PCL-gelatin electrospun membrane. In addition, they investigate how the airway reopening, after a cyclic collapse, can affect the alveolar-capillary barrier and cell injury.

Materials and Methods

The device consists of two PDMS layers, fabricated by soft lithography, and a PCL-gelatin membrane produced by the electrospinning technique (Figure 1.18).

The blend's components are dissolved in hexafluoro-2-propanol (HFP) for 24 hours, with four different weight ratios: 75/25, 50/50 and 25/75 (PCL/Gel) and 100% PCL. After that the blend is electrospun at 26 kV with a flow rate of 16 mL/h and 25 cm of distance to the collector. The chip is, then, assembled with the plasma oxygen and incubated at 70°C in oven for 10 minutes for promoting the PDMS-PDMS bonding.

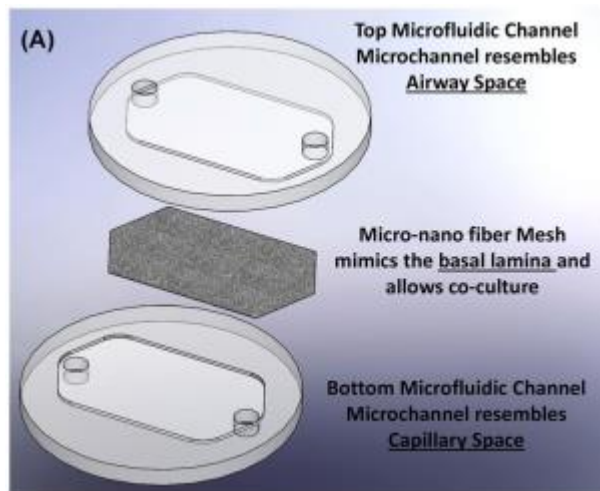


Figure 1.18. Schematic representation of the microfluidic device conformation

Results

The first property explored is the stiffness. Fibers with a higher amount of gelatin have a lower elastic modulus in fact 50/50 (PCL/Gel), 75/25 (PCL/Gel) and pure PCL have 0.36, 2.10, and 7.20 MPa median modulus, respectively. The exactly opposite result is found counting the fibers diameter, indeed, increasing the gelatin content also the diameter increases, finding 5.9, 1.12, 0.88 and 0.57 μm for 25/75 (PCL/Gel), 50/50 (PCL/Gel), 75/25 (PCL/Gel) and PCL fibers. After the evaluation of the membrane properties, human alveolar epithelial cells (A549) and human umbilical vein endothelial cells (HUVEC) are seeded in the device. The epithelial cells exhibit a more spread morphology in softer fibers, whereas the endothelial cells grow well both on more rigid and softer membranes. Instead, tight junctions (ZO-1 and occludin) are more identified in co-culture on stiffer fibers than in softer ones. To assess the barrier function, dextran transport is measured discovering that on 75/25 (PCL/Gel) meshes the transport decreases, underlining good barrier properties, in comparison with 50/50 fibers. By an airway reopening simulation after five reopening event cells death occurs mostly on PCL fibers than in meshes contain gelatin.

Conclusion

In this study is shown how changes on the seeding substrate can affect cells growth and barrier functions. So, it is important fabricate materials with features and morphology that mimic the native tissue.

2. AIM OF THE WORK

This work aims to develop an *in vitro* model of lung tissue inside an alveolus-on-a-chip, which allows to study the organ under dynamic conditions. In particular, the alveolar-capillary barrier, where the main phenomena of oxygen/carbon dioxide diffusive exchange take place, was recreated *in vitro*. This barrier is an air-liquid interface which is composed of alveolar epithelial cells in direct contact with the inhaled air, a basement membrane and endothelial cells of the capillary, in contact with the blood flow. Another important physiological lung feature to be mimicked is the mechanical stress imposed by respiratory motion on the cells, which causes the alveoli to expand and contract. Membrane microfluidic devices are the best solution to fulfil these objectives.

During this work, several steps were performed in order to achieve the ultimate goal of recreating *in vitro* a miniaturized alveolar-capillary barrier. After CAD design, PDMS molds and replicas were fabricated, evaluating, with optical microscope, that the obtained result was comparable with the desired one. Then, PCL/gelatin nanofibrous mats were fabricated to mimic the basement membrane, using the electrospinning technique, which allows the fabrication of scaffolds with a structure like the extracellular matrix. These fibers were then evaluated both morphologically through SEM and mechanically, to ensure that the material was elastic enough to implement respiratory motion. The fabricated device elements were assembled through the plasma oxygen process, validating the chip with leakage tests. Finally, a co-culture of A549 (human lung adenocarcinoma cells) and Hulec-5a (pulmonary capillary endothelial cells) on PCL/gelatin membranes were performed, implementing the conditions in ALI three days after seeding. The quality of the formed barrier were analyzed by confocal microscopy by staining the nuclei and cytoskeleton. The chip design provides for the mechanical stimulation of the formed alveolar/capillary barrier, which will be implemented in future works

3. MATERIALS AND METHODS

3.1. Materials

3.1.1 Polydimethylsiloxane (PDMS)

PDMS is a non-toxic, transparent, biocompatible and non-fluorescent material [37]. In addition, it has a high elasticity and it is gas permeable, which is important for a long-term cell culture [34]. SYLGARD 184 is the silicon elastomer, employed in this work, for fabricating the two layers of the alveolus-on-a-chip (Figure 3.1). Generally, it has two components: the base (the pre-polymer) and the curing agent (the cross-linker) (Table 3.1).

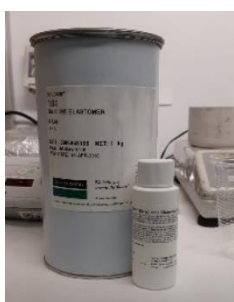


Figure 3.1. Sylgard 184

Product name	Sylgard 184
Base form	Viscous (5100 cP)
Curing agent form	Liquid
Color	Colorless
Cure time at 25 °C	48 h
Tensile strength	6.7 MPa

Table 3.1. Sylgard 184, product properties [55]

3.1.2 Polycaprolactone (PCL)

The PCL is a polyester obtained by ring-opening polymerization of cyclic monomer ϵ -caprolactone (Figure 3.2). This semi-crystallin polymer has a glass transition temperature of -60°C and a melting point between 59°C - 64°C [56]. It is hydrophobic and biodegradable. This last property involves the scission of the hydrolytic chains of the ester bonds and it is, generally, a slower process (1-2 years). The synthetic polymer has good mechanical properties and it is biocompatible. In fact, it is, often, selected for biomedical applications, such as for the realization of the scaffold in tissue engineering [53][56][57]. The PCL was purchase from Sigma-Aldrich (Table 3.2).

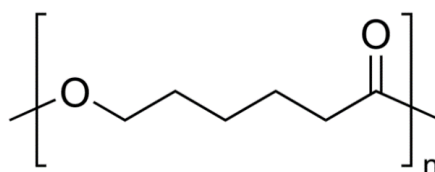


Figure 3.2. PCL Chemical formula [58]

Suppliers	Sigma-Aldrich
Form	Pellets (~3 mm)
Molecular weight	Mn 80,000
Impurities	< 0.5% water
Density	1.145 g/mL at 25°C

Table 3.2. PCL (Sigma-Aldrich) product description [58]

3.1.3 Gelatin

Partial hydrolysis of the collagen is used to extract the gelatin, which is a single chain protein [59]. Gelatin has a structure with heterogeneous and random macromolecules, which main components are hydroxyproline, glycine, and proline [60]. This natural polymer is biodegradable, biocompatible, less expensive, and less antigenic than the collagen [59]. Moreover, gelatin helps adhesion, migration and cell proliferation due to its natural properties and it can be mixed with synthetic polymer to increase its mechanical properties [59].

To achieve the gelatin type A, the collagen is soaked in a diluted acid solution at pH 4. Instead, gelatin type B is obtained by an alkali process. [60]. The gelatin was purchased from Sigma-Aldrich (Table 3.3).

Suppliers	Sigma-Aldrich
Biological source	Porcine Skin
Type	Type A
Form	Power
Solubility	H ₂ O: soluble 50 mg/mL

Table 3.3. Gelatin (Sigma-Aldrich), product description [61].

3.1.3.1 γ -glycidopropyltrimetossilano (GPTMS)

Gelatin is not stable in water, so it needs to be crosslinked. For this purpose, GPTMS is employed, which is a silane coupling agent (Figure 3.3). The crosslinking process occurs in two steps: in the first one, the oxirane rings on GPTMS chains react with the amino groups of the gelatin and pendent silanol groups are formed by the hydrolysis reaction of the GPTMS trimethoxy groups. The second step takes place during the fibers extrusion, when the solvent evaporates, in a condensation reaction of two silanol groups (Si-O-Si bonds are formed) [62]. The GPTMS was purchase from Sigm-Aldrich (Table 3.4).

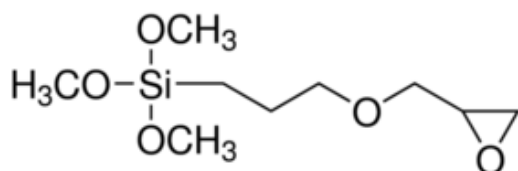


Figure 3.3. GPTMS, chemical formula.

Suppliers	Sigma-Aldrich
Form	Power
Density	1.07 g/mL at 25°C

Table 3.4. GPTMS (Sigma-Aldrich), product description [63].

3.1.4 Solution solvents

3.1.4.1 Acetic acid

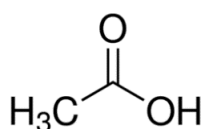


Figure 3.4. Acetic acid chemical, formula [65].

It is an organic carboxylic acid, weak and corrosive which has antibacterial properties and a sharp odour [64]. It was purchase from Sigma-Aldrich and has been used in electrophilic solutions to dissolve PCL and gelatin (Figure 3.4).

3.1.4.2 Formic acid

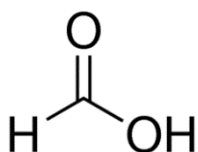


Figure 3.5. Formic acid, chemical formula [67].

The formic acid is a liquid clear, colourless, corrosive and with a pungent odour (Figure 3.5). It is obtained during the acetic acid production by liquid-phase oxidation of hydrocarbons. It was purchase from Sigma-Aldrich [66].

3.1.4.3 Chloroform



It is a chlorinate hydrocarbon volatile, clear, non-combustible and with a sweet smell [68]. It was purchase from Sigma-Aldrich and employed to dissolve the PCL (Figure 3.6).

Figure 3.6. Chloroform, chemical formula.

3.1.5 Cells

3.1.5.1 A549

The A549 cell line (lung adenocarcinoma cells) was used for cell testing on PCL and PCL/Gel samples, inserted into microfluidic devices, to mimic epithelial alveolar cells. A549 were purchased from the American type culture collection (ATCC) and derived from a 58-year-old male individual [69].

The cells are grown in Roswell Park Memorial Institute (RPMI) 1640 (Gibco, ThermoFisher scientific, Figure 3.7.) supplemented with:

- 10 % fetal bovine serum (FBS, Gibco ThermoFisher scientific), useful for cell maintenance and vitality [71].
- 1% L-glutamine, 200 nM (Gibco, THERMOFISHER scientific), an aminoacid
- 1% penicillin streptomycin (P/S, Gibco, ThermoFischer scientific), antibiotics used to prevent bacterial contamination due to their action against gram-positive and gram-negative bacteria [72].



Figure 3.7. RPMI 1640, Gibco [70].

The A549 cells, which are categorized as non-small cell lung carcinomas (NSLC), are squamous cells with a higher proliferative rate. [69] They are used as alveolar epithelial model. In fact, this cell line is select in numerous case studies even within microfluidic devices, as *in Higuita-Castro et al.* work [26], due to its features similar to the Type II alveolar epithelial cells, such as a distinct polarization, tight junctions and extensive cytoplasmatic extension [1].

3.1.5.2 HULEC-5a

The HULEC-5a cells, purchased from the American type culture collection (ATCC), are lung microvascular endothelial cells derived from a neonate male individual [73]. These cells were employed for the co-culture, together with the A549, to model the alveolar-epithelial barrier. The cells are grown in MCDB 131 (Gibco, ThermoFisher scientific, Figure 3.8.) supplemented with:

- 10 µg/mL Epidermal Growth Factor (EGF)
- 1 µ/mL Hydrocortisone
- 10 mM Glutamine
- 10 % fetal bovine serum (FBS)
- 1% P/S

These cells can be employed as an alternative for primary human lung endothelial cells for lung cancer research, for studying the endothelium function and investigating the role of endothelium in infection [73].



Figure 3.8. MCDB 131, Gibco [74].

3.1.6 Immunostaining

3.1.6.1 DAPI

DAPI was purchase from Invitrogen (ThermoFisher). It is a fluorescent dye (Figure 3.9) which emits in blue when binds with AT regions of DNA, so it is a nuclear stain used in fluorescent microscopy [75].

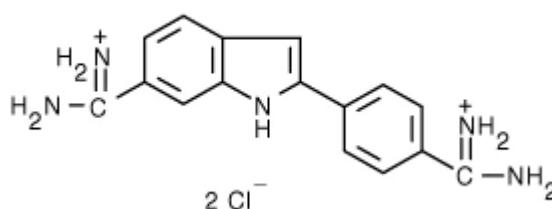


Figure 3.9. DAPI, chemical formula [76].

3.1.6.2 Phalloidin

Phalloidin is a bicycle peptide which strains with the actin filament (F-actin), it is usually conjugated with a fluorescent dye, such as FITC or Rhodamine (Figure 3.10) [77] [78]. Both phalloidin-FITC and rhodamine phalloidin were purchase from Invitrogen (ThermoFisher). The first one emits in green whereas the second one in red.

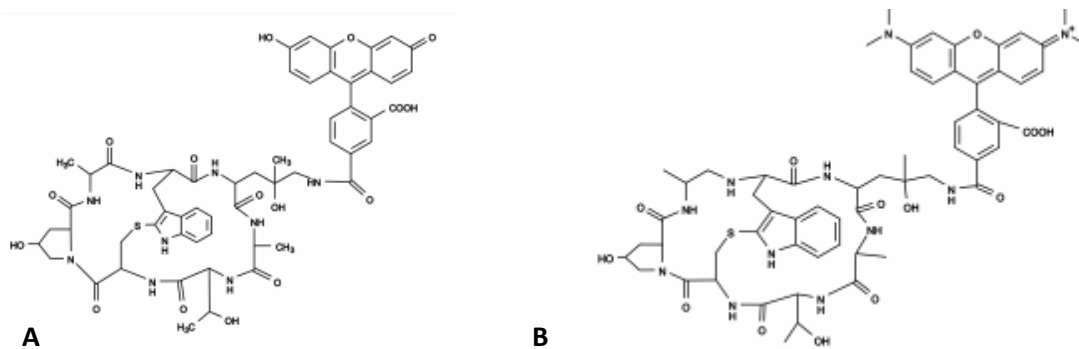


Figure 3.10. Chemical formula: A) FITC-Phalloidin, B) Rhodamine-Phalloidin

3.2 Methods

3.2.1 Alveolus-on-a-chip design

The device designed is a membrane-on-chip, it consists of:

- a top layer
- a PCL/Gel membrane, circular in shape to better mimic alveolar geometry. The A549 cells are seeded on the upper side of the membrane, while the HULEC-5a are seeded on the lower one, to form a cell co-culture
- a bottom layer

The project has been created by exploiting Rhinoceros, a CAD software. The measures chosen were inspired by the microfluidic device present in the literature [42] [45].

3.2.1.1 Top layer

The top layer is made of a central well of 3 mm in diameter for the PCL/Gel membrane housing, completely open to the atmosphere to allow to reproduce air-liquid interface (ALI) condition (Figure 3.11).

The inlet and outlet of the bottom channel (1.5 mm in diameter) can be also found in this layer, together with two side channels of dimensions 1 x 13.40 mm, for mechanical implementation.

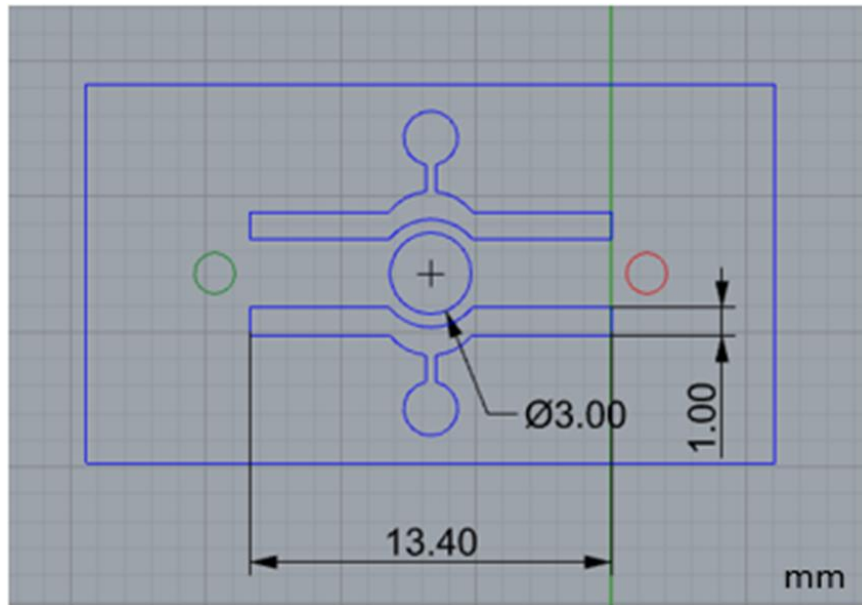


Figure 3.11. Top-layer CAD.

3.2.1.2 Bottom layer

Instead, the bottom layer features a central channel of size 1.5x16 mm, which allows the medium to pass through, and contains in the cell camera 10 pillar of 0.20 mm in diameter. The pillars are placed laterally for not disturbing the medium passage and they have the role of membrane support. Likewise, the channels for breathing actuation are conceived also in this layer with an inner hole of 1.5 mm in diameter (Figure 3.12). Finally, between the two layers the PCL/Gel membrane about 5 mm in diameter is blocked.

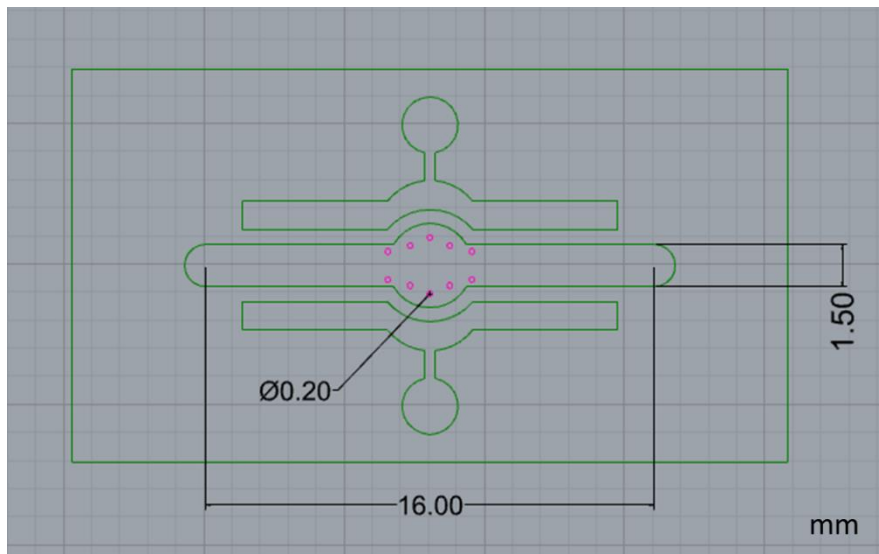


Figure 3.12. Bottom layer CAD.

3.2.2 Alveolus-on-a-chip fabrication

The soft lithography is the technology employed for the realization of the device. The first step concerns the development of the negative PMMA mold by laser ablation and then thanks to the replica molding the positive test-pieces are shaped. In the following, both the fabrication's processes of the mold and the replicas are described.

3.2.2.1 Mold fabrication

The technique chosen for this application is the laser ablation, which, through a laser beam, hits the material for drawing the design of interest in a rapid and reproducible way.

Laser slider (provided by Microla Optoelectronics) was employed by which a wide range of materials can be machined, such as paper, plastic and glass (Figure 3.13). This machine uses a CO₂ laser beam with a power of 25-50 W and a wavelength of 10.6 μm. Moreover, it is supplemented with a computer with a dedicated software for uploading the CAD project to be reproduced [79].



Figure 3.13. Laser marker slider: A) lateral B) front view

Firstly, the PMMA sheet (of about 5 mm of thickness), on which the pattern is going to be drawn, was placed easily inside the laser machine thanks to the slider. Then, the focus needs to be done to assess the beam targets correctly the material. Lastly, the working parameters are chosen, and the laser can be activated.

There two types of parameters upon which the operator can act: the filling ones and the laser ones. The first ones allow to work on the drawing plot, by selecting how the beam must move along the material for generating the lines of the design. The filling parameters picked to produce the alveolus-on-a-chip are reported in Table 3.5, together with the laser ones which enable to operate on the physic features of the CO₂. The PMMA mold, drawn by the laser ablation, is the negative of the final geometry

and has a 2D pattern. So, it is necessary to create a boundary to permit the casting of the PDMS inside the mold and the formation of a 3D replica. To do that, a rectangular edge was cut from a 2 mm thick sheet of PMMA, by exploiting the laser ablation technique. The cutting parameters chosen are also listed in Table 3.5. By using the same parameters it was, also, possible to produce a cylinder of PMMA (with 3 mm in diameter) to be stucked on the top layer mold in correspondence of the cellular central well to ensure the formation of a hole of the same dimension in the PDMS replica. Finally, both the cylinder and the edge were glued to the 2D mold by employing a double-side adhesive tape.

Filling parameters	Crossed lines	45°C angle
	Line spacing	0.03 mm
Laser parameters	Power	5%
	Frequency	2000 Hz
	Velocity	75 mm/s
Cutting parameters	Power	20%
	Frequency	17x10 ³ Hz
	Velocity	50 mm/s
	Number of cycles	8

Table 3.5. Summary table of the laser parameters chosen for the mold fabrication

3.2.2.2 Top and bottom layers fabrication

The replica molding technique was used for achieving the two layers in PDMS, by pouring the PDMS solution inside the negative mold and allowing it to crosslink. In detail, the solution must be prepared in fume hood by adding the curing agent to the base with a ratio of 1:10, respectively. The two elements were, then, mixed strongly with the help of a glass stick, obtaining a viscous solution full of bubbles. These last ones must be removed through the degassing in vacuum until a clear and transparent solution is gained. Afterward, the negative mold can be filled with about 2 mL of the PDMS solution, taking care to avoid the formation of additional bubbles during the casting process; in the eventually they can be removed by employing a sharp object, like pipette tips or needles. Finally, the mold filled with the PDMS was placed in the oven for one hour and a half at 70° C to allow the PDMS crosslinking. Once the replicas were solidified, they can be peeled off the PMMA with the support of the ethanol, which makes the peeling easier without ruining the PDMS layers.

To create the holes of inlet, outlet and lateral channels a puncher 1.5 mm in diameter was used of after the removal of the top layer from the mold. The entire process was carried out in a cleanroom to ensure the maximum cleanliness of the samples.

3.2.3 Nanofibrous mats fabrication

The membrane was fabricated by the electrospinning technique by employing the Novaspider V5 (Figure 3.14). This tool allows to place the needle vertically to the collector enabling the solution top-down extrusion. This electrospinning machine provides: a syringe pump where the syringe, filled with the solution, is mounted; a flat plate, which is covered with an aluminium foil to collect the fibers; and a gear system which job is to move the needle during the working time. The process is easily controlled by monitoring the parameters in real-time with a web user interface. The voltage must be set for both the needle and the flat plate, choosing for the collector a low voltage, in this work the value used for all the process was 4 kV [80].



Figure 3.14. Novaspider V5 device.

A blend PCL/Gel has been selected as material of choice, instead pure PCL fibers matrices have been chosen as control. First of all, the protocol for the fabrication of PCL electrospun matrices were optimized in order to obtain defect-free fibers.

3.2.3.1 Preparation of PCL electrospun mats

750 mg of PCL were dispersed in a 5 mL solution of acetic acid and formic acid (50:50 ratio). The solution was placed on a stirrer for 24h at 200 rpm at room temperature. The PCL obtained solution

(15% w/v), was loaded in a 5 mL syringe and processed by electrospinning. The process parameters used for optimizing the fabrication protocol are reported in Table 3.6.

Test code	Flow rate ($\mu\text{l}/\text{min}$)	Voltage (kV)	Distance (cm)
PCL 14_400	400	14	12
PCL 16_400	400	16	12
PCL 20_400	400	20	12
PCL 14_500	500	14	12
PCL 16_500	500	16	12
PCL 20_500	500	20	12
PCL 16_550	550	16	12
PCL 16_600	600	16	12
PCL 20_600	600	20	12

Table 3.6. Electrospinning parameters used for the optimization of the PCL solution

3.2.3.2 Preparation of PCL/gelatin mats

The PCL/Gel solution (15% w/v) was obtained by mixing PCL and GL (80/20 w/w) in a 5 mL solution of acetic acid and formic acid with a 50:50 ratio [80]. The solution was stirred for 24 h at room temperature at 200 rpm. The gptms (3,68% (v/v)) was added to the PCL/Gel solution, which was preserved under stirring for 30 minutes. The PCL/Gel was then inserted in a 5mL syringe and electrospun with a voltage of 20 kV, a distance of 12 cm and a flow rate of 500 $\mu\text{l}/\text{min}$

3.2.4 Microfluidic device assembling

The plasma oxygen technique is used to bond the replicas, by employing the Diener electronic low-pressure plasma lab system Atto (Figure 3.15). This machine promotes the surface activation of the material increasing the hydrophilicity for ensuring the adhesion between the two parts.

Before starting the process, the samples were washed in ethanol by ultrasound for 30 second, to make sure that dust and debris do not interfere with the adhesion. Next, the layers were placed in the working chamber of the plasma system, being careful to put upward the surfaces to be treated. Also, the membrane was plasma treated for ensuring the hydrophilicity and consequently the cellular adhesion [3]. So, the membranes were cut with a five mm diameter puncher and placed in the plasma system together with the samples. Afterwards, the program of interest, controlled automatically by the Diener plasma, was chosen.

There are four process steps (Table 3.7):

- the first one is called the pumping down period, where the pressure inside the chamber is lowered until reaching 0.3 mbar.
- The second step is the gas supply period where the working gas (oxygen) joins the samples with a pressure of 0.70 mbar for one minute
- Then the high frequency generator is activated and the plasma process period takes place for 30 seconds with a power of 22%.
- The last step is the venting where the chamber is, once more, filled with air.

After this process the samples and the membrane were ready for the bonding which requires to put the top layer inside the alignment box, a container produced by the laser ablation that supports the operator in the alignment of the replicas, then the membrane was placed on the central well and blocked by matching the bottom layer on the top one. Finally, the completed device was placed in the oven at 70°C for ten minutes to help the PDMS-PDMS bond, how is recommended in literature [26].



Figure 3.15. Diener electronic low -pressure plasma lab system Atto

Plasma process parameters		
<i>Pumping down period</i>	<i>PRESSURE</i>	<i>0.3 mbar</i>
<i>Gas supply period</i>	<i>TIME</i>	<i>1 min.</i>
	<i>GAS</i>	<i>O2 100%</i>
	<i>PRESSURE</i>	<i>0.70 mbar</i>
<i>Plasma process period</i>	<i>TIME</i>	<i>30 sec.</i>
	<i>POWER</i>	<i>22%</i>
<i>Venting period</i>	<i>TIME</i>	<i>1 min.</i>

Table 3.7. Summary of the parameters of the plasma process

3.2.5 Field Emission Scanning Electron Microscopy (FE-SEM)

SEM is a high-resolution technique which allows to analyse the specimen surface by displaying its topography [10]. The sample is scanned with a high energy electron beam, which is focused spot by spot with a set of electromagnetic lenses. In particular, the electrons are accelerated with about 1-30 kV voltage by the electron gun, composed by a cathode, an electron source which is, conventionally, a tungsten strand, and an accelerating anode. The negative charges hit the metal ions of the specimen, which is placed in a vacuum chamber with a pressure of $0.1 \cdot 10^{-4}$, leading to electron emission (the secondary electrons). Thereafter, some detectors collect the signal emitted [10] [82] [83].

To improve the spatial resolution and to increase the electron focusing, a field emission gun is required where electrons are released very close to the filament tip. Indeed, FESEM enables to carry out analysis with a higher stability and a smaller spot size compared to SEM. In addition, FESEM has a resolution of 1 nm, whereas SEM can achieve resolution of 3 nm [82] [84].

For this project, the electrospun PCL and PCL/Gel membranes have been analysed by using the Zeiss SUPRA 40 (Figure 3.16), which employs the Schottky filed emission gun to achieve high resolution images and measures [84].

The samples must be prepared carefully. The meshes were cut into little pieces and placed on stubs covered with double side adhesive tape, and then sputter-coated with a thin platinum layer (to make the samples conductive) using the Quorum Q150s at 20 mA for 20s.



Figure 3.16. Zeiss Supra 40 FE-scanning electron microscope where the samples were analysed by employing an accelerating voltage of 10KV.

3.2.6 Images analysis

The SEM images have been examined by employing Image J (National Institute of Health, USA), a software which allows to evaluate the nanofibers and pores diameters. Using the command *analyze-measure*, 30 diameters for each SEM images were measured. Instead, the pores areas were derived from the command *analyze particles*, assuming a circular shape of the pores. Then the values have been reported on Excel where the pores diameters and the distribution of the nanofibers diameters were calculated.

3.2.7 Mechanical characterization of electrospun nanofibers

The cyclic tests (both uniaxial and biaxial) were performed using the planar biaxial testbench instruments (electroforce testing solutions, Figure 3.17), fitted with a 225 N load cell, at room temperature. The instrument is composed of four linear motors placed perpendicular to each other and a chamber, controlled in temperature, which can be filled with water/PBS for the wet conditions [85]. The Win Test software is employed to select the working parameters. For all the trials carried out (100 cycles for each test) the parameters were chosen according to the physiological breathing motion: frequency of 0.2 Hz and 10% of displacement (sinusoidal wave form) [45].



Figure 3.17. Planar biaxial testbench instruments.

3.2.7.1 Uniaxial mechanical tests

The samples were cut with a dog-bone shape, which were 19mm long and 5mm wide. The thickness was measured for each sample. Three test-pieces were tested for both PCL and PCL/Gel membranes. The software returns the data of displacement and force, which were processed with Excel. To find the strain, the displacement was normalized for the initial sample length (l_0), defined as follow: $\epsilon = \frac{\Delta l}{l_0}$.

Instead, the stress was defined as the ratio between the applied force and the cross-sectional sample area: $\sigma = \frac{F}{A}$.

Afterwards, the stress-strain curves were filtered (only the force data, which were noisy) and plotted with Matlab using the following code:

% PSD calculation

```
Ncycles=100;
nsamples=length(load)/Ncycles; %number of samples for each cycle.
w=hamming(nsamples); %PSD window
fc=0.25; % sampling rate
NFFT=length(w);
[P f]=pwelch(stress,w,[],NFFT,fc); %sig: signal to analyze
```

%plot of the PSD curve, where the cutoff frequency can be selected

```
plot(f,P),xlabel('frequency (Hz)'),title('PSD')
```

% cheby filter

```
Wp=(ft*2)/fc; %passband edge frequency
Ws=(fs*2)/fc; %stopband corner frequency
Rp=1; %peak-to-peak pass band ripple
Rs=20; %stopband attenuation
```

```

[ordine,Wp]=cheb1ord(Wp,Ws,Rp,Rs);
[b,a]=cheby1(ordine,Rp,Wp,'low'); %low-pass filter
stressf=filtfilt(b,a,stress);
plot(strain,stressf_filt,xlabel('strain'),ylabel('stress (MPa)'),title('stress-stain curve'))

```

Instead, the young modulus (E) was calculated as angular coefficient of the linear tract for each cycle, after that the average and standard deviation were calculated for each test carried out

3.2.7.2 Biaxial mechanical tests

In this case two load cells were employed, one for horizontally placed motors and one for vertically placed engines. The parameters chosen were the same as in the previous case and the results were also analyzed by exploiting Excel and Matlab. The stress-strain graphs obtained were two, one for each pair of motors. The square shape specimens (3mm x 3mm) were tested for both PCL and PCL/Gel membranes, measuring the thickness of the sample for each test.

3.2.8 Cell culture

The samples were sterilized by ultraviolet radiation for 30 minutes per each side, before cells seeding. The cells were maintained in 75 cm² culture flasks at 37°C in a humidifier incubator under 5% CO₂ in air. The alveolar and endothelial cells must be detached from the flask before being seeded on the membrane, according to the following process. The waste medium was aspirated from the culture flask and the cells were washed with 5 mL of PBS (without calcium and magnesium, to promote the cell detachment). After removing the PBS 2 mL of trypsin was added, and the cells were incubated for 3 minutes. At the end of incubation time, the cell detachment was checked with a microscope and trypsin is inhibited with 5 mL of new culture medium. This time the cell suspension was moved in a falcon of 50 mL, from which 10 µl of medium were taken and placed in a Neubauer counting chamber, to proceed to the cell count. In the following figure (Figure 3.18), the Neubauer chamber is showed, in which cells, located in each red square, are counted. The total number of cells was averaged for the number of squares, multiplied for the millilitres of cell suspension (7 mL) and again multiplied for 10000, a constant factor.

$$\text{Total_cell number} = \frac{\text{tot cells number in the red squares}}{4} \times \text{ml of cells suspension} \times 10000$$

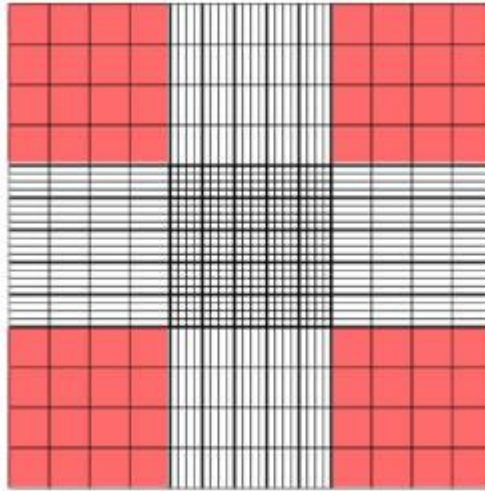


Figure 3.18. Neubauer grid employed for cell count [86]

Knowing the number of cells contained inside the falcon, throughout a mathematical proportion, the millimeters of medium necessary to get the desired number of cells can be collected from the falcon and filled in an Eppendorf.

Total cell number: ml of cell suspension = desired number of cell: x

The Eppendorf with the cell suspension were centrifugated at 1000 rpm, for 8 minutes at 25°C, obtaining cells pellet that is resuspended in pre-warmed (37°C) growth medium.

Next, cells were seeded on slides covered with electrospun PCL and PCL/Gel fibers, on transwell, and on microfluidic devices. On the slides, cells were seeded with a concentration of 30,000 cells/cm². Initially, 20 µl of cell suspension was placed on the slides coated with the nanofibers and on the glass-alone used as control, leaving the epithelial cells to adhere for one hour and the endothelial cells for 4h. Finally, 500 µl of fresh medium was added to the wells of the 48 multiwell containing the slides. Instead, different concentrations were used to seed on the transwell. Specifically, the concentrations employed for A549 cells were 12x10⁴cells/cm², 14x10⁴cells/cm², 16x10⁴cells/cm² and 18x10⁴cells/cm² whereas for HULEC-5a were 10x⁴cells/cm², 12x10⁴cells/cm², 14x10⁴cells/cm², 16x10⁴cells/cm² 18x10⁴cells/cm² and 20x10⁴cells/cm². HULEC-5a were seeded first on the basal side of the membrane, by flipping the transwell, and they could adhere for 4 h, after which 500 µl of endothelial medium was added in the multiwell. Then, A549 were seeded on the upper surface of the membrane and after 1h 300 µl of epithelial medium was added.

On microfluidic devices, A549 were seeded on the top of the membrane at about 14x10⁴cells/cm², instead HULEC-5a were seeded into the lower channel at about 16x10⁴cells/cm². The HULEC-5a were seeded first, along the lower channel, by inserting 10 µl of cell suspension and letting the cells adhere for 4 h, inverting the microdevice. After that, returning the device to its original configuration, a fresh medium is added to the channel and the A549 were seeded by putting a 10 µl cell suspension drop

into the well with the membrane. The epithelial cells could adhere for 1h, at the end of which new medium is added.

The microfluidic devices were maintained in static and submerged culture conditions for three days, taking care to change the medium every 24h hours. Once the alveolar epithelial cells reached the confluence the medium was aspirate from the apical side and the ALI conditions were implemented. 50:50 mixture of epithelial and endothelial medium was introduced in the lower channel to nourish both cells lines. The chips were maintained in a humidified incubator at 37°C for all the experimental time (7d).

3.2.9 Immunostaining

To qualitatively examine the cell culture, occurred on microfluidic devices, the cells were stained with DAPI, which marks the nuclei, and with phalloidine, which binds to actin filaments.

Next, the protocol used is reported. Firstly, the cellular medium was aspired of the chips with a micropipette, after which the cells are rinsed with PBS (without calcium and magnesium). The cells must be fixed with 4% paraformaldehyde for 30 minutes and permeabilized with 0.5% TRITON-X in PBS for 10 minutes by placing the chips on the rocker-shaker. Between these two steps, devices need to be washed for 5-minute PBS on the rocker-shaker. The cells were blocked with 1% (w/v) bovine serum albumin (BSA, Sigma-Aldrich) in PBS for 30 minutes and rinse in PBS.

For the DAPI/Phalloidin protocol, firstly the Phalloidin FTIC or rhodamine phalloidin was incubated in the dark for 40 minutes, preparing a 1:60 BSA solution. After rinsing the samples with PBS for three times, the DAPI solution (1:1000 in PBS) was added, incubated in the dark for 10 minutes and rinsed. Finally, the membrane can be disassembled from the device and analyzed under a microscope

3.2.10 Confocal laser scanning microscopy

The confocal laser scanning microscopy is the imaging technology most used for cell models, which is based on exciting fluorophores with tuneable laser. It features a pinhole between the sensor and the lens assembly, which allows only the focused light to get to the sensor, whereas light not focused is blocked [10]. The technique allows to isolate a specific fluorophore by using a single wavelength without producing noise or background. By labelling the cells with fluorescent dye, high resolution images can be done where cells are localized [10].

In this work, confocal laser scanning microscopy was used to display the nuclei and the cytoskeleton of the two cell lines by using the Nikon eclipse Ti2 (Figure 3.19). Images have been captured by employing the 20x and 60x objectives, the last one was used in oil immersion to reproduce high quality and high contrast images [87]. Image J was exploited to merge the images from different channels.



Figure 3.19. Nikon eclipse Ti2 confocal laser scanning.

3.2.11 Cell viability assay

Cell viability was quantifying through CellTiter-Blue® Cell Viability Assay (Promega), based on the ability of the living cells to transform a redox dye (resazurin) into a fluorescent product (resorufin) [88]. In this work, cell viability was estimated on slides on which PCL and PCL/Gel fibers were spun, to evaluate the material biocompatibility and on transwell, where a concentration optimization was done. Different time points were considered (24h,72h, 1w,2w). In addition, to compare the cellular metabolic activity between submerged and ALI conditions vitality was assess on microfluidic devices after one week of culture. The working solution was obtained by mixing 20 µl of CellTiter-Blue® Reagent to each 100 µl culture medium. The multiwell containing the samples were filled with the working solution. The samples seeded with A549 were incubated for 90 min and the HULEC-5a for 120 min. The data obtained from the Synergy HTX BIOTEK plate reader (Figure 3.20.) were analysed using Excel.



Figure 3.20. BioTek™ Synergy™ HTX Multi-Mode Microplate Reader [89]

4. RESULTS AND DISCUSSION

4.1 Fabrication of the lung on chip

Here, the fundamental steps, that led to the realization of the complete device, are reported together with the optical characterisation at the microscope carried out.

4.1.1 Laser ablation and production of the PMMA mold

4.1.1.1 Top layer mold

After manufacturing the mold through the laser ablation technique, the geometry was analysed with the Leica digital optical microscope. The measurements are in agreement with the CAD nominal value. In particular, the side channels measure 1.16 x 12.95 mm; instead the inlet and the outlet of the central channel measure 1.6 mm in diameter; and the well for the cells housing 2.77 mm in diameter. In the figure below (Figure 4.1), the image taken under the optical microscope and the photo of the complete mold are shown. These images highlighted as the lens of laser galvo head did not produce a perpendicular cut to the surface, in fact the geometry narrows in height. Despite that the fabricated mold maintained a good resolution, in fact the obtained dimensions are comparable with the ones requested. In this regard, all measurements were taken considering the outermost edge. Instead, in the photo on the right (Figure 4.1 (B)) the external frame and the cylinder for the creation of the central well, created by laser ablation, are shown.

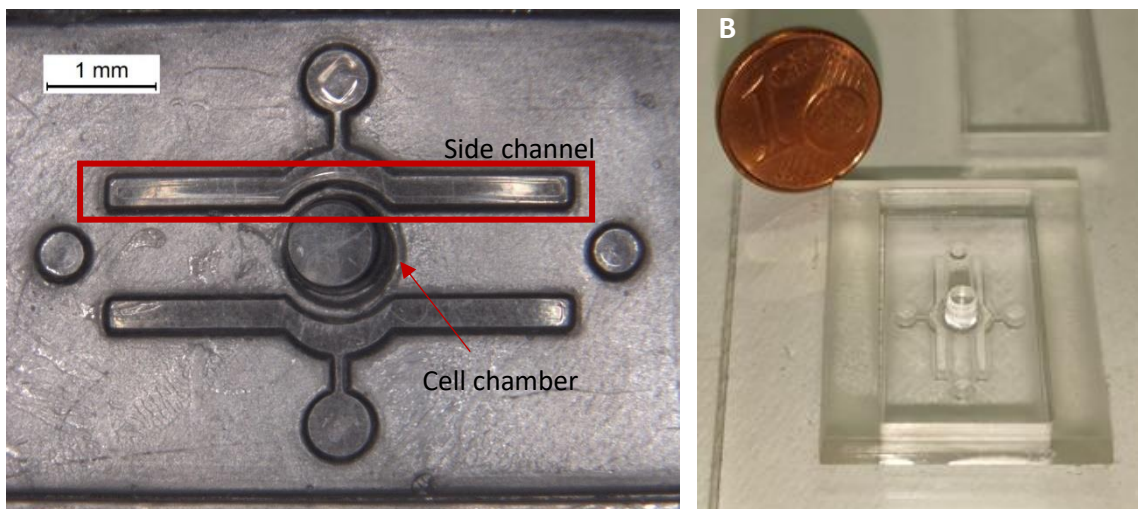


Figure 4.1. Top layer mold: A) optical microscope image, B) photo of the top layer mold.

4.1.1.2 Bottom layer mold

Likewise, the optical microscope was exploited to derive the measurements of the obtained geometry (Figure 4.2). The measures of the central channel are 1.68 x 17.40 mm, the cell chamber has a diameter of 3.15 mm and, instead, the pillars an average diameter of 390 μm . The measures have been carried out considering the external edge of the pattern, as in the previous case. In Figure 4.2, a magnification of the pillars is shown to demonstrate that the laser ablation allows to replicate the desired geometry. In addition, the side and central channels are also easy to identify. Also, in this case the external frame, designed to ensure a 2mm thick replica, is clearly visible from the photo taken (Figure 4.2 (B)).

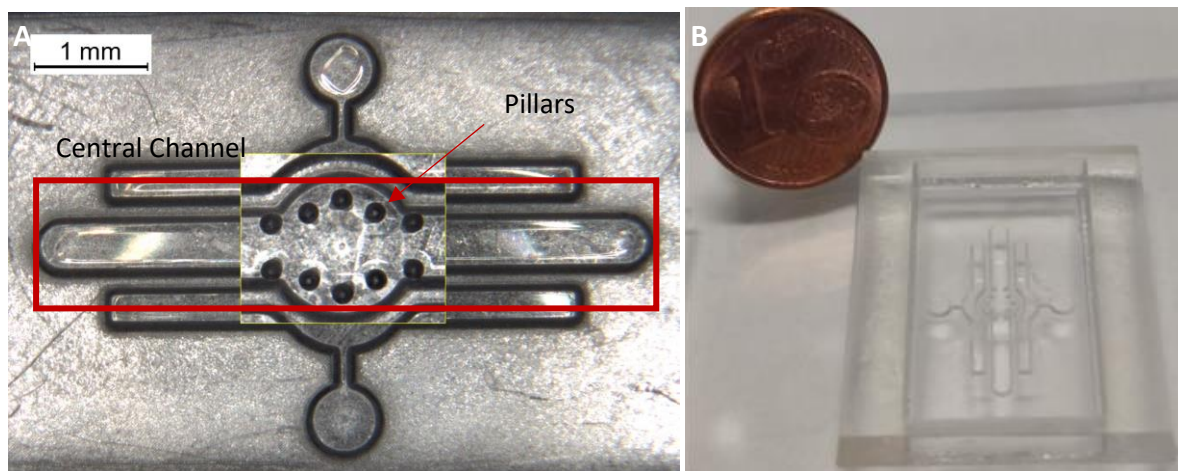


Figure 4.2. Bottom-layer mold: A) optical microscope image, B) photo of the bottom layer mold.

To achieve the mold configurations showed in the figure above, the laser parameters were varied. In particular, the velocity was reduced passing from 100 mm/s to 75 mm/s, because the laser, proceeding more slowly along the material, can reproduce the geometry more precisely. In fact, a higher velocity leaves lower time at the CO₂ beam to burn and vaporize the material losing in resolution and digging less deep in the PMMA. This is not convenient, mainly for the pillars formation that must be higher enough to support the membrane, purpose which they are designed for. In addition, also the filling parameters, the space lines and the angles, were changed in order to improve the texture of the pattern and to eliminate the defects on the mold created, for examples, by choosing an angle of 90°. SU-8, used in the photolithography technique, is challenging to process because it requires careful optimization of the process parameters [37]. In addition, the produced mold is likely to break easily when the replica is peeled off [36]. For these reasons, in this work, the laser ablation technique was chosen, which allowed to obtain the molds quickly, maintaining a good geometry resolution and respecting the required measures, as demonstrated previously.

4.1.2 Replica molding and fabrication of the layers in PDMS

Replicas were also measured under an optical microscopy, finding values comparable to the theoretical values set on the CAD (Table 4.1).

4.1.2.1 Top layer

The characteristic sizes of the first layer are: side channels of 0.96 x 11.30 mm, central well for the housing of the membrane of 2.75 mm in diameter and inlet and outlet holes of the central channel of 1.51 mm in diameter. In the Figure 4.3, the optical microscope image of the top replica is shown. The PDMS is an optical transparent material, in fact all the components (the side chamber, central well and inlet and outlet) are visible by optical microscopy, confirming that the replication was successful.

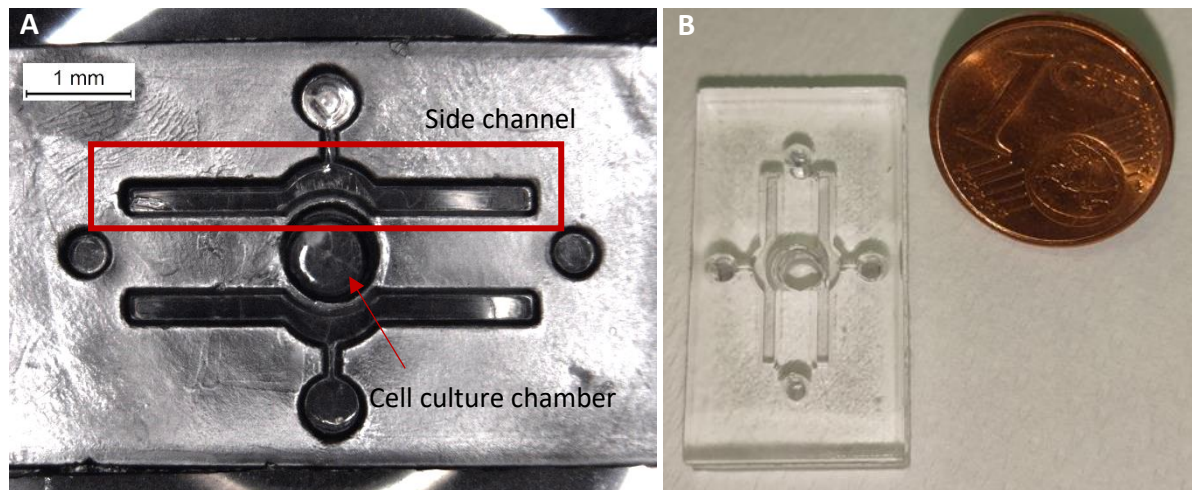


Figure 4.3. Top layer replica: A) optical microscope image, B) photo of the top layer replica.

4.1.2.2 Bottom layer

In the bottom layer the values obtained are the following: central channel of 1.33 x 14.93 mm, cell chamber of 2.6 mm in diameter and pillars with an average diameter of 480.55 μm . Also, in this case the geometry was evaluate by optical microscopy, to assess that all the elements have been realized correctly. Pillars are clearly visible from Figure 4.4. All the pillars required were produced, remaining separated from one another.

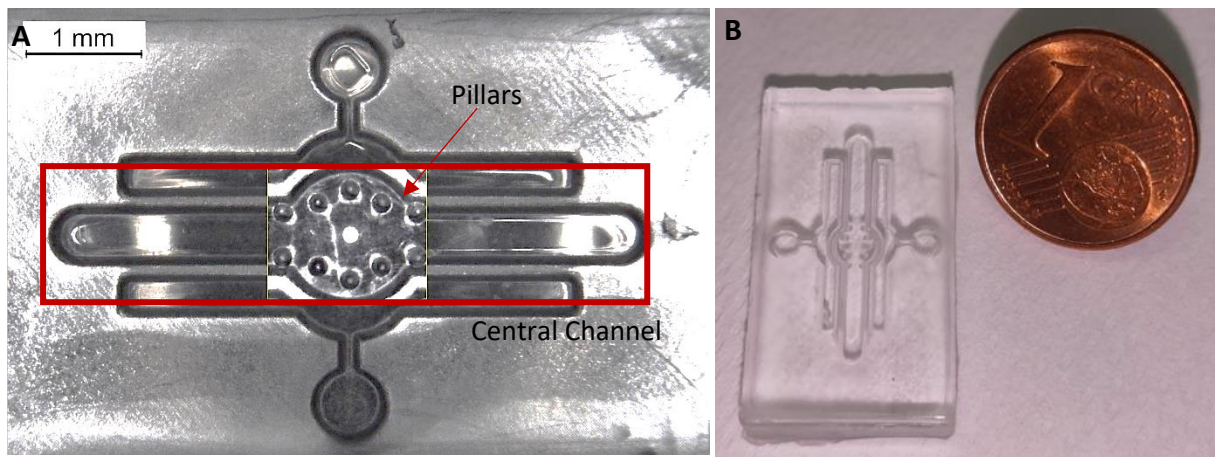


Figure 4.4. Bottom-layer replica: A) optical microscope image, B) photo of the bottom layer replica.

MEASURE (mm)				
LAYER		CAD	MOLD	REPLICA
TOP	Side channels	1x 13.40	1.16 x 12.95	0.96 ± 0.03 x 11.30 ± 0.42
	Central well	3	2.77	2.75 ± 0.04
	Inlet/outlet holes	1.5	1.6	1.51 ± 0.06
BOTTOM	Central channel	16	1.68 x 17.40	1.33 ± 0.07 x 14.93 ± 0.42
	Central chamber	3	3.15	2.6 ± 0.1
	Pillars	0.2	0.39	0.480 ± 14

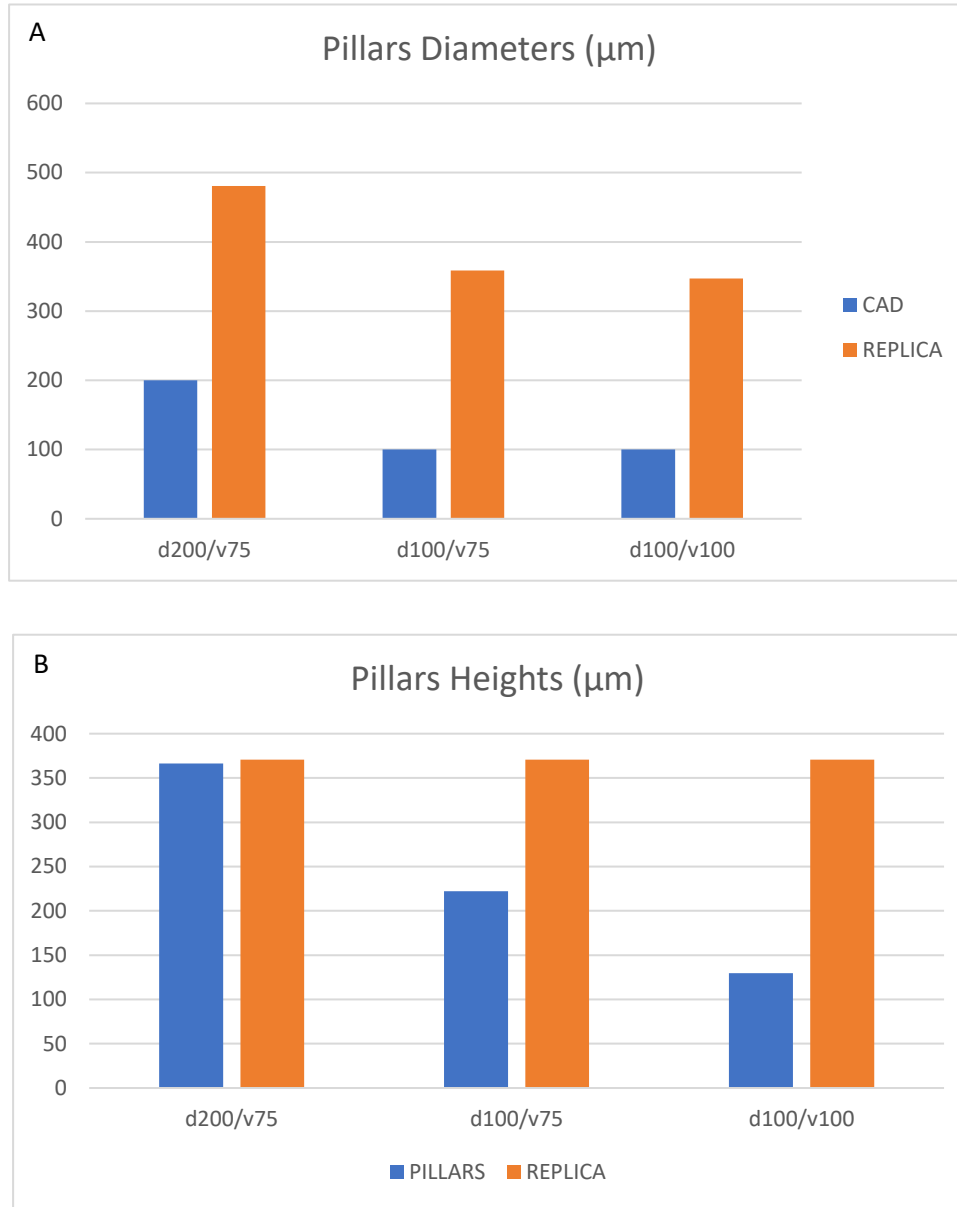
Table 4.1. Summary table of the layers measures and standard deviation

Pillars

As proven by the table above, the diameter of the pillars (both in the mold and in the replica) is very different from the desired one (200 μm). To optimize its measure, two different laser speeds were tested (75 mm/s and 100 mm/s) and the diameter on the CAD was halved (100 μm). In order to select the optimal set of parameters (speed and diameter), considering the membrane support role that the pillars are called to play, the sections were examined under optical microscopy.

In the following, the graphs (Graph 4.1) of the diameters and heights of the three different tests performed (d.200 μm/vel. 75 mm/s; d.100 μm/vel. 75 mm/s; d.100 μm/vel. 100 mm/s) are shown. From the first one it can be observed that the decrease of the CAD diameter allows to obtain replicas with smaller pillar diameters (without a significant difference between the two speeds). Instead, the heights graph (Graph 4.1) shows that by increasing the speed and by decreasing the diameter, pillars with a height considerably lower compared to the rest of the geometry reproduced are obtained. This

involves, as the images of the sections under the microscope (Figure 4.5) demonstrated, the formation pillars that does not allow them to perform the task of support. In conclusion, the set of parameters selected was the starting one (200 $\mu\text{m}/75\text{mm/s}$), which despite leading to the formation of pillars with larger diameters, allows them to perform the task for which they were designed.



Graph 4.1. A) graph of the pillars diameters, B) graph of the pillars height



Figure 4.5. Section of A) d200/v75, B) d100/v75, C) d100/v100 samples, scale bar:500 μm . Pillars are circled in red.

The project was modified during the work to facilitate its connection, through the silicone tubes, to the pump for trials of the mechanical implementation. The adjustments were conducted only for the side channels, which were enlarged, for allowing a stronger application of the mechanical force, and the holes of inlet and outlet were halved planning an only hole for each lateral channel, so less tubes are needed. In the figure, a CAD of the old project is shown to provide an idea of the changings occurred (Figure 4.6.).

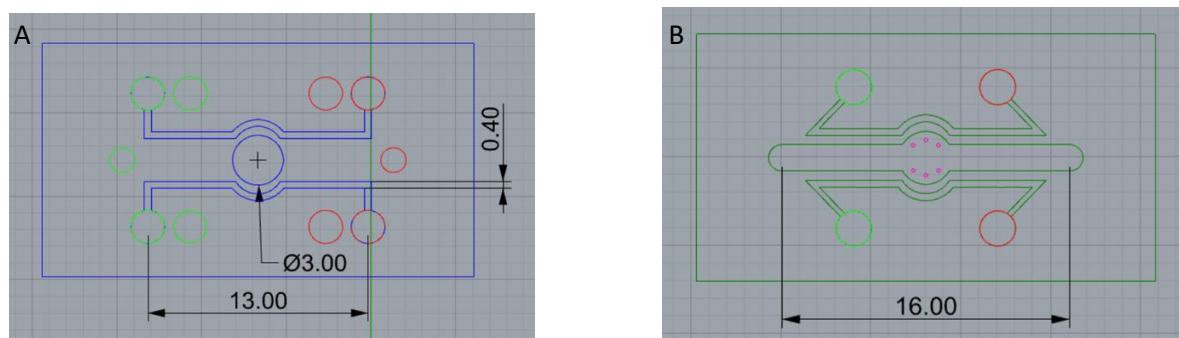


Figure 4.6. First version of A) Top-layer CAD, B) Bottom-layer CAD

4.1.3 Electrospinning and membranes production

Polymeric membranes were fabricated by electrospinning after preparing PCL and PCL/Gel solutions. The electrospinning flow rate and voltage of the PCL solution were optimized to obtain homogeneous and bead-free fibers. Then, the morphological and mechanical properties of electrospun membranes were investigated. Lastly, the membranes were placed inside the device to perform cellular tests.

4.1.3.1 Parameters optimization

Optimization was performed only for PCL membranes by varying the flow rate and voltage. In particular, the former was evaluated in a range of 400 $\mu\text{l}/\text{min}$ -600 $\mu\text{l}/\text{min}$ while the latter was increased from 14 kV up to 20 kV, instead the distance was kept constant to 12 cm. Table 3.6, reported in section 3.2.3.1 of chapter 2, summarizes all the parameters used for the different tests. A first evaluation of the trend of the tests was carried out from the SEM images (Figure 4.7) that show the presence of defects when low flow rate and voltage parameters were used (Figure 4.7, B-G, I). For this reason, a more detailed morphological investigation was performed only for the membranes A and H showed in Figure 4.7.

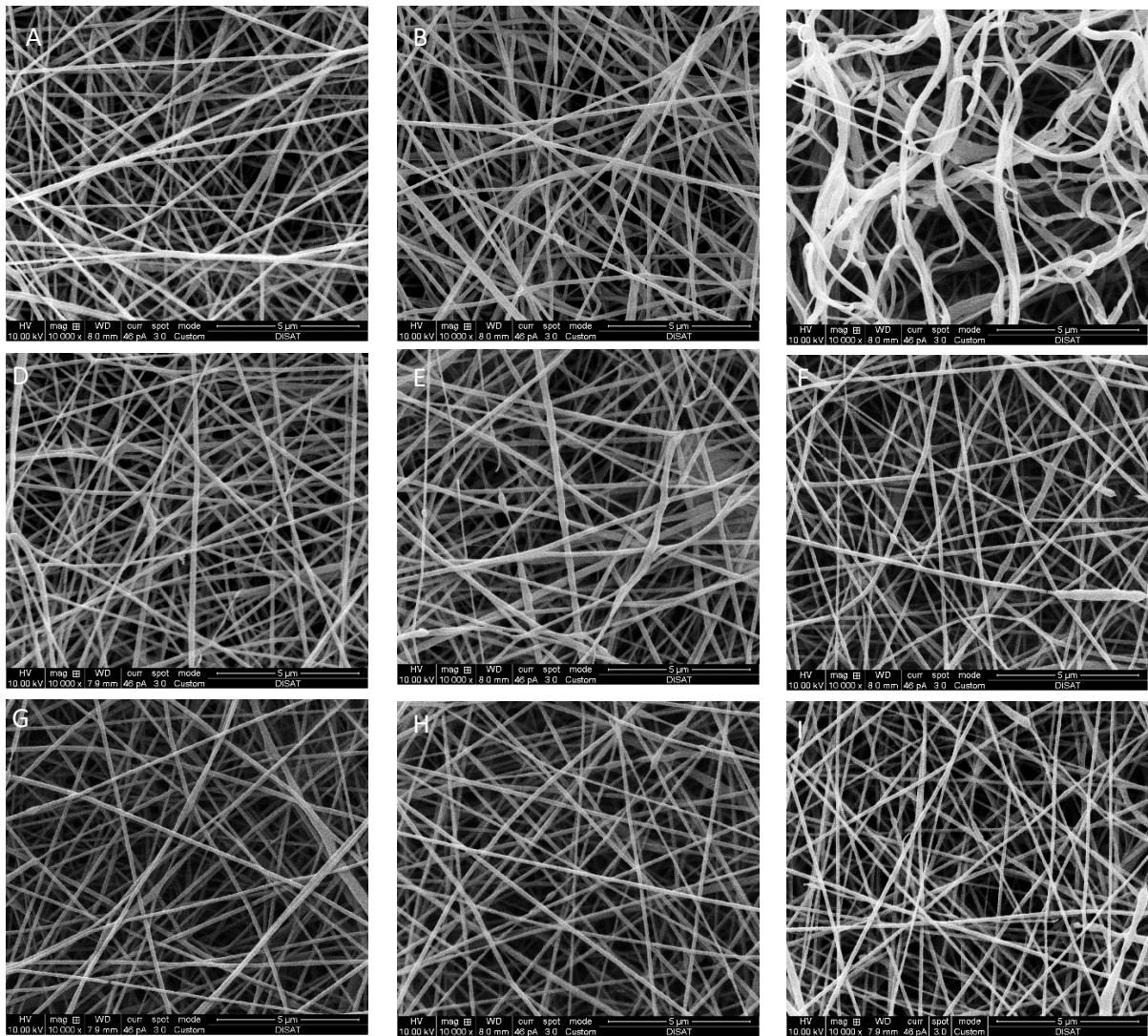


Figure 4.7. SEM images of: A-C) 500 μ l/min and 16 kV(A); 20kV(B); 14kV(C); D-F) 400 μ l/min and 16kV(D); 20kV(E);14 kV(G); GH) 600 μ l/min and 16kv (G); 20kV (H); I) 550 μ l/min-16kV PCL membranes. Magnification bars: 5 μ m

The combinations of parameters that allow to obtain more uniform fibers are: 16kV-500 μ l/min and 20kV-600 μ l/min. For this two-best set of parameters, the diameter distribution and porosity were evaluated to select the most suitable one.

4.1.3.2 Morphological characterization

The membrane morphology was analysed by FE-SEM microscopy. The images of the PCL 16_500, PCL 20_600 and PCL/Gel membranes can be observed in the figure below (Figure 4.8.).

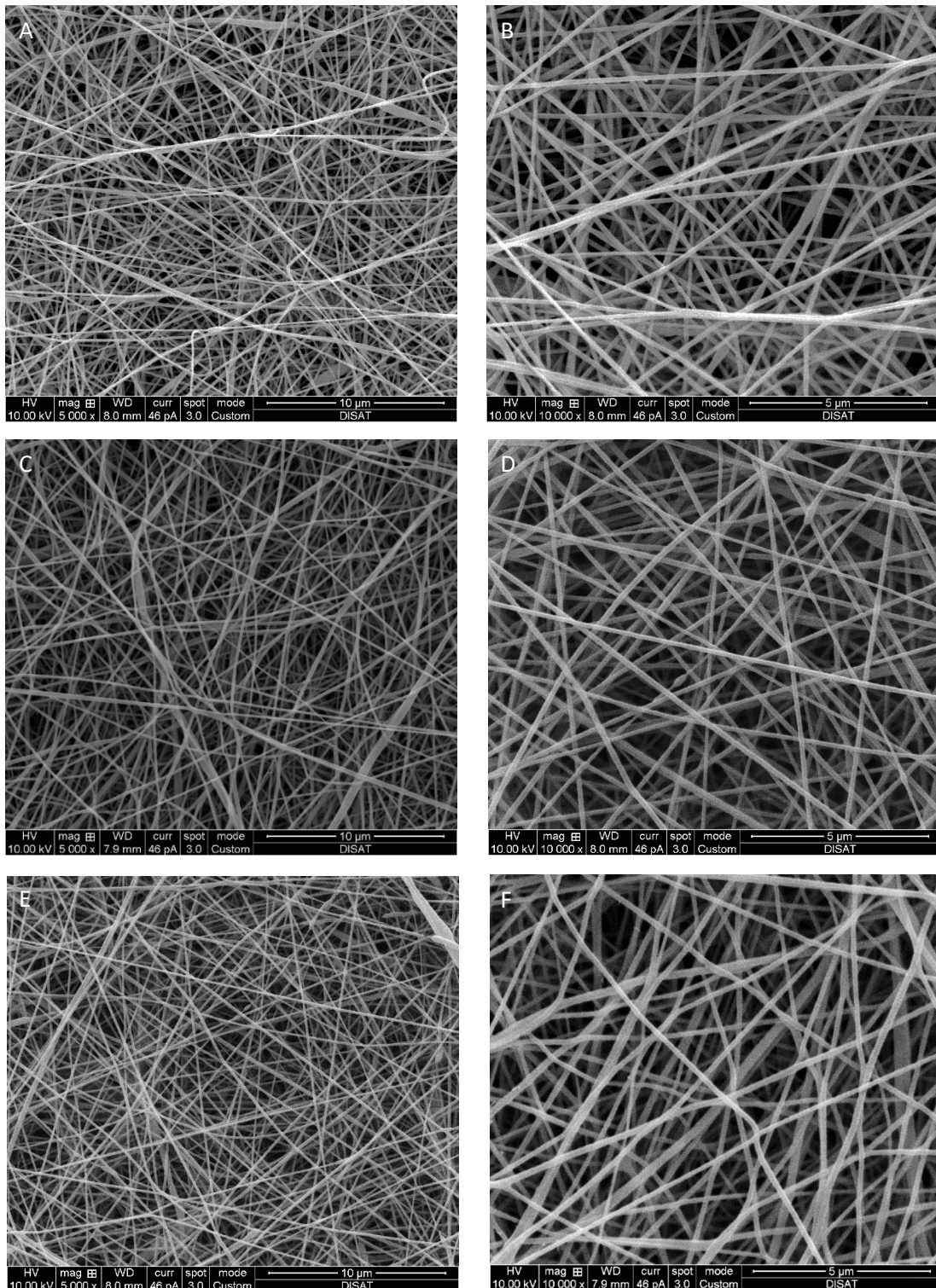
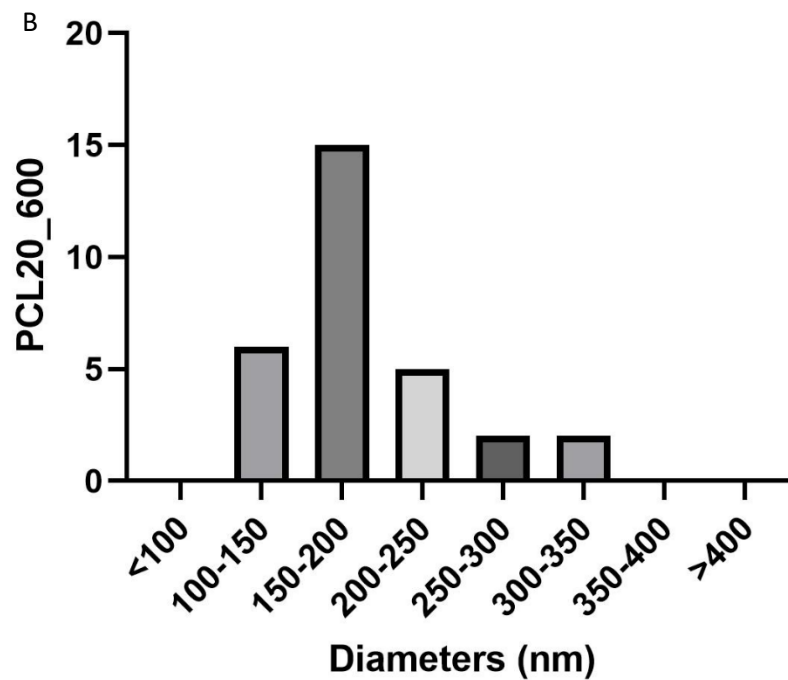
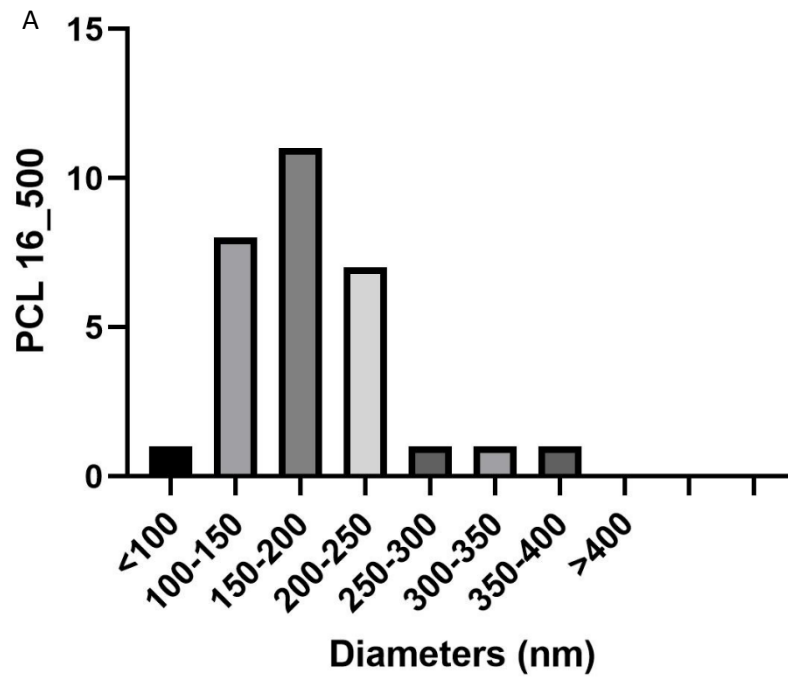
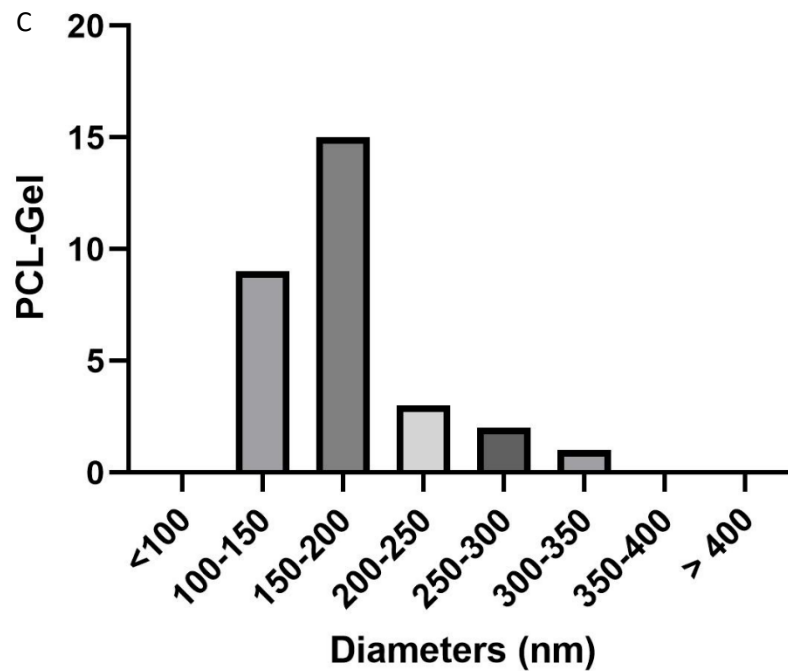


Figure 4.8. SEM images of: A-B) PCL 16_500 membrane. C-D) PCL 20_600 membrane; E-F) PCL/gel membrane. Magnification bars: 10 µm (A-C-E), 5 µm (B-D-F).

The PCL/Gel membranes show a bead-free, random, and smooth fibers as proven in *Gautam et al. work* [90].

The diameters distribution obtained through the analysis with Image J is displayed for each membrane (Graph 4.2.). Moreover, in the table below a summary of the fiber diameter and the pore diameters is listed (Table 4.2.).





Graph 4.2. Diameters distribution of A) PCL 16_500; B) PCL 20_600; C) PCL/gel

	PCL 16_500	PCL 20_600	PCL/Gel
Fiber diameters (nm)	191± 74	185± 52	177± 47
Pore diameters (nm)	511 ± 373	463 ± 314	394 ± 227

Table 4.2. Summary table of the pores and fibers dimensions

Due to the presence of smaller diameters and pore in the PCL 20_600, membranes used for further investigation were prepared by setting this process parameters. Moreover, these results indicate that the fiber diameters and pore diameters of PCL/Gel membranes are smaller than that of PCL fibers, as shown in the work of *Gautam et al.* and of *Ghasemi-Mobarakeh et al.* [90] [91]. In fact, gelatin is a polyelectrolyte polymer that has several ionizable groups and releases ions within the solvent, as opposed to PCL, which is a non-ionic synthetic polymer. This was demonstrated by *Son et al.*, who proved that the addition of a polyelectrolyte to the solution increases its charge density resulting in the formation of thin and smooth fibers [92].

4.1.3.3 Mechanical characterization

Cyclic mechanical tests were conducted, performing 100 cycles of stress with 10% strain and 0.2 Hz frequency (about 12 cycles per minute counted). These values were picked in accordance with the physiological parameters of a healthy lung, which are, also, used in the literature for the actuation of respiratory motion in microfluidic devices [42][45]. To evaluate the fatigue resistance of PCL and PCL/gel membranes under physiological parameters, uniaxial and biaxial tests were performed.

Cyclic uniaxial testing

The data of the tests were examined with excel, yielding very noisy graphs that needed to be filtered with Matlab. In the following, the stress-strain graphs (before and after filtering) are shown for both materials (Figure 4.9.).

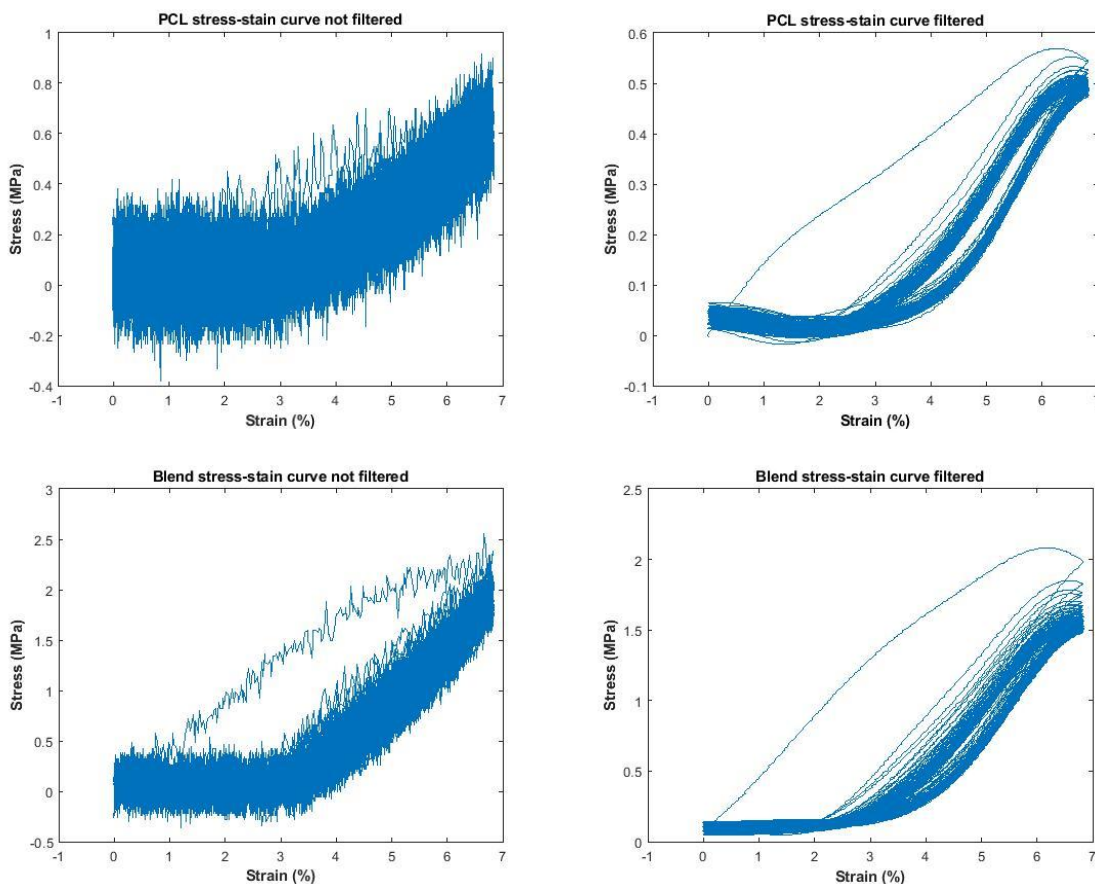


Figure 4.9. Stress-strain curves of PCL and PCL/gelatin membranes (not filtered and filtered)

From the figures obtained, it can be observed that each cycle forms a hysteresis, from which the Young's modulus has been obtained as the angular coefficient of the linear section visible from the graph itself. Finally, the Young's modulus of the material was calculated by averaging the moduli of all 100 cycles. For PCL membranes, a modulus of 16.60 ± 1.45 MPa was obtained, while for PCL/Gel membranes a value of 40.16 ± 2.14 MPa was calculated. These outcomes are in accordance with the work of *Ghasemi-Mobarakeh et al.* which establish that by adding gelatin to PCL, the elastic modulus

increases compared to PCL-alone fibers [91]. Thus, the addition of gelatin implies a decrease in the mechanical strength of the fibers due to its poor mechanical properties but mixing it with PCL allows to obtain membranes with good fatigue resistance.

Cyclic biaxial testing

The biaxial tests were implemented on square specimens with 3 mm side, keeping the same parameters used for uniaxial tests. The data were analysed through excel and filtered with matlab. Two graphs were achieved from every specimen one for each axis, testing three specimens for both materials (Figure 4.10). As in the previous tests, the Young's modulus of PCL is lower than the one of the PCL/Gel, due to the presence of gelatin. In particular, the elastic modulus obtained for PCL/gel are 27.72 ± 1.09 Mpa for one direction and 28.22 ± 1.19 Mpa for the second, instead for PCL we found 8.63 ± 1.86 Mpa and 6.88 ± 0.074 Mpa. The data obtained in the biaxial trials are in accord with the uniaxial ones in fact the modulus for each direction is about half of that found in the uniaxial case, showing the stress has not a favoured direction. It was not possible to find scientific evidence for this type of test and it is therefore necessary to repeat them to evaluate if the behaviour is reproducible.

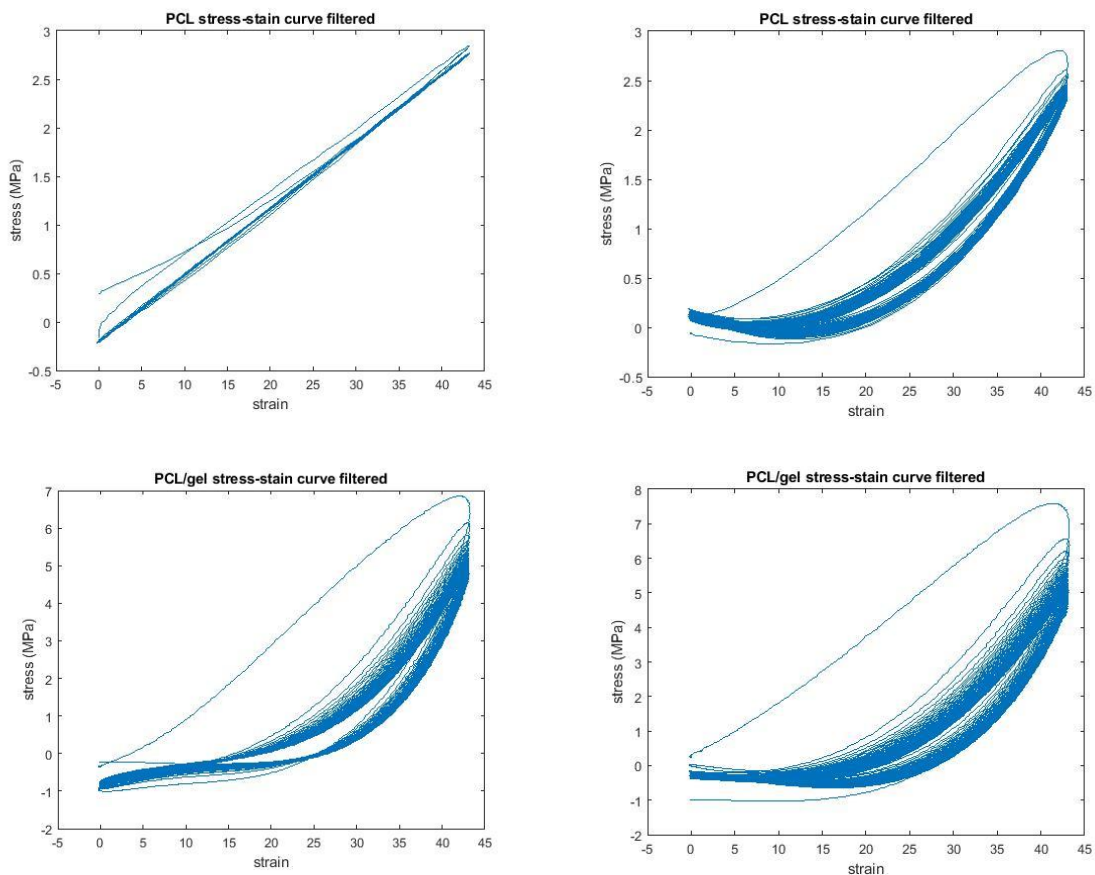


Figure 4.10. Stress-strain curves of PCL and PCL/gelatin membranes, biaxial tests. One graph for each direction.

4.1.4 Assembly of the device

The plasma is an ionized gas with a total zero electric charge, and it is considered the fourth state of the material. By adding energy to a gas, the shell of atom breaks down into ions, electrons and charge molecules. There are a wide range of application in which the plasma technology can be employed such as surface cleaning, etching, coating and surface activation [93]. The latter is the one used in this thesis's work by exploiting the low-pressure plasma technology, which consists in producing the vacuum inside the working chamber with a vacuum pump. After this the working room is filled with the process gas until it reaches the exercise pressure, when the high frequency generator is activated and the plasma can be done on the samples [93].

By exposing the PDMS to the plasma oxygen the methyl groups (Si-CH_3) on the surface are replaced by the hydrophilic silanol groups (Si-OH) achieving a decrease of hydrophobicity. At this point, the process of adhesion can be carried out by putting in contact two PDMS replicas which, after the surface modification, can form Si-O-Si irreversible bond [35] [37].

Also, the PCL and the PCL/Gel membranes need to be treated to ensure the hydrophilicity and to guarantee the same boundary conditions respectively, like already explained in the materials and methods section.

In the figure below, a section image at the optical microscopy and a photo of the bonded device are reported (Figure 4.11). The first one shows how the electrospun membrane fits perfectly inside the chip and it can stay completely stretched out on the sustaining pillars.

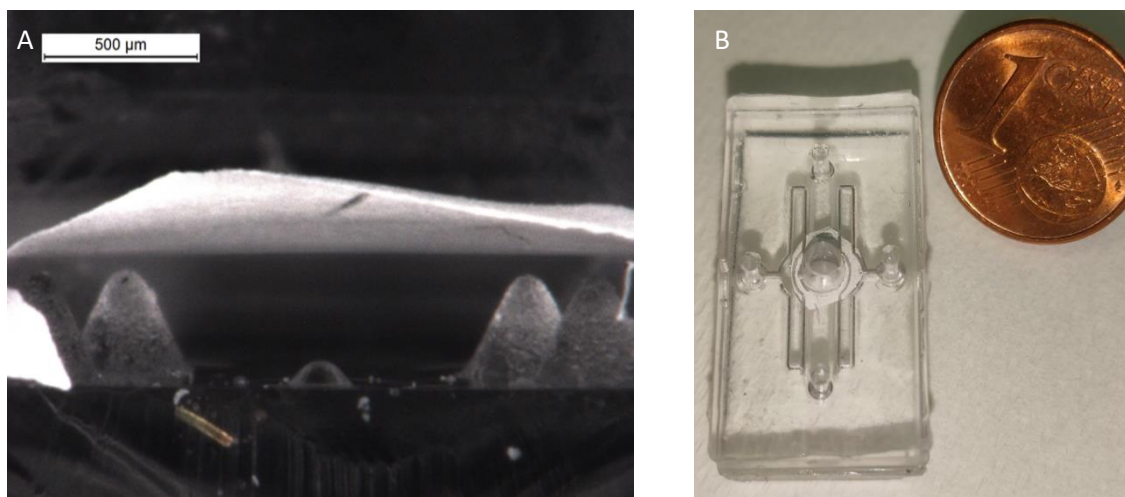


Figure 4.11. A) bonded device section at the optical microscopy; B) photo of the entire chip

For evaluating if the bonding process is correctly made some leakage tests must be performed. In the following paragraph they are described in detail.

4.2 Leakage tests

These tests were performed to validate the chip layers design and bonding, they were conducted by the usage of blue food dye (from Fulgar SpA) dispersed in distilled water under a digital microscope (Leica DVM 2500), as reported by *Marasso et al.* [94]. A syringe was filled with the solution described above which was pushed inside the microfluidic geometry to check that the fluid stays confined to the channels. Indeed, the leakage test is necessary to evaluate that the assembling process correctly occurred and that the bonding between the two replicas is enough strength. All the process can be conducted with a static or a dynamic method, if, in the first mode, the liquid is driven manually along the pattern, in the second case the flux is controlled by a syringe pump. The photo below (Figure 4.12) shows how by sliding the flow throughout the device pattern no leakage happens, proving that the bonding process enables to form a PDMS-PDMS bond desired for the task required.

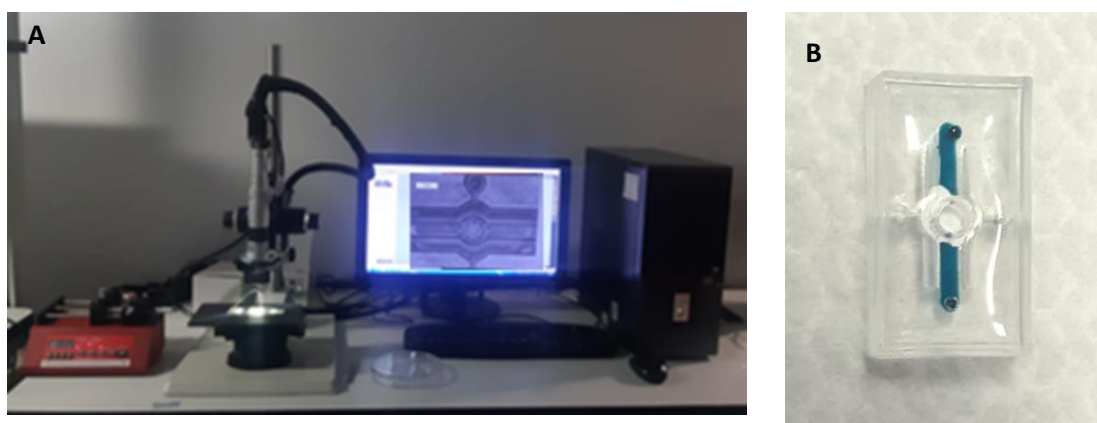


Figure 4.12. A) complete setup of the leakage test: a syringe pump, an optical microscope, and a computer. B) a photo of the device filled with dye which confirms its good tightness.

To assure that all the test-pieces fabricated have a good tightness, it is necessary that the bonding process benefits from specific features. Firstly, the PDMS replicas should not contain dust and debris which can affect the bond between the two; for this reason the layers are washed in ethanol with ultrasound. In addition, the assembly should be rapid, to not lose the surface modification carried out, and precise in order to perfectly match the two replicas. So, through the laser ablation technique a container was produced, with the same width and length dimensions and the same thickness of the complete device, which has the purpose to help in the alignment of the replicas, inside which the PDMS layers were bonded (Figure 4.13).



Figure 4.13. Photo of the box of alignment produced by laser ablation.

4.3 Cellular tests

To assess cell adhesion, fluorescence microscopy analyses were conducted, staining nuclei and actin filaments; instead, the cells viability assay (resazurine) was implemented to study cells metabolic activity. Both tests were performed firstly on electrospun fibers on slides, then on transwells and finally on microfluidic devices. In particular, to evaluate the material biocompatibility, cellular assays were performed on glass coverslip slides coated with both PCL nanofibers (used as controls) and PCL/Gel membranes. Then, the seeding was performed only on PCL/Gel mats, both on the transwell inserts to optimize cell density that allowed to reach the confluence after 72h of co-culture, and on the chips. Specifically, a co-culture of alveolar epithelial cells (A549), and pulmonary capillary endothelial cells (HULEC-5a), seeded respectively on the upper and lower side of the membrane, was carried out. After three days, when the cells have reached the confluence, air/liquid conditions are generated with the purpose of compare the submerged culture conditions with those in ALI.

4.3.1 Evaluation of the material biocompatibility

PCL and PCL/Gel solutions were electrospun directly on laboratory slides, which were moved inside the multiwell for cell seeding, along with a glass-alone control. To assess and compared the cell adhesion and viability on the two different mats, A549 and HULEC-5a were seeded with a density of 30.000 cells/cm²).

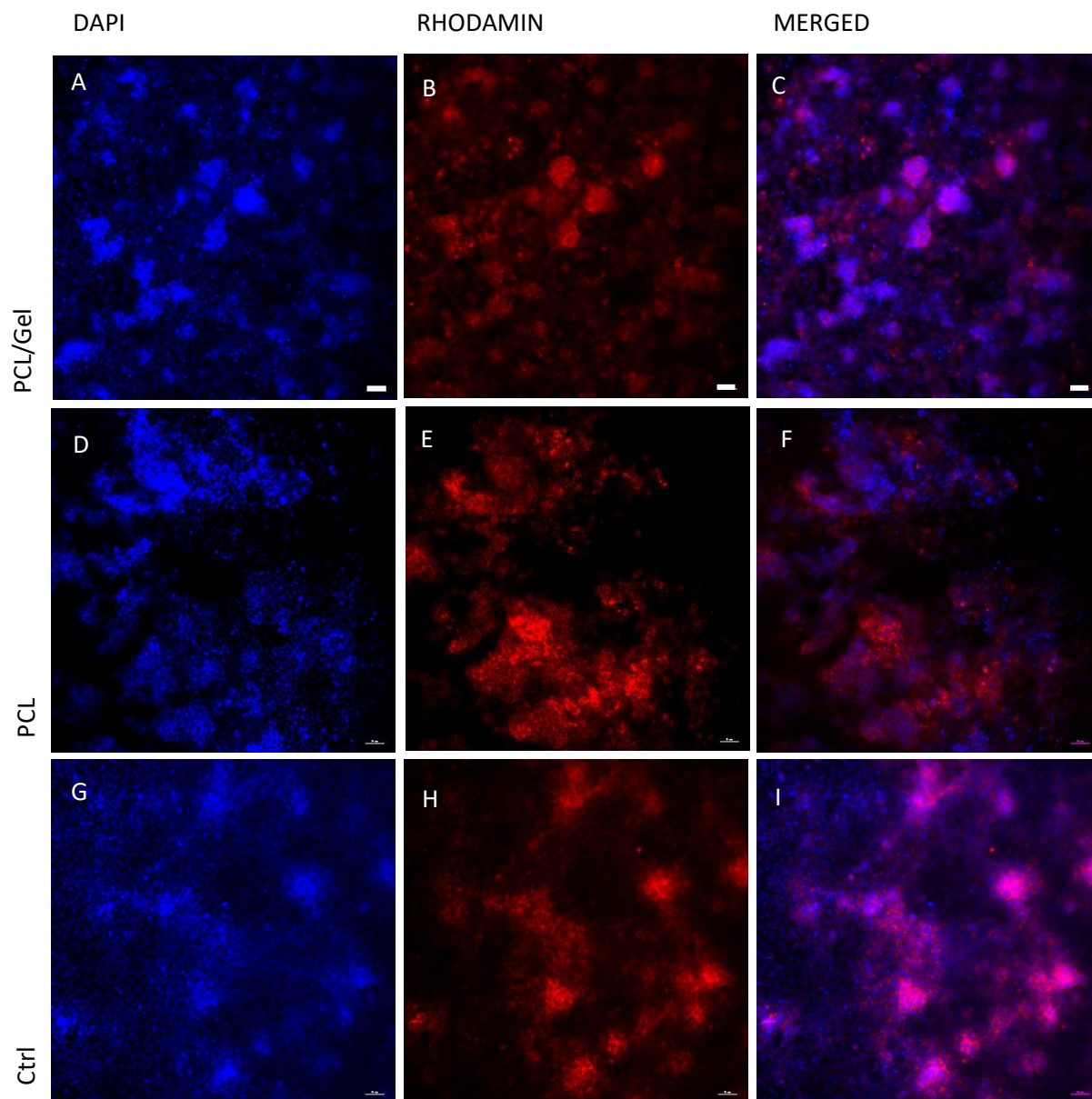


Figure 4.14. Confocal fluorescent images of A549 seeded on: A-C) PCL/Gel, which shows the better adhesion; D-F) PCL, and G-I) glass, as control. The cells were stained with: A-D-G) DAPI for showing the nuclei and B-E-H) Rhodamine, for evaluating the actin filament. C-F-I) DAPI and Rhodamine images merged with image J. Scale bar 50 μ m.

The Figure 4.14 shows that A549 cells, after two weeks of culture, grow on the substrate forming clusters of cells, on the contrary HULEC-5a (photos below, Figure 4.15) grow creating a uniform monolayer.

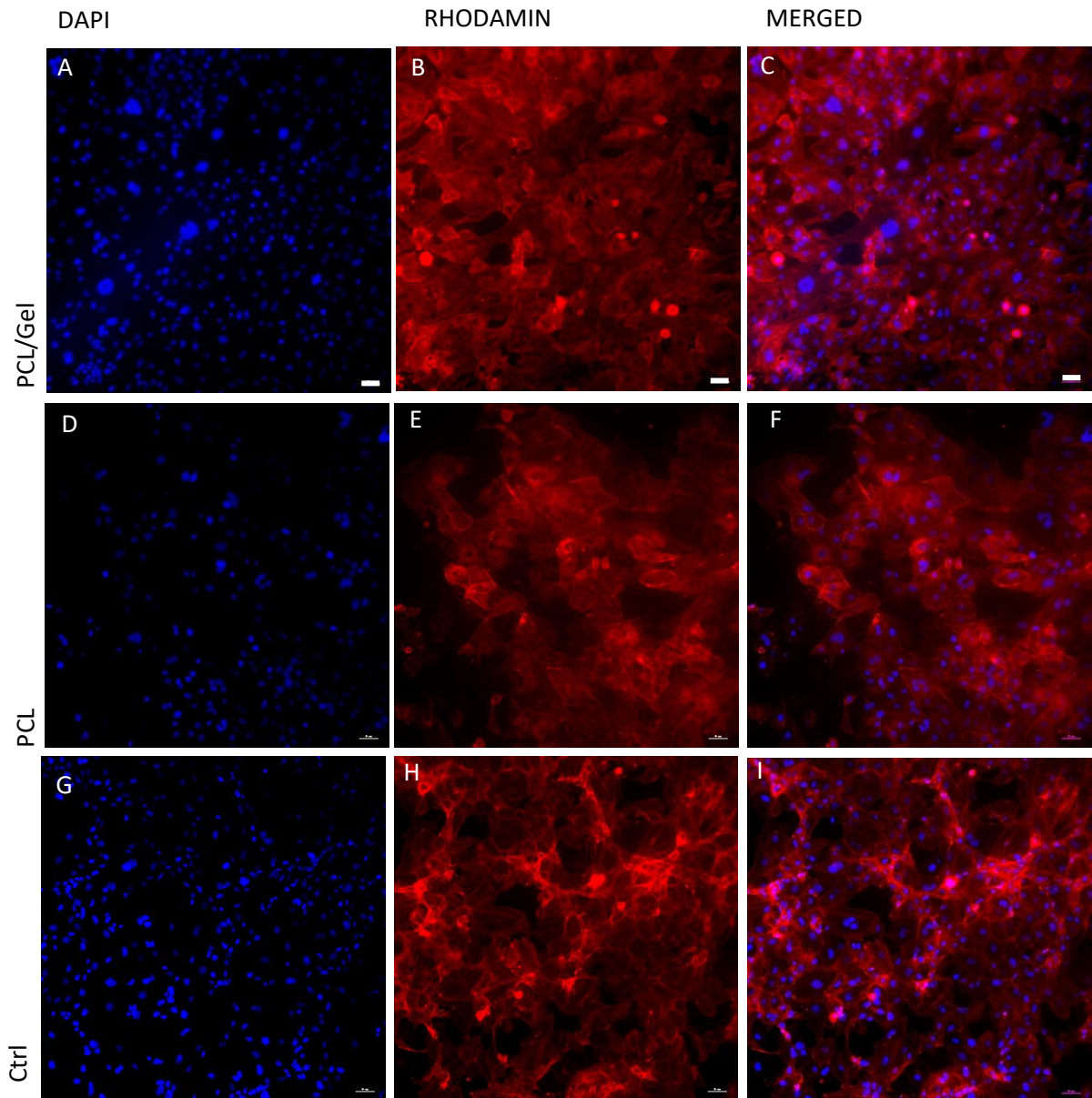
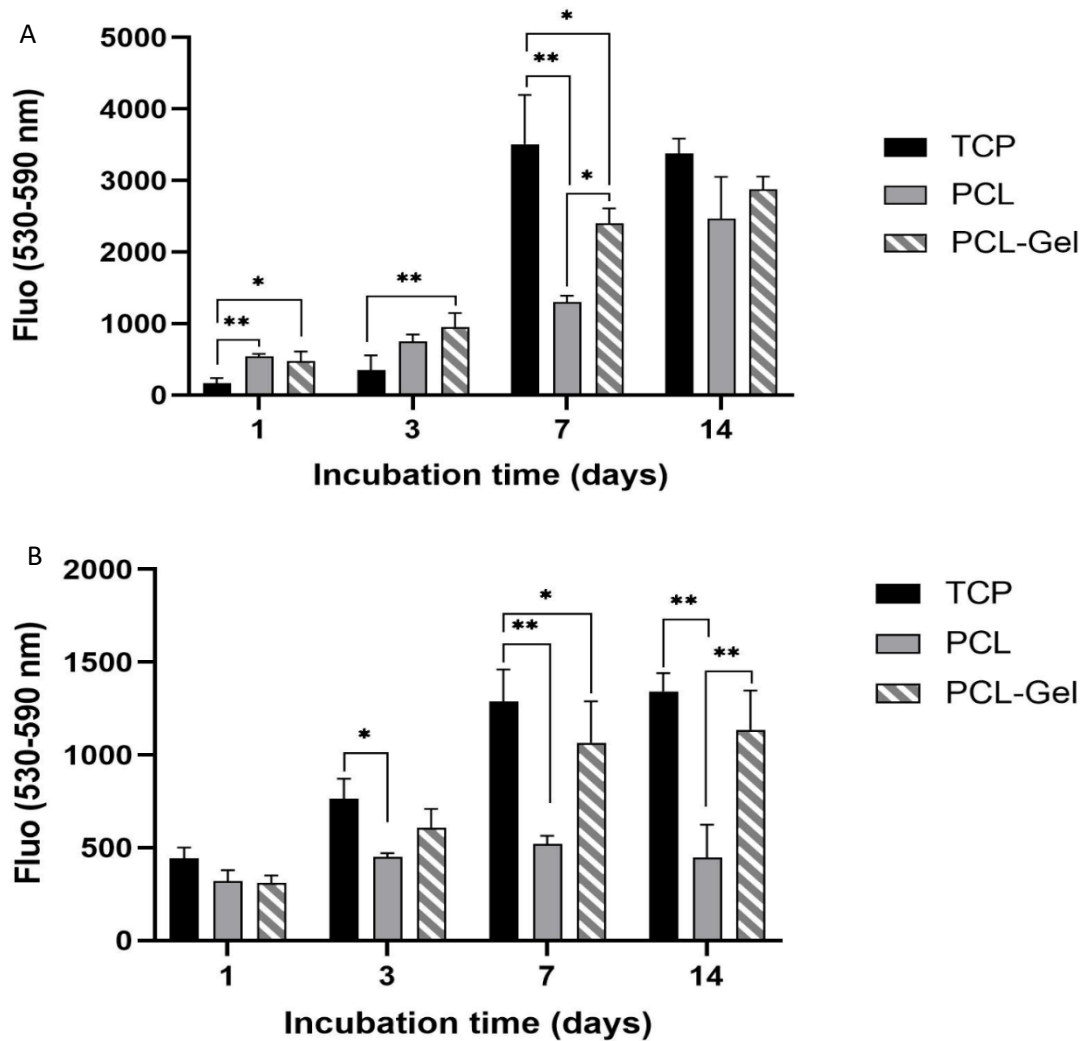


Figure 4.15. Confocal fluorescent images of HULEC-5a seeded on: A-C) PCL/Gel, which shows the better adhesion; D-F) PCL, and G-I) glass, as control. The cells were stained with: A-D-G) DAPI for showing the nuclei and B-E-H) Rhodamine, for evaluating the actin filament. C-F-I) DAPI and Rhodamine images merged with image J. Scale bar 50 μ m.

Despite both cell lines could grow and adhere on PCL and PCL/Gel membrane, the adhesion is higher on PCL/Gel membrane, as demonstrate by DAPI and rhodamine staining. These results are in line with the work of *Zhang et al.* and confirmed the good compatibility of PCL/gelatin scaffolds for both A549 and HULEC-5a cells, promoting their growth [95]. In fact, the presence of the gelatin imparts hydrophilic property to the blended material, resulting in a cell friendly substrate, unlike PCL which is hydrophobic material. Moreover, the natural polymer have peptide sequences able to generate a

favourable environment for cell adhesion and proliferation [95]. Indeed, the addition of gelatin to PCL allows to recruit cell adhesion molecules, generating greater interaction forces between cells and the scaffold than the PCL-alone fibers [91]. Finally, cell migration on PCL/Gel substrates is also improved due to the gradual dissolution of the gelatin component during cell culture [95].

Results achieved by the staining of the nuclei and cytoskeleton were validated by the assessment of the cell metabolic activity, which was performed at 24h, 72h, 7d and 14d, to compare cell viability on the different materials. Tissue culture plates were used as control. The data obtained were and the graphs are shown below (Graph 4.3).



Graph 4.3. Cell viability assay on: A) A549 and B) HULEC-5a at 1d, 3d, 7d, 14d. Non normalized values. Data are reported as the mean \pm SD * p <0.05 and ** p <0.005.

The two graphs represent the trend of cell viability for up to two weeks on the two materials considered, the PCL and the PCL/Gel. In particular, the results confirmed that the A549 and the HULEC-5a can adhere and grow on both materials, as already demonstrated by *Ghasemi-Mobarakeh et al.*, increasing their activity over time [91]. As found by *Dias et al.*, after 24h and 72h there are no substantial differences between PCL alone and the blend probably because many of the cells are still adhering or adapting to the substrate surface [96]. On the other hand, by increasing the incubation time, cells on blend display a higher metabolic activity than those on the PCL due to the presence of integrin-binding sites on the gelatin [96]. The confluence on TCP is reached after 7 days instead in the membranes 14d are necessary to reach the confluency. In general, greater metabolic activity in A549 than in HULEC-5a was observed.

4.3.2 Optimization of the cell concentration.

Cell density optimization was performed for both cell lines on transwell. Epithelial and endothelial cells were seeded on PCL/Gel at different concentrations and grown for three days under submerged conditions. This test was performed in order to choose the cell density that ensures the confluence after 72h. Since ALI is generated on chips after three days of cell seeding, as suggested by *Ingber et al* [46], this test was necessary to guarantee that both cell lines reach confluence state before removing the epithelial medium. Four concentrations were tested for A549 (120,000 cells/cm², 140,000 cells/cm², 160,000 cells/cm², 180,000 cells/cm²) while six increasing concentrations were considered for Hulec-5a (100,000 cells/cm², 120,000 cells/cm², 140,000 cells/cm², 160,000 cells/cm², 180,000 cells/cm², 200,000 cells/cm²). The optimal concentration was selected by marking nuclei with DAPI as well as by performing the Celltiter-blue © vitality test. Microscopic photographs of the membranes at different concentrations are shown in the images below (Figure 4.16).

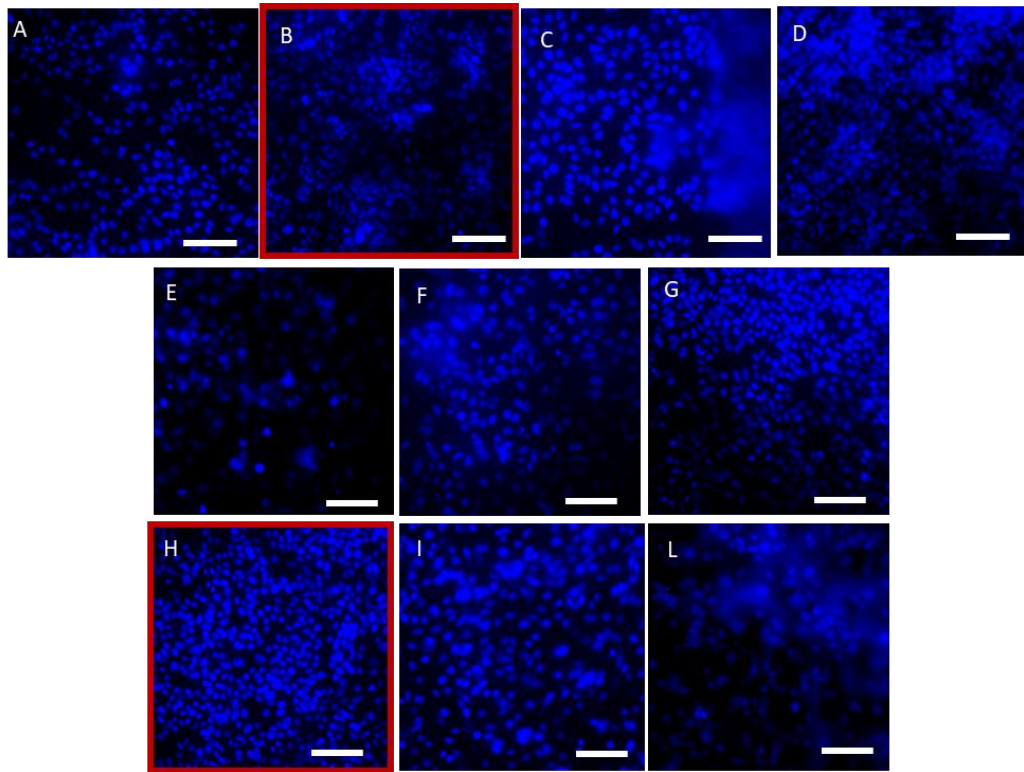
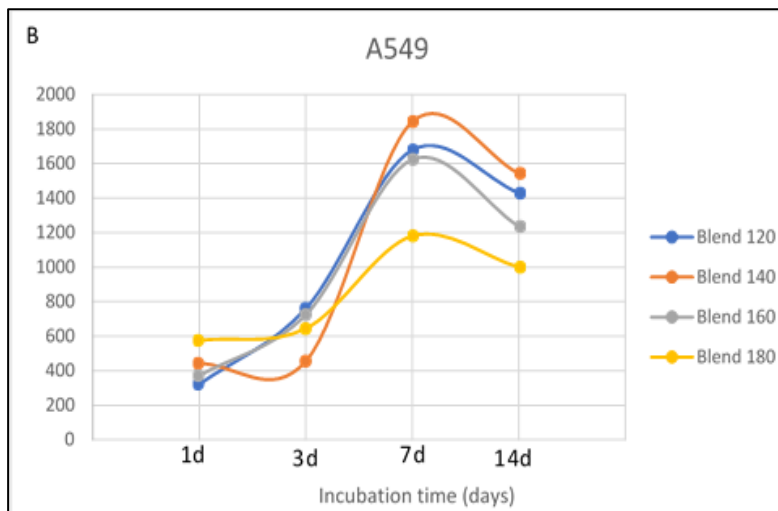
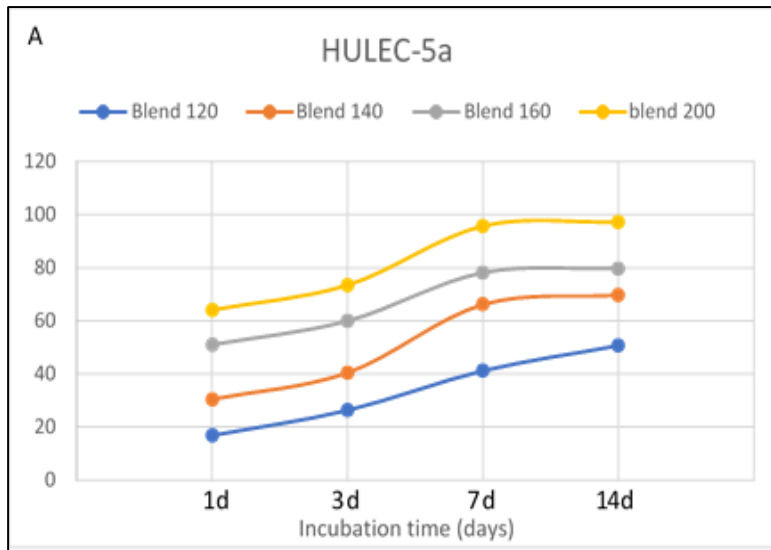


Figure 4.16. Staining of nuclei (DAPI) in: A-D) A549 cells with a concentration of 120.000 cells/cm² (A); 140.000 cells/cm² (B), 160.000 cells/cm² (C) ; 180.000 cells/cm² (D); E-L) HULEC-5a cells with a concentration of 100.000 cells/cm² (E), 120.000 cells/cm² (F); 140.000 cells /cm² (G); 160.000 cells/cm² (H); 180.000 cells/cm² (I); 200.000 cells/cm² (L). Scale bar: 50 μ m.

Cell viability test was also carried out for different concentrations on transwell at 24h, 72h, 7d and 14d. In general, viability at 7 days is confirmed for both cell types, as demonstrate by the graphs below (Graph 4.4). The metabolic activity of endothelial cells continued to constantly increase up to a week, reaching a plateau between 7d and 14d (except in the case of the lowest concentration), because confluence has probably been achieved. A549 cells showed a significant proliferation between 72h and 7d, due to their tendency to grow as clusters [97]. For this reason, the selected concentration was the one which allowed to obtain a confluent and uniform monolayer at 72h. In conclusion, the two best concentrations (selected in red in Figure 4.16 B and H) were 140,000 cells/cm² for A549 and 160,000 cells/cm² for HULEC-5a.



Graph 4.4. Cell viability assay (resazurin) on A) Hulec-5a and B) A549 at different concentrations. Incubation time of 1d,3d,7d and 14d.

4.3.3 Cells adhesion and vitality in the microfluidic device

Finally, the co-culture of A549 and HULEC-5a were performed on chips. First, seeding methods and cell adhesion were evaluated. A549 were seeded at a density of 140.000 cells/cm², by adding a 10 µl drop of cells suspension on the apical side of the PCL/Gel membrane. After 1h of adhesion, the cell culture well was filled with fresh medium. Adhesion was evaluated by staining the nuclei at 24h and 72h, demonstrating that epithelial cells adhere well to the membrane already after 24h (Figure 4.17.)

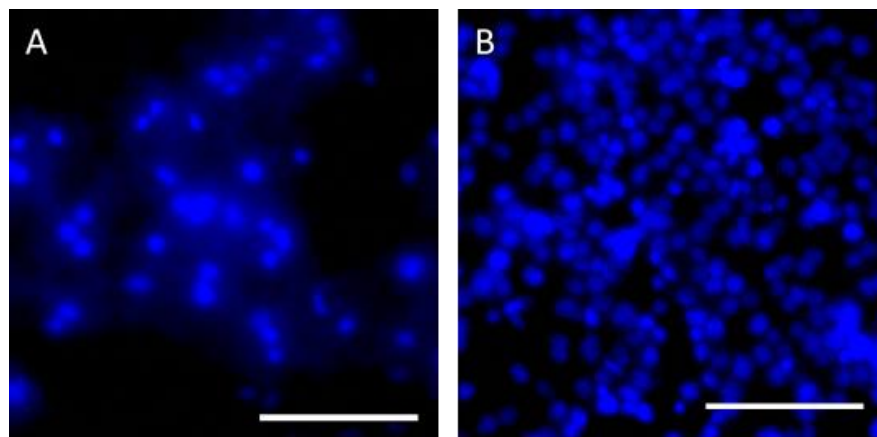


Figure 4.17. Staining of the nuclei with DAPI on A549 after A) 24h and B) 72h. Scale bar: 100 µm

Furthermore, after 72h the A549 were also labelled with FITC-phalloidin, expressing already the tight junctions formation, clearly visible in the figure 4.18, as also demonstrated by *Higueta-Castro et al.* [26].

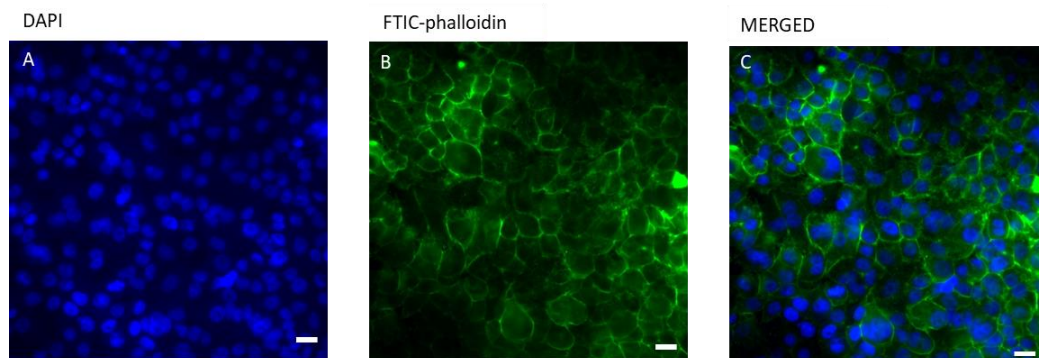


Figure 4.18. Confocal fluorescent images (60x) of A549 cells at 72h grown on blend labelled with A) DAPI, B) FITC-Phalloidin. C) merge of A and B; Magnification bar 20µm

HULEC-5a cells were initially seeded ($160.000 \text{ cells/cm}^2$) on the basal side of the membrane, pushing the cell suspension up to the membrane with a micropipette. Subsequently, two adhesion tests were conducted: the cells were left to adhere for 1h and or 2h. Results of the staining with the DAPI on these tests were not satisfactory, in fact only a few cells adhered. So, both the adhesion time and the seeding method were varied. Specifically, cells were seeded throughout the channel by inserting $10 \mu\text{l}$ of cell solution. Again, two time parameters of adhesion were tested, 4h and 24 h. For all tests performed the chip is flipped during the adhesion process, to exploit gravity, and at the end fresh medium is added. In Figure 4.19 the staining of the nuclei is shown for all the tests carried out selecting as optimal parameters 4h adhesion time and seeding along the entire channel, where a good cell adhesion can be observed (Figure 4.19 (C)). Rhodamine was performed on these samples, and the merged images are shown in Figure 4.19 E and F at two different magnifications (20x and 60x).

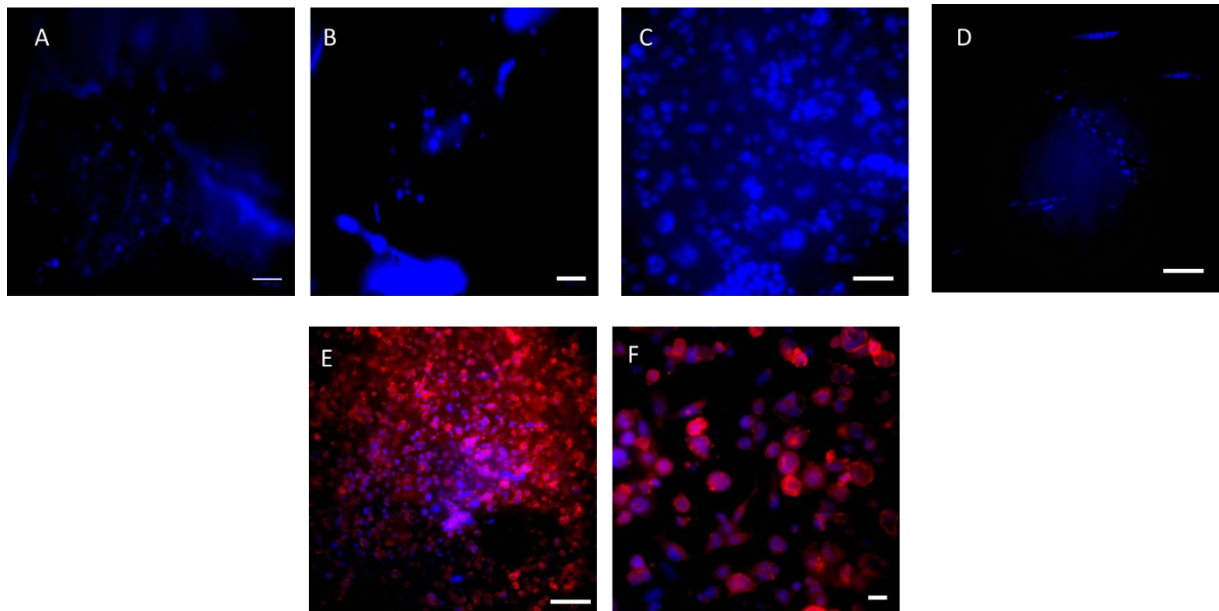
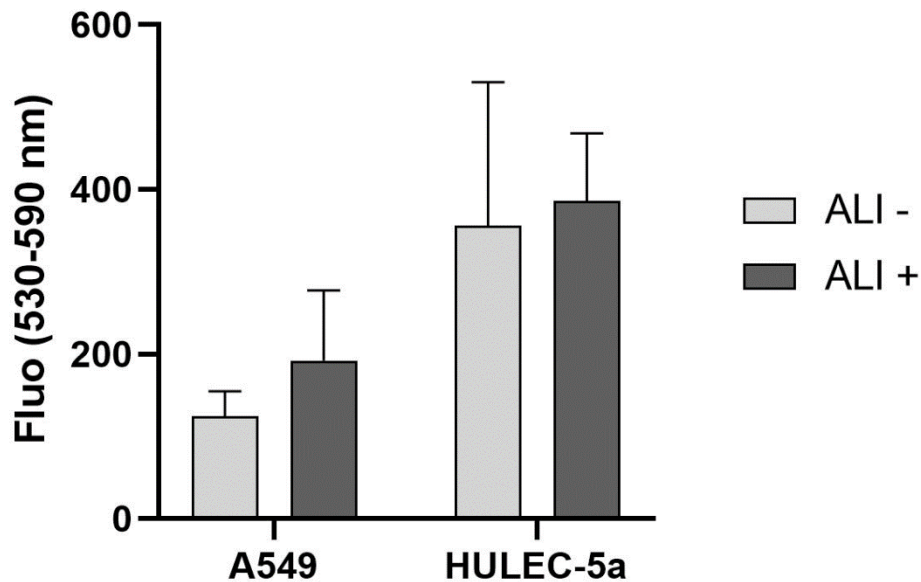


Figure 4.19. A-B) HULEC-5a seeded on the basal membrane and adhered for 1h (A) and 2h (B), scale bar :100 μm ; C-D) Hulec-5a seeded along the entire channel and adhered for 4h (C) and 24 h (D), scale bar 50 μm . E-F) confocal images at 20x (E) and 60x (F) of Hulec-5a after 4h of adhesion, scale bars: 50 μm (E) and 20 μm (F).

Afterwards, both A549 and HULEC-5a were seeded in the chips for 7 days at the previously optimized seeding parameters and cell viability was analysed. After three days of submerged culture ALI was generated on some chips, by aspirating the medium from the apical chamber to leave the epithelial cells fully exposed to air. Cell viability was analyzed by Celltiter-blue®, incubating the devices for 1h. After that 2µl of this medium was transferred inside a plate reader. In the following, the data obtained after one week of seeding in microfluidic devices on PCL-gel membranes are shown (Graph 4.5), which allow to compare the two culture conditions (submerged and ALI). The viability expressed by the two cell lines is comparable for both culture conditions. Thus, the cells are metabolically active seven days after seeding even under air-liquid conditions, which allow epithelial cells to polarize, increasing the presence of tight junctions [3]. This result suggests that cells seeded on chip are viable after one week, demonstrating the good functionality of the projected device.



Graph 4.5. Cell viability on microfluidic devices for ALI and submerged conditions.

5.CONCLUSIONS

Lung diseases have increased in recent years due to environmental pollution and smoking, for example [6]. Indeed, lung cancer is the leading cause of cancer death worldwide [2]. Lung cells behaviour must be investigated to find individual therapies, suitable for each patient [6]. *In vitro* models can be useful in reaching this goal because they allow to mimic the *in vivo*-like environment by recreating biological features and cell-cell interactions. Moreover, they enable to overcome the use of animal models that involve several ethical, economic and scientific problems [10] [11]. However, real-time analysis and dynamic conditions cannot be performed by exploiting the classical *in vitro* models, 2D and 3D [18] [19]. For this reason, organ-on-chips have been introduced, thanks to the development of micro-machining technologies, such as soft lithography [6]. Microfluidic devices reproduce the fundamental unit of the treated organ, mimicking both its biological and mechanical characteristics. In this thesis work, an alveolus-on-a-chip was developed with the aim of simulating the alveolar-capillary barrier, where the main phenomena of diffusive exchange take place. The two physiological features to be considered in the device are the air-liquid interface, because the alveolar cells are directly in contact with air, and the cyclic stress imposed by respiration on the alveoli. For the development of the project geometry, the works of *Ingber et al* and *Stucki et al* were taken as a reference [42] [45]. In fact, both examine cell growth under ALI conditions and deploy the respiratory movement through mechanical actuation in vacuum. In this project biomimetic membranes were employed to mimic the alveolar geometry as *Stucki et al.* did [42], moreover the cells are directly exposed to the atmosphere thanks to the circular chamber completely open to the atmosphere. On the other hand, for the mechanical actuation, side channels were designed as proposed by *Ingber et al.* [45]. The membrane is the distinguishing element from the two mentioned works. The choice of the material and the technique was based on *Higuera-Castro et al.* scientific paper [26]. They developed a two-level microfluidic device with an electrospun PCL/Gel membrane between the two. In fact, electrospinning allows to reproduce biomimetic membranes with a morphology similar to the cellular ECM. A co-culture of alveolar epithelial cells (A549) and pulmonary capillary endothelial cells (HULEC-5a) was performed on the membrane which has the role of mimicking the basal membrane of the alveolar-capillary barrier. The first step was to design the device, drawing the CAD from Rhinoceros. Afterwards, the mold was manufactured by exploiting the laser ablation technique to reproduce the negative of the projected pattern in the PMMA. Inside the mold, PDMS was subsequently poured (in a 10:1 ratio between base and curing agent) and cross-linked in an oven for one hour and thirty minutes at 70°C, obtaining the replicas of the top and bottom layer. Indeed, PDMS is a biocompatible, optically transparent, flexible and thermally resistant material [37]. For these reasons it is suitable for microfluidics applications in the biomedical field and therefore chosen for this thesis work. Subsequently, both the mold and the

replicas were analyzed under optical microscopy to provide that the obtained geometry and dimensions were comparable with the desired ones. In particular, the laser parameters were optimized for the pillars choosing those which ensure to perform the task of membrane support. In general, the sizes obtained are similar to those on the CAD.

The membrane was produced by electrospinning in two different polymeric materials: PCL, used as control, and PCL-gel. For both solutions, the solvents used to dissolve polymers were acetic acid and formic acid (50:50 v/v). Finally, GPTMS crosslinker was added to the PCL/Gel solution. The electrospinning voltage and flow rate parameters were optimized for the pure PCL solution, keeping the distance constant. The morphology of the fibers obtained for both solutions was analyzed by SEM, thanks to which it was possible to choose the best set of parameters for the fibers in PCL. In particular, the fibers show a random configuration with smaller diameters and pores in the blended membranes. Subsequently, the mechanical properties of the nanofibers were evaluated with uniaxial and biaxial cyclic tests (100 cycles), both exhibiting good fatigue resistance. The addition of gelatin to PCL increases the value of the elastic modulus compared to the pure PCL fibers.

The PCL/Gel membranes were inserted into the microfluidic devices, cutting out a piece of 5mm in diameter. In order to bond the two layers, a surface modification was made with oxygen plasma, which allows the formation of irreversible Si-O-Si bonds. The membrane is blocked in between the two layers. Thereafter, the cellular tests were performed on the two polymeric materials to evaluate their effect on the cells. To study the cell adhesion and therefore the biocompatibility of the materials, a seeding (with a concentration of 30,000 cells/cm²) was first conducted on electrospun slides with PCL and PCL/Gel fibers, using glass-alone as control. Results suggested that cells can adhere on both polymeric materials, as also demonstrated by cell viability assay. This test was carried out on slides at different time point (24h, 72h, 7d and 14d) showing an increasing activity on both substrates as the incubation time advance. Viability on PCL/Gel membrane turns out higher than that on PCL as well as adhesion, evaluated by staining the nuclei and actin filament with DAPI and phalloindin.

Since the tests performed confirmed that the PCL/Gel is a suitable substrate for cell growth, subsequent tests were accomplished only on PCL/Gel membranes. Initially, optimization of cell concentration was carried out to ensure confluence after 72h. In fact, ALI is generated within microfluidic devices three days after seeding as seen in literature, when cells reach the confluence [46]. Optimization was performed on transwell by seeding increasing concentrations of cells for both cell lines. Staining and cell viability were conducted in order to define the two optimal concentrations. For A549 the concentration chosen was 140,000 cells/cm², which ensures, after 72h, the formation of a uniform monolayer on the membrane. In contrast, increasing concentrations show the creation of cell clusters on the scaffolds. In contrast, a concentration of 160,000 cells/cm² was selected for HULEC-5a. Endothelial cells viability increases up to one week and then reaches a plateau at two weeks.

Finally, the seeding was carried out inside the microfluidic devices under static conditions using the optimized concentrations. After three days, air-liquid interface was generated on some chips and after 7 days cellular metabolic activity was evaluated. By comparing classical growth conditions with those in ALI, viability has turned out confrontable between the two methods. Thus, the developed microfluidic device maintained cells viable with both liquid-liquid interface and air-liquid interface.

Staining of the nuclei and cytoskeleton was also implemented in the chips by obtaining confocal microscopy images, such as the one shown in Figure 4.18 (C) in Chapter 4. From this, the cell-cell tight junctions formed on A549 cells were visible. In this regard, a possible future work to be done is the characterization of the alveolus-capillary barrier growth inside the chips. Several methods can be used to assess the quality of the barrier. For example, immunostaining of the characteristic antibodies of the tight junctions, such as ZO-1-occludin for epithelial cells and VE-cadherin for endothelial cells, can be done on the membranes, displaying results with confocal microscopy [1]. In addition, the expression of ATI and ATII cell-specific markers, AQP-5 and SP-C respectively, can also be conducted by staining. In particular, these specific markers should be clearly visible in the case of ALI [16] culture conditions. Barrier integrity may be investigated by measuring transepithelial electrical resistance (TEER) and by studying permeability. The former is a real-time analysis which measures the strength of cell-cell interactions and may be performed using electrodes placed in the apical chamber and in the basal chamber [1] [10]. The second exploits the use of fluorescein-sodium, filling the apical chamber with the permeability solution by incubating the devices for a few hours. Finally, from basal chamber is retrieved the supernatant and transferred to a plate reader for the fluorescence reading [42].

Since the tests performed in this thesis work were done in static, so the cellular behaviour in dynamic should be examined. To do this the device can be connected to a syringe pump containing cellular medium with silicone tubes. An optimization of the flow rate of the pump should be made before performing the cellular assays. In addition, the effect of respiration on the alveolar-capillary barrier could be studied by mechanically stimulating the cells. As mentioned above, this device is already equipped with channels for the mechanical actuation that must be connected to a pump (e.g. vacuum or solenoid) which would allow the membrane traction and compression by stretching the PDMS. In literature, dedicated software is exploited in which the desired frequency and deformation parameters are entered in order to control the movement of the pump [45].

Finally, to reach the ambitious goal of personalized medicine, human primary cells could be seeded to study therapies and to perform drug screening to each patient or specific genetic group [43].

Bibliography

- [1] Rothen-Rutishauser, B., Müller, L., Blank, F., Brandenberger, C., Mühlfeld, C., & Gehr, P. (2008). A newly developed in vitro model of the human epithelial airway barrier to study the toxic potential of nanoparticles. *Altex*, 25(3), 191–196. <https://doi.org/10.14573/altex.2008.3.191>
- [2] Dellaquila, A., Thomée, E. K., McMillan, A. H., & Lesher-Pérez, S. C. (2019). Lung-on-a-chip platforms for modeling disease pathogenesis. In *Organ-on-a-chip: Engineered Microenvironments for Safety and Efficacy Testing*. <https://doi.org/10.1016/B978-0-12-817202-5.00004-8>
- [3] Doryab, A., Tas, S., Taskin, M. B., Yang, L., Hilgendorff, A., Groll, J., Wagner, D. E., & Schmid, O. (2019). Evolution of Bioengineered Lung Models: Recent Advances and Challenges in Tissue Mimicry for Studying the Role of Mechanical Forces in Cell Biology. *Advanced Functional Materials*, 29(39), 1–20. <https://doi.org/10.1002/adfm.201903114>
- [4] Evans, K. V., & Lee, J. H. (2020). Alveolar wars: The rise of in vitro models to understand human lung alveolar maintenance, regeneration, and disease. *Stem Cells Translational Medicine*, 9(8), 867–881. <https://doi.org/10.1002/sctm.19-0433>
- [5] Tenenbaum-Katan, J., Artzy-Schnirman, A., Fishler, R., Korin, N., & Sznitman, J. (2018). Biomimetics of the pulmonary environment in vitro: A microfluidics perspective. *Biomicrofluidics*, 12(4). <https://doi.org/10.1063/1.5023034>
- [6] Li, K., Yang, X., Xue, C., Zhao, L., Zhang, Y., & Gao, X. (2019). Biomimetic human lung-on-a-chip for modeling disease investigation. *Biomicrofluidics*, 13(3), 1–8. <https://doi.org/10.1063/1.5100070>
- [7] Wang, C., Tang, Z., Zhao, Y., Yao, R., Li, L., & Sun, W. (2014). Three-dimensional in vitro cancer models: A short review. *Biofabrication*, 6(2). <https://doi.org/10.1088/1758-5082/6/2/022001>
- [8] R. Carrington, S. Jordan, Y.J. Wong, S.C. Pitchford, C.P. Page, A novel murine model of pulmonary fibrosis: the role of platelets in chronic changes induced by bleomycin, *Journal of Pharmacological and Toxicological Methods*, Volume 109, 2021, 107057, ISSN 1056-8719, <https://doi.org/10.1016/j.vascn.2021.107057>.
- [9] You, M. S., Rougely, L. C., You, M., & Wang, Y. (2013). Mouse models of lung squamous cell carcinomas. *Cancer and Metastasis Reviews*, 32(1–2), 77–82. <https://doi.org/10.1007/s10555-012-9406-4>

- [10] Konar, D., Devarasetty, M., Yildiz, D. V., Atala, A., & Murphy, S. V. (2016). Lung-On-A-Chip Technologies for Disease Modeling and Drug Development. *Biomedical Engineering and Computational Biology*, 7s1, BECB.S34252. <https://doi.org/10.4137/becb.s34252>
- [11] Wu, Q., Liu, J., Wang, X., Feng, L., Wu, J., Zhu, X., Wen, W., & Gong, X. (2020). Organ-on-a-chip: Recent breakthroughs and future prospects. *BioMedical Engineering Online*, 19(1), 1–19. <https://doi.org/10.1186/s12938-020-0752-0>
- [12] Leininger, M. (2016). UC San Diego UC San Diego Electronic Theses and Dissertations by. *UC San Diego Electronic Theses and Dissertations*, 290, 214.
- [13] Grainger, C. I., Greenwell, L. L., Lockley, D. J., Martin, G. P., & Forbes, B. (2006). Culture of Calu-3 cells at the air interface provides a representative model of the airway epithelial barrier. *Pharmaceutical Research*, 23(7), 1482–1490. <https://doi.org/10.1007/s11095-006-0255-0>
- [14] Kreft, M. E., Jerman, U. D., Lasič, E., Hevir-Kene, N., Rižner, T. L., Peternel, L., & Kristan, K. (2015). The characterization of the human cell line Calu-3 under different culture conditions and its use as an optimized in vitro model to investigate bronchial epithelial function. *European Journal of Pharmaceutical Sciences*, 69, 1–9. <https://doi.org/10.1016/j.ejps.2014.12.017>
- [15] Miller, A. J., & Spence, J. R. (2017). In vitro models to study human lung development, disease and homeostasis. *Physiology*, 32(3), 246–260. <https://doi.org/10.1152/physiol.00041.2016>
- [16] Wu, J., Wang, Y., Liu, G., Jia, Y., Yang, J., Shi, J., Dong, J., Wei, J., & Liu, X. (2018). Characterization of air-liquid interface culture of A549 alveolar epithelial cells. *Brazilian Journal of Medical and Biological Research*, 51(2), 1–9. <https://doi.org/10.1590/1414-431x20176950>
- [17] Dekali, S., Gamez, C., Kortulewski, T., Blazy, K., Rat, P., & Lacroix, G. (2014). Assessment of an in vitro model of pulmonary barrier to study the translocation of nanoparticles. *Toxicology Reports*, 1, 157–171. <https://doi.org/10.1016/j.toxrep.2014.03.003>
- [18] Azizipour, N., Avazpour, R., Rosenzweig, D. H., Sawan, M., & Ajji, A. (2020). Evolution of biochip technology: A review from lab-on-a-chip to organ-on-a-chip. *Micromachines*, 11(6), 1–15. <https://doi.org/10.3390/mi11060599>
- [19] Bhatia, S. N., & Ingber, D. E. (2014). Microfluidic organs-on-chips. *Nature Biotechnology*, 32(8), 760–772. <https://doi.org/10.1038/nbt.2989>
- [20] Xu, W. H., Han, M., Dong, Q., Fu, Z. X., Diao, Y. Y., Liu, H., Xu, J., Jiang, H. L., Zhang, S. Z., Zheng, S., Gao, J. Q., & Wei, Q. C. (2012). Doxorubicin-mediated radiosensitivity in multicellular spheroids from

a lung cancer cell line is enhanced by composite micelle encapsulation. *International Journal of Nanomedicine*, 7, 2661–2671. <https://doi.org/10.2147/IJN.S30445>

[21] Tian, L., Gao, J., Garcia, I. M., Chen, H. J., Castaldi, A., & Chen, Y. W. (2020). Human pluripotent stem cell-derived lung organoids: Potential applications in development and disease modeling. *Wiley Interdisciplinary Reviews: Developmental Biology*, January, 1–16. <https://doi.org/10.1002/wdev.399>

[22] Miller, A.J., Dye, B.R., Ferrer-Torres, D. *et al.* Generation of lung organoids from human pluripotent stem cells in vitro. *Nat Protoc* **14**, 518–540 (2019). <https://doi.org/10.1038/s41596-018-0104-8>

[23] Wilkinson DC, Alva-Ornelas JA, Sucre JM, Vijayaraj P, Durra A, Richardson W, Jonas SJ, Paul MK, Karumbayaram S, Dunn B, Gomperts BN. Development of a Three-Dimensional Bioengineering Technology to Generate Lung Tissue for Personalized Disease Modeling. *Stem Cells Transl Med*. 2017 Feb;6(2):622-633. doi: 10.5966/sctm.2016-0192. Epub 2016 Sep 15. PMID: 28191779; PMCID: PMC5442826.

[24] Doryab, A., Amoabediny, G., & Salehi-Najafabadi, A. (2016). Advances in pulmonary therapy and drug development: Lung tissue engineering to lung-on-a-chip. *Biotechnology Advances*, 34(5), 588–596. <https://doi.org/10.1016/j.biotechadv.2016.02.006>

[25] Ghaedi, M., Calle, E. A., Mendez, J. J., Gard, A. L., Balestrini, J., Booth, A., Bove, P. F., Gui, L., White, E. S., & Niklason, L. E. (2013). Human iPS cell-derived alveolar epithelium repopulates lung extracellular matrix. *Journal of Clinical Investigation*, 123(11), 4950–4962. <https://doi.org/10.1172/JCI68793>

[26] Higueta-Castro, N., Nelson, M. T., Shukla, V., Agudelo-Garcia, P. A., Zhang, W., Duarte-Sanmiguel, S. M., Englert, J. A., Lannutti, J. J., Hansford, D. J., & Ghadiali, S. N. (2017). Using a Novel Microfabricated Model of the Alveolar-Capillary Barrier to Investigate the Effect of Matrix Structure on Atelectrauma. *Scientific Reports*, 7(1), 1–13. <https://doi.org/10.1038/s41598-017-12044-9>

[27] Shigemura, N., Okumura, M., Mizuno, S., Imanishi, Y., Matsuyama, A., Shiono, H., Nakamura, T., & Sawa, Y. (2006). Lung tissue engineering technique with adipose stromal cells improves surgical outcome for pulmonary emphysema. *American Journal of Respiratory and Critical Care Medicine*, 174(11), 1199–1205. <https://doi.org/10.1164/rccm.200603-406OC>

[28] De Hilster, R. H. J., Sharma, P. K., Jonker, M. R., White, E. S., Gercama, E. A., Roobeek, M., Timens, W., Harmsen, M. C., Hylkema, M. N., & Burgess, J. K. (2020). Human lung extracellular matrix hydrogels resemble the stiffness and viscoelasticity of native lung tissue. *American Journal of Physiology - Lung Cellular and Molecular Physiology*, 318(4), L698–L704. <https://doi.org/10.1152/AJPLUNG.00451.2019>

- [29] Horvath, L., Umehara, Y., Jud, C., Blank, F., Petri-Fink, A., & Rothen-Rutishauser, B. (2015). Engineering an in vitro air-blood barrier by 3D bioprinting. *Scientific Reports*, 5. <https://doi.org/10.1038/srep07974>
- [30] Zhu, J. (2020). Application of Organ-on-Chip in Drug Discovery. *Journal of Biosciences and Medicines*, 08(03), 119–134. <https://doi.org/10.4236/jbm.2020.83011>
- [31] Maschmeyer, I. (2020). *Organ-on-a-Chip*.
- [32] Esch, E. W., Bahinski, A., & Huh, D. (2015). Organs-on-chips at the frontiers of drug discovery. *Nature Reviews Drug Discovery*, 14(4), 248–260. <https://doi.org/10.1038/nrd4539>
- [33] Kurth, F., Györvary, E., Heub, S., Ledroit, D., Paoletti, S., Renggli, K., Revol, V., Verhulsel, M., Weder, G., & Loizeau, F. (2019). Organs-on-a-chip engineering. In *Organ-on-a-chip: Engineered Microenvironments for Safety and Efficacy Testing*. <https://doi.org/10.1016/B978-0-12-817202-5.00003-6>
- [34] Ren, K., Zhou, J., & Wu, H. (2013). Materials for microfluidic chip fabrication. *Accounts of Chemical Research*, 46(11), 2396–2406. <https://doi.org/10.1021/ar300314s>
- [35] Wu, W. I., Rezai, P., Hsu, H. H., & Selvaganapathy, P. R. (2013). Materials and methods for the microfabrication of microfluidic biomedical devices. In *Microfluidic Devices for Biomedical Applications*. <https://doi.org/10.1533/9780857097040.1.3>
- [36] Becker, H., & Gärtner, C. (2008). Polymer microfabrication technologies for microfluidic systems. *Analytical and Bioanalytical Chemistry*, 390(1), 89–111. <https://doi.org/10.1007/s00216-007-1692-2>
- [37] Mata, A., Fleischman, A. J., & Roy, S. (2005). Characterization of Polydimethylsiloxane (PDMS) Properties for Biomedical Micro/Nanosystems. *Biomedical Microdevices*, 7(4), 281–293. <https://doi.org/10.1007/s10544-005-6070-2>
- [38] Faustino, V., Catarino, S. O., Lima, R., & Minas, G. (2016). Biomedical microfluidic devices by using low-cost fabrication techniques: A review. *Journal of Biomechanics*, 49(11), 2280–2292. <https://doi.org/10.1016/j.jbiomech.2015.11.031>
- [39] Gale, B. K., Jafek, A. R., Lambert, C. J., Goenner, B. L., Moghimifam, H., Nze, U. C., & Kamarapu, S. K. (2018). A review of current methods in microfluidic device fabrication and future commercialization prospects. *Inventions*, 3(3). <https://doi.org/10.3390/inventions3030060>
- [40] Benam, K. H., Königshoff, M., & Eickelberg, O. (2018). Breaking the in vitro barrier in respiratory medicine: Engineered microphysiological systems for chronic obstructive pulmonary disease and

beyond. *American Journal of Respiratory and Critical Care Medicine*, 197(7), 869–875. <https://doi.org/10.1164/rccm.201709-1795PP>

[41] Artzy-Schnirman, A., Lehr, C. M., & Sznitman, J. (2020). Advancing human in vitro pulmonary disease models in preclinical research: opportunities for lung-on-chips. *Expert Opinion on Drug Delivery*, 17(5), 621–625. <https://doi.org/10.1080/17425247.2020.1738380>

[42] Stucki, J. D., Hobi, N., Galimov, A., Stucki, A. O., Schneider-Daum, N., Lehr, C. M., Huwer, H., Frick, M., Funke-Chambour, M., Geiser, T., & Guenat, O. T. (2018). Medium throughput breathing human primary cell alveolus-on-chip model. *Scientific Reports*, 8(1), 1–13. <https://doi.org/10.1038/s41598-018-32523-x>

[43] Shrestha, J., Razavi Bazaz, S., Aboulkheyr Es, H., Yaghobian Azari, D., Thierry, B., Ebrahimi Warkiani, M., & Ghadiri, M. (2020). Lung-on-a-chip: the future of respiratory disease models and pharmacological studies. *Critical Reviews in Biotechnology*, 40(2), 213–230. <https://doi.org/10.1080/07388551.2019.1710458>

[44] Jain, A., Barrile, R., van der Meer, A. D., Mammoto, A., Mammoto, T., De Ceunynck, K., Aisiku, O., Otieno, M. A., Loudon, C. S., Hamilton, G. A., Flaumenhaft, R., & Ingber, D. E. (2018). Primary Human Lung Alveolus-on-a-chip Model of Intravascular Thrombosis for Assessment of Therapeutics. *Clinical Pharmacology and Therapeutics*, 103(2), 332–340. <https://doi.org/10.1002/cpt.742>

[45] Huh, D., Matthews, B. D., Mammoto, A., Montoya-Zavala, M., Yuan Hsin, H., & Ingber, D. E. (2010). Reconstituting organ-level lung functions on a chip. *Science*, 328(5986), 1662–1668. <https://doi.org/10.1126/science.1188302>

[46] Hassell, B. A., Goyal, G., Lee, E., Sontheimer-Phelps, A., Levy, O., Chen, C. S., & Ingber, D. E. (2017). Human Organ Chip Models Recapitulate Orthotopic Lung Cancer Growth, Therapeutic Responses, and Tumor Dormancy In Vitro. *Cell Reports*, 21(2), 508–516. <https://doi.org/10.1016/j.celrep.2017.09.043>

[47] Huh, D., Leslie, D. C., Matthews, B. D., Fraser, J. P., Jurek, S., Hamilton, G. A., Thornehoeloe, K. S., McAlexander, M. A., & Ingber, D. E. (2012). A human disease model of drug toxicity-induced pulmonary edema in a lung-on-a-chip microdevice. *Science Translational Medicine*, 4(159). <https://doi.org/10.1126/scitranslmed.3004249>

[48] Benam, K. H., Novak, R., Nawroth, J., Hirano-Kobayashi, M., Ferrante, T. C., Choe, Y., Prantil-Baun, R., Weaver, J. C., Bahinski, A., Parker, K. K., & Ingber, D. E. (2016). Matched-Comparative Modeling of Normal and Diseased Human Airway Responses Using a Microengineered Breathing Lung Chip. *Cell Systems*, 3(5), 456-466.e4. <https://doi.org/10.1016/j.cels.2016.10.003>

- [49] Tavana, H., Zamankhan, P., Christensen, P. J., Grotberg, J. B., & Takayama, S. (2011). Epithelium damage and protection during reopening of occluded airways in a physiologic microfluidic pulmonary airway model. *Biomedical Microdevices*, *13*(4), 731–742. <https://doi.org/10.1007/s10544-011-9543-5>
- [50] Giannitelli, S. M., Costantini, M., Basoli, F., Trombetta, M., & Rainer, A. (2018). Electrospinning and microfluidics: An integrated approach for tissue engineering and cancer. In *Electrofluidodynamic Technologies (EFDTs) for Biomaterials and Medical Devices: Principles and Advances*. Elsevier Ltd. <https://doi.org/10.1016/B978-0-08-101745-6.00008-6>
- [51] Liu, Z., Ramakrishna, S., & Liu, X. (2020). Electrospinning and emerging healthcare and medicine possibilities. *APL Bioengineering*, *4*(3). <https://doi.org/10.1063/5.0012309>
- [52] Nishiguchi, A., Singh, S., Wessling, M., Kirkpatrick, C. J., & Möller, M. (2017). Basement Membrane Mimics of Biofunctionalized Nanofibers for a Bipolar-Cultured Human Primary Alveolar-Capillary Barrier Model. *Biomacromolecules*, *18*(3), 719–727. <https://doi.org/10.1021/acs.biomac.6b01509>
- [53] Dohle, E., Singh, S., Nishigushi, A., Fischer, T., Wessling, M., Möller, M., Sader, R., Kasper, J., Ghanaati, S., & Kirkpatrick, J. C. (2018). Human Co- and Triple-Culture Model of the Alveolar-Capillary Barrier on a Basement Membrane Mimic. *Tissue Engineering - Part C: Methods*, *24*(9), 495–503. <https://doi.org/10.1089/ten.tec.2018.0087>
- [54] Morris, G. E., Bridge, J. C., Brace, L. A., Knox, A. J., Aylott, J. W., Brightling, C. E., Ghaemmaghami, A. M., & Rose, F. R. A. J. (2014). A novel electrospun biphasic scaffold provides optimal three-dimensional topography for in vitro co-culture of airway epithelial and fibroblast cells. *Biofabrication*, *6*(3). <https://doi.org/10.1088/1758-5082/6/3/035014>
- [55] Chemical., T. D. C. (2017). SYLGARD™ 184 Silicone Elastomer Technical Datasheet. *Silicone Elastomer Technical Data Sheet*, *11*, 4. <https://consumer.dow.com/en-us/document-viewer.html?randomVar=3835418757322904567&docPath=/documents/en-us/productdatasheet/11/11-31/11-3184-sylgard-184-elastomer.pdf>
- [56] Mohamed, R. M., & Yusoh, K. (2015). A Review on the Recent Research of Polycaprolactone (PCL). *Advanced Materials Research*, *1134*, 249–255. <https://doi.org/10.4028/www.scientific.net/amr.1134.249>
- [57] Rahmani Del Bakhshayesh, A., Annabi, N., Khalilov, R., Akbarzadeh, A., Samiei, M., Alizadeh, E., Alizadeh-Ghodsi, M., Davaran, S., & Montaseri, A. (2018). Recent advances on biomedical applications of scaffolds in wound healing and dermal tissue engineering. *Artificial Cells, Nanomedicine and Biotechnology*, *46*(4), 691–705. <https://doi.org/10.1080/21691401.2017.1349778>

- [58] "Polycaprolacthone|Sigma-Aldrich." (n.d.). Retrieved June 29, 2021, from <https://www.sigmaaldrich.com/IT/en/product/aldrich/440744>
- [59] Hassan, S., Heinrich, M., Cecen, B., Prakash, J., & Zhang, Y. S. (2020). Biomaterials for on-chip organ systems. In *Biomaterials for Organ and Tissue Regeneration*. LTD. <https://doi.org/10.1016/b978-0-08-102906-0.00019-2>
- [60] Nikkhah, M., Akbari, M., Memic, A., Dolatshahi-pirouz, A., & Khademhosseini, A. (2016). for Tissue Engineering and. *Biomaterials from Nature for Advance Devices and Therapies*, 37–62.
- [61] "Gelatin from porcine skin |Sigma-Aldrich" (n.d.). Retrieved June 29, 2021, from https://www.sigmaaldrich.com/IT/en/product/sigma/g2500?gclid=CjwKCAjwieuGBhAsEiwA1Ly_nb0G9a5emGSS1_ACU3GvHm1W06XQ5MQPjwbUNEJVKjQMNj1B6g2TUxoC2c0QAvD_BwE
- [62] Tonda-Turo, C., Cipriani, E., Gnani, S., Chiono, V., Mattu, C., Gentile, P., Perroteau, I., Zanetti, M., & Ciardelli, G. (2013). Crosslinked gelatin nanofibres: Preparation, characterisation and in vitro studies using glial-like cells. *Materials Science and Engineering C*, 33(5), 2723–2735. <https://doi.org/10.1016/j.msec.2013.02.039>
- [63] "(3-Glycidyloxypropyl)trimethoxysilane ≥98%|Sigma-Aldrich." (n.d.). Retrieved June 29, 2021, from <https://www.sigmaaldrich.com/IT/en/product/aldrich/440167>
- [64] Wagner, F.S. and Staff, U.b. (2014). Acetic Acid. In *Kirk-Othmer Encyclopedia of Chemical Technology*, John Wiley & Sons, Inc (Ed.). <https://doi.org/10.1002/0471238961.0103052023010714.a01.pub3>
- [65] "Acetic acid ACS reagent, ≥99.7%|Sigma-Aldrich." (n.d.). Retrieved June 29, 2021, from https://www.sigmaaldrich.com/IT/en/product/sigma/a0808?gclid=CjwKCAjwieuGBhAsEiwA1Ly_nVpj5PxcN5K1Zf31Lsvsxufp44fpS9XQ5imWhCJPVvNThkvrwiPuEBoCGtcQAvD_BwE
- [66] Sheet, S. D. (2017). Formic acid Formic acid. *ICIS Chemical Business*, 1(29), 1–12. <https://doi.org/10.1002/14356007.a12>
- [67] "Formic acid|Sigma-Aldrich." (n.d.). Retrieved June 29, 2021, from https://www.sigmaaldrich.com/IT/en/product/mm/822254?gclid=CjwKCAjwieuGBhAsEiwA1Ly_nd1rtMvwkh_btrLROCo4yUqMg82-Vo2CZjAJR0R02lw5L3yvAARZoBoCwokQAvD_BwE
- [68] "Chloroform|Sigma-Aldrich." (n.d.). Retrieved June 29, 2021, from <https://www.sigmaaldrich.com/IT/en/product/sigald/c2432?context=product>
- [69] "A549| ATCC." Retrieved June 29, 2021, from <https://www.atcc.org/products/ccl-185>

- [70] "Gibco™ RPMI 1640 Medium." (n.d.). Retrieved June 29, 2021, from <https://www.fishersci.it/shop/products/rpmi-1640-medium-41/p-7076212>
- [71] "Fetal Bovin Serum|Gibco™." (n.d.). Retrieved June 29, 2021, from <https://www.thermofisher.com/it/en/home/life-science/cell-culture/mammalian-cell-culture/fbs.html>
- [72] "Gibco™ Penicillin-Streptomycin (10,000 U/mL)." (n.d.). Retrieved June 29, 2021, from <https://www.thermofisher.com/order/catalog/product/15140122#/15140122>
- [73] "HULEC-5a|ATCC." (n.d.). Retrieved June 29, 2021, from <https://www.atcc.org/products/crl-3244>
- [74] "Gibco™ MCDB 131 Medium, no glutamine." (n.d.). Retrieved June 29, 2021, from <https://www.thermofisher.com/order/catalog/product/10372019#/10372019>
- [75] Palu', G., Valisena, S., Barcellona, M. L., Masotti, L., & Meloni, G. A. (1987). DAPI - pUC8 complex: A tool to investigate biological effects of nucleic acid-drug interaction. *Biochemical and Biophysical Research Communications*, 145(1), 40–45. [https://doi.org/10.1016/0006-291X\(87\)91284-8](https://doi.org/10.1016/0006-291X(87)91284-8)
- [76] "DAPI (4',6-Diamidino-2-Phenylindole, Dihydrochloride)|ThermoFisher." (n.d.). Retrieved June 30, 2021, from https://www.thermofisher.com/order/catalog/product/D1306?gclid=CjwKCAjwrPCGBhALEiwAUI9X07mOkb5rkOhdlg1ScnbOVZ9sP0gQk3qaUg3BamK1c5Hqab3eVormzhoC29oQAvD_BwE&ef_id=CjwKCAjwrPCGBhALEiwAUI9X07mOkb5rkOhdlg1ScnbOVZ9sP0gQk3qaUg3BamK1c5Hqab3eVormzhoC29oQAvD_BwE:G
- [77] "Invitrogen™ Fluorescein Phalloidin." (n.d.). Retrieved June 30, 2021, from <https://www.thermofisher.com/order/catalog/product/F432#/F432>
- [78] "Invitrogen™ Rhodamine Phalloidin." (n.d.). Retrieved June 30, 2021, from <https://www.thermofisher.com/order/catalog/product/R415#/R415>
- [79] "Marcaturation laser stand-alone LASER Slider|MicroLa Optoelectronics." (n.d.). Retrieved July 1, 2021, from <https://www.micro-la.com/open/product/7/laser-slider-sistema-di-marcaturation-laser-standalone>
- [80] "Novaspider v5." (n.d.). Retrieved June 30, 2021, from <http://novaspider.com/equipment-and-services/>
- [81] Giuntoli G, Muzio G, Actis C, Ganora A, Calzone S, Bruno M, Ciardelli G, Carmagnola I and Tondaturro C (2021) *In-vitro* Characterization of a Hernia Mesh Featuring a Nanostructured Coating. *Front. Bioeng. Biotechnol.* 8:589223. doi: 10.3389/fbioe.2020.589223

- [82] Brabazon, D., & Raffer, A. (2014). Advanced characterization techniques for nanostructures. In *Emerging Nanotechnologies for Manufacturing* (Second Edition). Elsevier Inc. <https://doi.org/10.1016/B978-0-323-28990-0.00003-8>
- [83] Inkson, B. J. (2016). Scanning Electron Microscopy (SEM) and Transmission Electron Microscopy (TEM) for Materials Characterization. In *Materials Characterization Using Nondestructive Evaluation (NDE) Methods*. Elsevier Ltd. <https://doi.org/10.1016/B978-0-08-100040-3.00002-X>
- [84] “ZEISS. (2015). *SUPRA*® Series. 1–25.” (n.d.). Retrieved July 4, 2021 from <https://wiki.smfi.unipr.it/dokuwiki/lib/exe/fetch.php?media=lmn:brochure.pdf>
- [85] “Tissue, A. TestBench Test Instrument ElectroForce® Planar Biaxial TestBench Test Instrument.” (n.d.). Retrieved July 4, 2021 from https://www.tainstruments.com/wp-content/uploads/sellsheet_TBPlanarBiaxial_022009_low.pdf
- [86] “Neubauer Chamber.” (n.d.). Retrieved July 1, 2021, from <https://www.molecularlab.it/protocolli/protocol.asp?id=57>
- [87] “*Ti2_e_2CE-MPLH-8.pdf*.” (n.d.). Retrieved July 4, 2021 from https://www.microscope.healthcare.nikon.com/it_EU/products/inverted-microscopes/eclipse-ti2-series
- [88] Rampersad, S. N. (2012). Multiple applications of alamar blue as an indicator of metabolic function and cellular health in cell viability bioassays. *Sensors (Switzerland)*, 12(9), 12347–12360. <https://doi.org/10.3390/s120912347>
- [89] “BioTek™ Synergy™ HTX Multi-Mode Microplate Reader.” (n.d.). Retrieved July 1, 2021, from <https://www.fishersci.com/shop/products/biotek-synergy-htx-multi-mode-microplate-reader-5/p-4911692>
- [90] Gautam, S., Dinda, A. K., & Mishra, N. C. (2013). Fabrication and characterization of PCL/Gelatin composite nanofibrous scaffold for tissue engineering applications by electrospinning method. *Materials Science and Engineering C*, 33(3), 1228–1235. <https://doi.org/10.1016/j.msec.2012.12.015>
- [91] Ghasemi-Mobarakeh, L., Prabhakaran, M. P., Morshed, M., Nasr-Esfahani, M. H., & Ramakrishna, S. (2008). Electrospun poly(ϵ -caprolactone)/gelatin nanofibrous scaffolds for nerve tissue engineering. *Biomaterials*, 29(34), 4532–4539. <https://doi.org/10.1016/j.biomaterials.2008.08.007>
- [92] Son, W. K., Youk, J. H., Lee, T. S., & Park, W. H. (2004). The effects of solution properties and polyelectrolyte on electrospinning of ultrafine poly (ethylene oxide) fibers. *Polymer*, 45(9), 2959–2966. <https://doi.org/10.1016/j.polymer.2004.03.006>

[93] "Plasma oxygen/Diener." (n.d.). Retrieved July 2, 2021, from https://d3krux2s64mzgx.cloudfront.net/fileadmin/user_upload/Downloads/Plasmatechnik_IT_Kunde.pdf

[94] Marasso, S. L., Puliafito, A., Mombello, D., Benetto, S., Primo, L., Bussolino, F., Pirri, C. F., & Cocuzza, M. (2017). Optimized design and fabrication of a microfluidic platform to study single cells and multicellular aggregates in 3D. *Microfluidics and Nanofluidics*, 21(2). <https://doi.org/10.1007/s10404-017-1872-0>

[95] Zhang, Y., Ouyang, H., Chwee, T. L., Ramakrishna, S., & Huang, Z. M. (2005). Electrospinning of gelatin fibers and gelatin/PCL composite fibrous scaffolds. *Journal of Biomedical Materials Research - Part B Applied Biomaterials*, 72(1), 156–165. <https://doi.org/10.1002/jbm.b.30128>

[96] Dias, J. R., Baptista-Silva, S., Sousa, A., Oliveira, A. L., Bártolo, P. J., & Granja, P. L. (2018). Biomechanical performance of hybrid electrospun structures for skin regeneration. *Materials Science and Engineering C*, 93(March), 816–827. <https://doi.org/10.1016/j.msec.2018.08.050>

[97] Stearns, R. C., Paulauskis, J. D., & Godleski, J. J. (2001). Endocytosis of ultrafine particles by A549 cells. *American Journal of Respiratory Cell and Molecular Biology*, 24(2), 108–115. <https://doi.org/10.1165/ajrcmb.24.2.4081>